Marit Reiso

The Tower Shadow Effect in Downwind Wind Turbines

Thesis for the degree of Philosophiae Doctor

Trondheim, May 2013

Norwegian University of Science and Technology
Faculty of Engineering Science and Technology
Department of Civil and Transport Engineering

NTNU – Trondheim
Norwegian University of
Science and Technology

NTNU
Norwegian University of Science and Technology

Thesis for the degree of Philosophiae Doctor

Faculty of Engineering Science and Technology
Department of Civil and Transport Engineering

ISBN 978-82-471-4489-3 (printed ver.)
ISBN 978-82-471-4490-9 (electronic ver.)
ISSN 1503-8181

Doctoral theses at NTNU, 2013:188

Printed by NTNU-trykk

Abstract

Scarcity of land sites applicable for wind turbines is pushing the technology offshore. By going offshore the expenses of nearly all components increases, which has triggered extensive research with the aim of decreasing component costs, and increasing reliability, as also maintenance costs increase as going offshore.

The focus of this thesis is to look at ways to reduce aerodynamic loads which can contribute in lowering structural fatigue loads and thereby component costs for offshore wind turbines. The loading is mainly reported as blade root flapwise bending moment on wind turbines intentionally made for bottom fixed offshore sites. The load reduction is investigated using a different wind turbine configuration with a downwind mounted rotor and further compared with the conventional upwind mounted rotor on a monopile tower. Blades on downwind mounted rotors are exposed to the fluctuating wake behind the towers, known as the tower shadow. The influence from the tower shadow on blade fatigue loads is investigated using three different types of towers; a full height truss type tower, a faring (airfoil shaped) tower and a monopile tower.

For reliable wind turbine simulations with downwind mounted rotors, an accurate tower shadow model is essential. Thorough investigations of the tower shadow is presented, including the detailed flow picture of the mean velocity deficit, unsteady and turbulent motions, as well as velocity spectra. The tower shadow is investigated in three different ways; using three dimensional physical model scale experiments, steady tower shadow models and two dimensional computational fluid dynamic (CFD) simulations.

By use of the tower shadow from the CFD simulations, an artificial increase in blade fatigue loading is seen as the transversal grid is made coarser. Although this is a 'safe-fail' design (for the coarser grid), it should be kept in mind as this 'simulated' safety factor from the coarse grid simulations could increase wind turbine costs.

A method for improving the accuracy of the steady tower shadow models (currently the most frequently used model in commercial software) through a preprocessing

step, where the results are directly applicable in commercial software for full wind turbine simulations, is presented. This method will improve the reliability of the simulated results. The parameters of the steady tower shadow model and the turbulence intensity are fitted and calibrated with short CFD simulations of the relevant tower geometries. This method accounts for any deviation between the mean velocity deficit obtained from the steady tower shadow model and the CFD simulations, as well as the unsteady motions and turbulence due to the presence of the tower through the calibration of the turbulence intensity (maximum deviation of ± 3 percent with respect to the tower shadow based on the CFD simulations, measured as blade fatigue loading).

The response measured as blade fatigue load show an increased loading for the blades on the downwind mounted rotors using the original blades, compared to the conventional upwind mounted rotor on a monopile tower. Introducing softer and lighter blades changed this result, with reductions in blade fatigue loading (compared to the upwind mounted rotor with the original blades) of three, four and five percent for the monopile, truss and fairing towers, respectively.

Acknowledgements

After four years of working at the Department of Civil and Transport Engineering (BAT) at the Norwegian University of Science and Technology (NTNU) my time as a PhD candidate has now come to an end. It has been an interesting journey focusing on parts of the technical complexity of offshore wind turbines and also getting knowledge in related practical and political matters related to wind turbine technology and erection world wide.

I would like to thank my former supervisor Professor Geir Moe for taking me on and giving me the opportunity to work within the field of offshore wind turbine research. And also to the administration at BAT for arranging a new supervisor after Professor Moe passed away. Thanks to Associated Professor Michael Muskulus for supervising me through the last months of my PhD. I would also like to acknowledge the Research Council of Norway through the project *Offshore Wind Energy in Norway: Setting the basis* (contract no. 186952/I30) for funding my research work.

Parts of my work was carried out in the wind tunnel at the Aerodynamic Laboratory, Department of Energy and Process Engineering, NTNU. I would like to thank laboratory technician Arnt Egil Kolstad and Olav Haldorsen for facilitating my experimental work. Thanks also to Professor Per-Åge Krogstad and PhD candidate Pål Egil Eriksen for valuable discussions in the wind tunnel, as well as master student Loup Suja for helping out during the experiment.

Also a great thanks to former and present colleagues at BAT for constructive discussions as well as social happenings, I would like to mention Haiyan Long, Danial Zwick, Eric Van Buren, Karl Merz, Mayilvahanan Alagan Chella, Fredrik Sandquist, Raed Khalil Lubbad, Johan Wåhlin, Wolfgang Kampel, Sergiy Sukhorukov, Anton Kulyakhtin, Sergiy Kulyakhtin, Ivan Metrikin, Ole-Christian Ekeberg, Torodd Skjerve Nord, Felix Breitschädel, Marat Kashafutdinov, Anna Pustogvar, Alex Klein-Paste, Christian Lønøy, Kim Yangkyun, Nicolas Serre, Ada Repetto-Llamazares, Paul Thomassen, Wenjun Lu, Jenny Trumars, Arne Gürtner, Hans Bihs, Kenneth Eik, Vegard Aksnes, Oddgeir Dalane, Lucie Strub-Klein,

Katherine Dykes, Jan Dubois and Torbjørn Ruud Hagen. A thanks also goes to the remaining PhD candidates within offshore wind turbine research at NTNU for fruitful discussions across our disciplines.

An enormous gratitude goes to my family for being understanding, helping and supportive throughout these years. And last but not least thanks to Steffan and Vilde for patiently waiting for me, I am looking forward spending more time with the two of you.

Marit Reiso

February 2013
Trondheim, Norway

List of Appended Papers and Declaration of Authorship

This thesis contains a total of seven papers, three of the papers are submitted to journals (whereof one is accepted and published) and the remaining papers are published in conference proceedings. The complete papers are found in appendix A.

1. M. Reiso, and G. Moe. *Blade response on offshore bottom fixed wind turbines with downwind rotors.* In Proceedings of the 29th International Conference on Ocean, Offshore and Arctic Engineering (OMAE2010), Shanghai, pages 1-6, 2010.

2. M. Reiso, M. Muskulus, and G. Moe. *Tower shadow - experiment comparing wake behind tubular and truss towers.* In Proceedings of the 21st International Offshore (Ocean) and Polar Engineering Conference (ISOPE2011), Maui, HI, pages 335-341, 2011.

3. T.R. Hagen, M. Reiso, and M. Muskulus. *Numerical tower shadow modeling for a downwind wind turbine truss tower.* In Proceedings of the 30th International Conference on Ocean, Offshore and Arctic Engineering (OMAE2011), Rotterdam, pages 1-12, 2011.

4. T.R. Hagen, M. Reiso, and M. Muskulus. *Numerical analysis of turbulent flow past a truss tower for offshore downwind turbines.* In Proceedings of the 21st International Offshore (Ocean) and Polar Engineering Conference (ISOPE2011), Maui, HI, pages 319-326, 2011.

5. M. Reiso, and M. Muskulus. *Resolution of tower shadow models for downwind mounted rotors and its effect on the blade fatigue.* Submitted to: Journal of Physics: The Science of Making Torque from Wind, Conference Series XX (2012), IOP Publishing, 2012.

6. M. Reiso, and M. Muskulus. *The simultaneous effect of a fairing tower and*

increased blade flexibility on a downwind mounted rotor. Journal of Renewable and Sustainable Energy 5, 033106 (2013); doi: 10.1063/1.4803749.

7. M. Reiso, T.R. Hagen, and M. Muskulus. *A calibration method for downwind wake models accounting for the unsteady behaviour of the wind turbine tower shadow behind monopile and truss towers.* Submitted to: Journal of Wind Engineering and Industrial Aerodynamics.

The PhD candidate carried out the experiments, performed the necessary calculations, provided the results and wrote up the papers. The two papers of where the PhD candidate is co-author, the CFD modelling was carried out by Hagen and the statistical analysis by Muskulus, with the PhD candidate advising Hagen throughout the modelling process, discussing the findings and collaborating in writing up the papers.

Throughout all the work both former and present supervisors, Professor Moe and Associated Professor Muskulus contributed in discussions of the experimental setups and findings and came with constructive feedback that in the end increased the quality of the papers.

Nomenclature

Abbreviation

ALS	Accidental limit state
BEM	Blade element method
CFD	Computational fluid dynamic
COE	Cost of energy
DEL	Damage equivalent loading
DLC	Design load case
DNS	Direct numerical simulations
DW	Downwind
F40-FXX	Fairing length
FLS	Fatigue limit state
HAWT	Horizontal axis wind turbine
kW	Kilowatt
LES	Large eddy simulations
MW	Megawatt
PDF	Probability density function
RANS	Reynolds averaged Navier-Stokes
RFM	Blade root flapwise bending moment
RMS	Root-mean square
RSM	Reynolds-stress model
SLS	Serviceability limit state
SST	Shear-stress transport
Sxx	xx percent reduction in stiffness (S)
TBM	Tower base bending moment
ULS	Ultimate limit state
UW	Upwind
VAWT	Vertical axis wind turbine
Wyy	yy percent reduction in weight (W)
xP	Blade passing frequencies at different rotational speeds

Roman symbols

b	Length parameter (Blevins' model)
c	Centreline deficit (Blevins' model)
C_d	Drag coefficient
$C_{\epsilon 1}$	RANS constant
$C_{\epsilon 2}$	RANS constant
C_μ	RANS constant
D	Diameter
d	Diameter
f	Frequency
$\mathbf{f}$	Body forces
J_m	Momentum deficit
K	Kinematic momentum
k	Turbulent kinetic energy
L	Length scale (Mann model)
l^*	Eddy length
l_m	Mixing length (Boussinesq assumption)
L_{1k}	Length scale (von Karman model)
L_{2k}	Length scale (Kaimal model)
N_i	Counter
n_i	Counter
P	Production rate of turbulent kinetic energy
p	Pressure
Re	Reynolds number
S_{ij}	Mean strain-rate tensor
S_k	Frequency spectrum
St	Strouhal number
TI	Turbulence intensity
U_0	Free stream wind velocity
U_{in}	Free stream wind velocity
$\langle u_i u_j \rangle$	Reynolds stresses
$\mathbf{U}$	Mean velocity
$\mathbf{u}$	Wind velocity
$\mathbf{u}^{'}$	Velocity fluctuations
u^*	Eddy velocity
V	Wind velocity
V	Time averaged velocity at that point (used in TI)
V_0	Free stream velocity
V_i	Truss tower member velocity
$\langle V_i \rangle$	Ensemble mean
V_x	Longitudinal velocity component
V_y	Velocity component normal to the flow direction
$\overline{V}$	Time averaged velocity

$\overline{v}$	Mean velocity
W	Wake width (Powles' model)
w	Wake width parameter (Powles' model)
w_r	Reference wake width parameter
x	Position vector in longitudinal direction
x_0	Virtual origin of the wake (Blevins model)
x_c	Factor (AeroDyn model)
x_r	Longitudinal reference plane
y	Position vector in transversal direction
y^+	Ratio between turbulent and laminar influence

Greek symbols

α	Spectral multiplier in inertial sub range (Mann model)
Δ	Velocity deficit (Powles' model)
Δ_r	Reference velocity deficit parameter
δ_{ij}	Kronecker delta
ϵ	Dissipation
η	Position dependent parameter (JET wake model)
Γ	Eddy lifetime constant (Mann model)
μ	Dynamic viscosity
μ_T	Eddy viscosity
ν	Kinematic viscosity
ν_T	Turbulent viscosity field (RANS)
π	Constant
ρ	Density of fluid
σ	Standard deviation
σ_ϵ	RANS constant
σ_k	RANS constant
σ_k	Standard deviation (von Karman and Kaimal models)
σ_ω	RANS constant
τ_{ij}	Reynolds stress tensor
ω	Dissipation term (RANS)

Contents

Chapter 1

Introduction

Many concepts for wind turbines have been proposed over the years. From Charles Brush' very first automatically operated wind turbine with several blades (Figure 1.1a), through vertical axis wind turbines (Figure 1.1b), the two bladed, full truss tower, Smith-Putman wind turbine (from 1941, Figure 1.1c) to today's conventional wind turbine, the land based monopile tower with an upwind, three bladed, horizontal axis rotor (Figure 1.1d). As exploiting offshore areas for installing wind turbines, the cost of erection, installation, operation and maintenance increases and hence new concepts that can contribute to a decrease in the cost of energy (COE) is interesting to look at. This is the basis for the work in the presented thesis and will be further detailed in the following chapters.

1.1 Thesis outline

The thesis is structured as a collection of papers. A general introduction (chapter 1) and relevant background (chapter 2) are first given. Thereafter chapter 3 summarizes and highlights the different papers separately. Chapter 4 concludes the work and give some interesting views on relevant further works. The full length papers (seven in total) are found in appendix A.

1.2 Motivation

As mentioned, research on offshore wind energy is about reducing the COE. To reduce the COE one might have to think *out of the box* and hence look at other technical ways of erecting energy from wind.

The dominating design with the three bladed, upwind mounted rotor on a monopile tower (often referred as the Danish design, [3]), may be challenged as going offshore. The overall objective of this thesis is to investigate a different configuration, using a downwind mounted rotor and focussing on the aerodynamic and structural

(a) 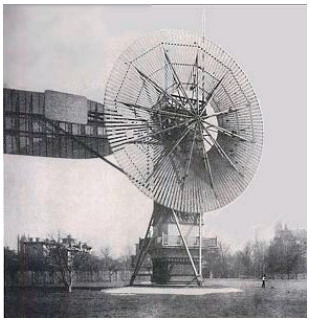 (b) 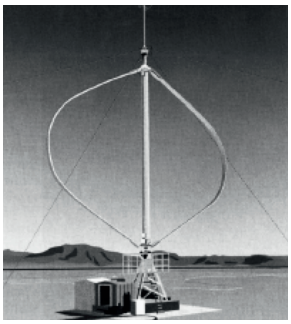

(c)  (d) 

Figure 1.1: Different wind turbine concepts; (a) worlds' first automatically operated wind turbine, courtesy to [1], (b) Darrieus vertical axis wind turbine, courtesy to [2], (c) worlds first MW size wind turbine, courtesy to [2], and (d) today's conventional three bladed horizontal axis wind turbine.

dynamic interaction between the tower and blade. The downwind configuration has benefits such as being more stable in yaw, reducing the risk of blade-tower strike and (from the latter) thereby allowing for more flexible (and lighter) blades (further detailed in section 2.2.1). The central research question is formulated:

How does the tower shadow, caused by different tower geometries, affect the fatigue loading and power production in a downwind mounted rotor?

In the search of answering this question, other more detailed questions arise:

- How does the wind field look like behind a tower at the position of a downwind mounted rotor?
- How can the wind field behind a tower at the position of a downwind mounted rotor be described?
- Will the accuracy of the tower shadow model influence the blade fatigue loads?

- Could softer and lighter blades improve blade fatigue loads on a downwind mounted rotor?
- Could a downwind mounted rotor be an alternative to the conventional upwind mounted rotor from a blade fatigue point of view?

These questions are tried answered through the seven papers of this PhD work. First through a coarse blade fatigue comparison of upwind and downwind rotor configurations using truss and monopile towers (with the tower shadow implemented as a steady parametric wake deficit) in paper 1. The steady parametric tower shadow model is based on certain simplifications, which should be validated with more accurate tower shadow representations. This was done in paper 2 through a physical model scale experiment of the flow field behind a monopile tower and a truss tower (including mean velocity profiles and turbulence spectra). And in papers 3 and 4 for the same tower geometries in full scale two dimensional CFD simulations. The steady parametric tower shadow models were then fitted with the mean velocity profiles from the CFD simulations and the physical model scale experiment.

In paper 5 the unsteady tower shadow (obtained from the CFD simulations) was converted into three dimensional space and implemented in full wind turbine simulations to obtain blade fatigue data for blades on the downwind mounted rotors. The contribution from the different CFD 'components' (mean velocity profile, unsteady motions from vortex shedding and turbulence) were investigated. Also a grid resolution study, to investigate the level of accuracy needed for the tower shadow model and grid to obtain reliable blade fatigue loads were investigated. Paper 6 discuss an optional tower design for downwind mounted rotors, using a fairing for parts of the tower height, and additionally introducing different blade stiffness and weights. Paper 7 suggests a calibration method for downwind steady wake models and the turbulence intensity with CFD simulations (which will increase the reliability of the steady wake model and limit the time consuming CFD simulations to short studies at a few cross-sections of the relevant tower geometries). Further the method is applied in a comparison study of upwind and downwind rotors, using two different blade stiffness and weights.

1.3 Contributions

Contributions to wind turbine research has been conducted in the area of downwind rotors. The main contributions of the thesis are:

- Giving a method for efficiently improving the accuracy of the steady parametric tower shadow models' (currently most frequent used tower shadow model in commercial software for full wind turbine simulations), using short CFD simulation of the relevant tower geometry (in a pre-processing step to the full wind turbine simulations), where the steady tower shadow parameters are fitted and the turbulence intensity calibrated. Due to the pre-processing

step, this will not increase the simulation time for the full wind turbine simulations (with the comprehensive number of design load cases described in wind turbine standards), but will improve the reliability of the simulated results. The method is applicable to any tower geometry, and is directly applicable to commercial software (e.g. Bladed, from GL Garrad Hassan; Bristol, UK).

- Highlighting the effect the wind field (including the tower shadow) grid resolution has on the blade fatigue loading in downwind mounted rotors.
- Showing how the tower shadow from different towers (monopile, truss and fairing), and adjusted blade flexibilities and weights influence the blade fatigue loading on downwind mounted rotors, and how their performance is compared to the conventional upwind mounted rotor.

In detail; the wind field behind a tower at the position of a downwind mounted rotor is complex, consisting of a mean velocity profile, unsteady motions and turbulence, as found in the model scale experiment and the CFD simulations. For blade fatigue loading the main contributors were found to be the mean velocity profile and the turbulence spectrum in the incoming wind, with minor contributions from the unsteady motions and turbulence due to the presence of the tower structure.

These results suggest that the time consuming CFD simulations can be replaced by steady wake (tower shadow) models. For reliable steady wake models, their parameters were fitted with the mean velocity profiles from the CFD simulations. The mean velocity profile for the monopile tower fitted well with the experiment and the CFD simulations. For the truss tower deficiencies were seen. These deficiencies were accounted for in the calibration of the turbulence intensity (refer pre-processing step in the first dot-point above). The calibrated turbulence intensity also accounted for the unsteady motions (vortices) and turbulence originating from the presence of the tower structure.

In addition to the accuracy of the tower shadow model, also the accuracy of the wind field (including tower shadow) grid resolution influenced the result accuracy (measured as blade fatigue loads). Full wind turbine simulations with a coarse grid gave higher blade fatigue loads, than simulations using a finer grid resolution. This is a 'safe-fail' design (for the less time consuming simulations using the coarser grid), but due to the possible increase in construction costs (originating from the artificial 'safety factor' caused by the coarse grid) it should be kept in mind as running simulations.

All downwind mounted rotors performed worse, measured as blade fatigue loads, than the conventional upwind mounted rotor when using the original blades. But with the option of softer and lighter blades in downwind rotors, the blade fatigue loading decreased in all the downwind mounted rotors (behind monopile, truss and fairing towers), while remaining the power production, compared to the upwind mounted rotor (still using the original blades). The blade fatigue loads measured

downwind the truss tower aligned at 0 degrees with the incoming wind direction performed slightly better compared to the measured loads behind the monopile tower, while the largest decrease in blade fatigue loads were found for the blades downwind the fairing tower (five percent lower than for the blades on the upwind mounted rotor), but came at the cost of an increased mean tower bending moment (due to the increased rotor overhang).

1.4 Readership

The thesis focus on the interaction between flow fields behind structures intended as towers for downwind wind turbines and the loads experienced by the rotor blades as passing through the flow field of these towers. The primary readership is students, researchers and engineers interested in or working with:

- wind turbine loading,
- complex dynamic behaviour of wind fields behind (tower) structures, and
- downwind wind turbine configurations.

Chapter 2

Background

The world as of 2013 is a world still demanding more power and electricity, especially with the upcoming economies of the BRIC countries (Brazil, Russia, India and China) [4]. The potential is out there, both as renewable energy and fossil fuels, as well as nuclear power. The choice of energy source is ours to decide.

After the tragic accident in Fukushima Daiichi in Japan in March 2011 the debate of nuclear power and its' catastrophic consequences have again come to live. E.g., in Germany where Chancellor Angela Merkel completely changed the agenda, announcing the ambitious plan of both shutting down the German nuclear power plants 10 years ahead of former Chancellor Gerhard Schröders plan (of 2022), and that the country by 2020 should have reached a 40 percent reduction in greenhouse-gas emissions compared to the 1990 levels (and 80 percent by 2050) based on renewable energy sources (wind energy being amongst them), without the use of nuclear power [5]. Germany has already installed a considerable amount of onshore wind (Figure 2.1), and would need new areas for further expansion. As onshore sites applicable for wind turbines are prone to conflicts with other interests, offshore sites have become interesting, and Germany is now installing offshore wind turbines both in the North Sea and the Baltic Sea [6]. Offshore installations for wind turbines are also being developed in other countries in the region (Belgium, The Netherlands, United Kingdom and Denmark to mention some) [7]. Looking at the wind resources (Figure 2.2) it is also understandable why offshore wind could be a good alternative to the already existing onland wind turbines, with higher mean wind speeds at the elevation of harvest it allows for a larger energy capture per area.

In the following, background on offshore concepts are outlined, together with relevant design requirements. With the focus on tower and blade interaction in downwind mounted rotors, a major part is dedicated to the flow behind the tower including theory on turbulence and tower wake modelling.

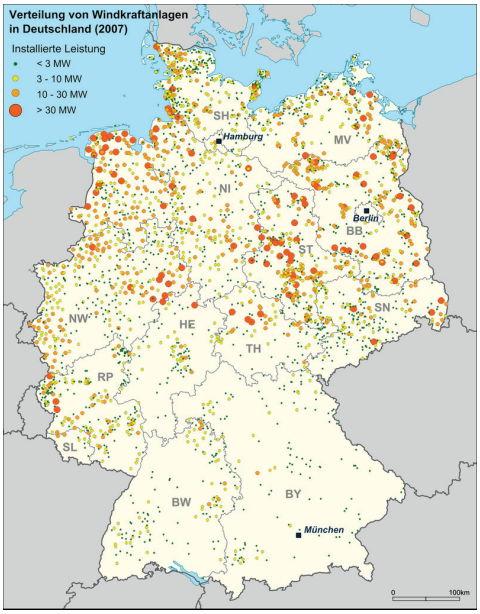

Figure 2.1: Installed onland wind turbines in Germany as of 2007. Courtesy to [8].

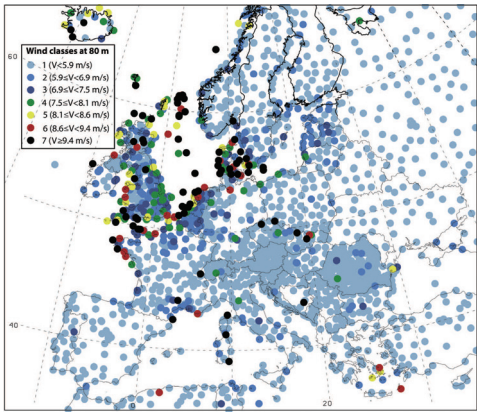

Figure 2.2: European offshore and onshore wind map, velocities taken at elevation 80m. Courtesy to [9].

2.1 Challenges and opportunities going offshore

From the start of the modern wind turbines up until today the growth in wind turbine size has been tremendous, ranging from the smaller kW size into today's MW size. The trend has been to up-scale existing technology into larger MW-size wind turbines (Figure 2.3). Also as going offshore the idea of up-scaling is tempting as it will reduce the number of foundations installed, which is reported to substantially increase in cost compared to onshore foundations [10]. In addition to increasing the power output, the up-scaling has contributed to a substantial weight increase, as the weight scales with the cube [11], or taking the actual development in blade design into account, a bit less [12], while the power scales to the square.

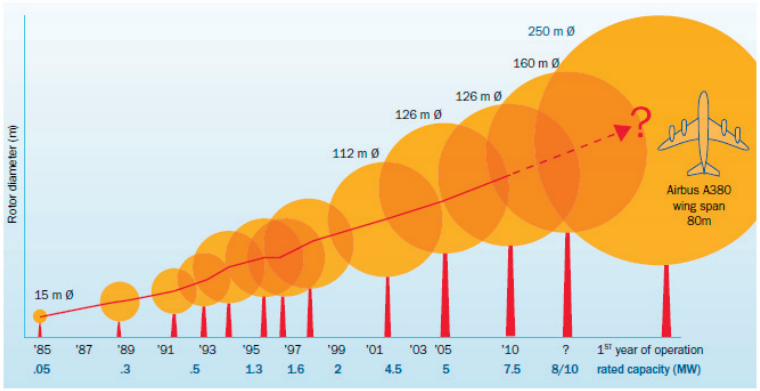

Figure 2.3: Increasing size of commercial and future wind turbines. Courtesy to [13].

As for the foundation, also maintenance cost increases offshore [10]. And with the harsher offshore climate (including large waves and strong winds), one needs a weather window to be able to maintain the wind turbine, which could cause a significant down-time cost associated with component failure [14] [15]. The need of corrosion protection further increases the component costs.

With the above weighting of the pros and cons, it may be questioned if the traditional up-scaling of the three bladed upwind rotor on a monopile tower is the best design from a COE point of view. Looking into other concepts may be beneficial.

2.2 Concepts

In this thesis, *concepts* are restricted to rotor configuration, rotor blades and tower geometries in horizontal axis wind turbines (HAWT). In the following a brief history of HAWT concepts is given, and a discussion in light of comparison with vertical axis wind turbines (VAWT) is omitted.

2.2.1 Rotor configuration

Upwind and downwind rotor configurations

The upwind mounted rotor on a monopile tower is the most commonly used configuration today, with the advantage that the tower shadow effect is much less for the same blade-tower spacing, reducing both dynamic loads on the blade and the audible 'thumping' noise (latter originating as the blade passes through the tower influenced flow region) [2]. The main drawback with the upwind configuration is the risk of a blade-tower strike, requiring accurate prediction of blade deflections under conditions such as wind gusts, fault conditions or emergency stops.

Clearance can be obtained through the use of a rotor overhang in combination with a coned or tilted rotor, or using out-of-plane pre-curved blades, Figure 2.4. Using a downwind mounted rotor would benefit from the tower clearance problem as the wind acts on the rotor in the direction away from the tower. If the blades are still coned away from the tower, the mean blade root bending moment will decrease (compared to the blades on the upwind mounted rotor) as the bending moments originating from the centrifugal loads will counteract parts of the thrust force from the incoming wind. Also the downwind rotor is referred as being more stable when it comes to aligning with the wind direction, hence a less powerful yaw system could be used, such as for the free yawing downwind wind turbine in the experiment by Verelst et al. [16], where the tower has a free yawing capability provided at the tower base. Such a configuration could also be interesting for a floating offshore wind turbine.

With the smaller likelihood of a blade-tower strike in a downwind configuration, this configuration also allows for more flexible blades. The more flexible and thereby lighter blades would further reduce the gravity loads transferred onto the remaining turbine, which could reduce the COE [17]. Such flexible blades also benefit by being less severely unloaded by the tower shadow, as the wind loads deflect them further away from the tower in the first place [2] [12].

The main challenge for the downwind mounted rotors is the tower shadow with its' mean velocity deficit and turbulent unsteady vortices, which give an impulsive loading on the blades (significantly contributing to the blade fatigue load) as they pass through the tower influenced region [18]. This is closer detailed is sections 2.5, 2.7 and 2.8.

Number of rotor blades

In the simple construction of the old wind mills used on, e.g., the Great Plains in the U.S. (for pumping water from the wells), a large number of short length blades were used to achieve torque and rotation also in low winds, while being self-regulated (stall controlled) in high winds. Today most modern wind turbines have either one, two or three long (and relatively thin) blades.

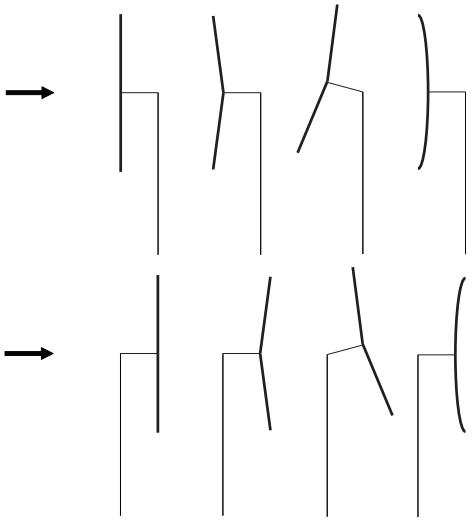

Figure 2.4: Rotor overhang, with cone and tilt angles and pre-curved blades (from left to right) for upwind (top) and downwind (bottom) rotor configurations.

The one and two bladed rotors need to rotate at a higher rotational speed to obtain the same 'solidity' and thereby power production as for the three bladed rotor. This will increase the acoustic noise emission, but for offshore application it may not be a problem. Still, the one bladed rotor will need a large counterweight (to balance the static rotor weight). From that point of view the two bladed rotor is a better option. For stability issues the two bladed rotor may be exposed to large cyclic loads originating from the fluctuating rotational inertia about the yaw axis. And with the higher rotational speed for both the one and two bladed rotors, blade edge erosion could occur, which would tremendously increase the offshore maintenance costs [12].

Based on these statements, the three bladed rotor is the preferred solution, both having the lowest rotational speed (benefiting the acoustic 'noise' emission and blade edge erosion) and having a constant rotational inertia about the yaw axis. Also from an aesthetic point of view (not as important offshore) and without any significant increase in rotor weight (compared to the two bladed rotor) [12], the three bladed rotor is preferred. But with the three bladed rotor occupying a larger three dimensional space compared to the two bladed rotor, the latter may be favourable from a transportation, erection and maintenance point of view.

2.2.2 Tower geometry

The tower needs to be designed to withstand the primary design loads, i.e., those transmitted from the rotor and nacelle, and those imposed directly on the tower. For a cost efficient tower, the fabrication, erection and maintenance costs should be minimized. The highly dynamic structure must also be designed to avoid resonance (i.e. tower excitation) with the blade passing frequencies of 1P and 3P (for a three bladed rotor), as well as the vortices shed from the tower [19].

The complex dynamic behaviour of a full wind turbine has not been possible to simulate with computational software until very recently. Back in the 1980's (after a lot of American wind turbines suffered catastrophic failures [20]) the land based Mod-1 wind turbine [21] was conservatively erected to avoid 1P and 3P resonance (frequency of one and three blades passing the tower at different rotational speeds), constructing a full height truss tower (all the way up to the nacelle) in the stiff-stiff region of the Campbell diagram (tower eigenfrequency higher than the 3P frequency at cut-out speed). Based on experience from the Smith-Putnam wind turbine [22], the truss tower was thought to be the most cost effective tower concept at that time. But experience with the fabrication and assembly of the Mod-1 wind turbine showed that the truss concept was a costly alternative for the megawatt size wind turbines. The preferred (onland) design in the U.S. changed from the rigidly stiff-stiff truss tower, to a more flexible monopile tower [19].

In Europe the trend was all along the monopile tower, which was more easily assembled [23], and as well the design was preferred from an aesthetic point of view. Today monopile towers are also used for offshore applications (monopile all the way down to the foundation at the sea bed), refer e.g. [3]. But as the offshore wind turbine technology is pushing for deeper waters, the eigenfrequencies of the taller monopile substructure (here referred as the section from approximately the sea level down to the foundation) will change and could be excited by the wave frequencies. Additionally mounting the foundation for a monopile substructure becomes more difficult as the monopile diameter gets larger in deeper waters. Using tripod and truss (jacket) substructures, e.g., Alpha Ventus [24] and Nordsee Ost [25], respectively, ease the mounting of the foundation (smaller diameter foundations, although more numerous with three and four legs for the tripod and truss, respectively) and the monitoring of the substructure eigenfrequencies, for the truss substructure through adjusting the leg spacing [26]. A downside of the truss substructure, is the large and heavy intersection piece (about 1.2 times the weight of the substructure itself) that is needed to connect the substructure with the monopile tower [23].

Another promising design for even deeper waters are floating wind turbines [23]. The worlds first floating wind turbine in the MW-size is the Statoils' test turbine *Hywind*, erected off the south-west coast of Norway in 2009. It has both shown promising stability behaviour in wind and waves, and a satisfying power production [27]. Still, for commercial use, it needs to be optimized to lower the overall costs

of the wind turbine construction. A summary of world wide offshore floating wind turbine foundations can be found in [28].

For downwind rotor configurations the idea of using a fairing tower, i.e., an airfoil shaped tower (to allow for a more narrow tower shadow profile) has been found promising in the perspective of decreasing the tower shadow effect on the rotor blades [29] [30]. But the increased rotor overhang, to obtain a satisfying blade-tower clearance, could outplay the benefit of the fairing [31].

2.2.3 Future offshore concepts

For offshore application, the heavy (and expensive) intersection piece between the truss substructure and the monopile tower (refer section 2.2.2) will be eliminated if using a full height truss tower (from nacelle down to the sea bed) [32]. Such a tower will also benefit from a significant reduction in weight and material cost, and produced in a cost effective way it will additionally be competitive with respect to erection and installation cost with other tower geometries. This indicates the need to, once again, look at which types of towers and substructures are the most cost efficient as wind turbines are moved offshore.

With the audible 'noise' and visual impact being of less concern offshore, the downwind rotor configuration, e.g., using a coning rotor [33] or a variable rotor diameter [34] to alleviate blade root loads in high wind speeds, could be interesting to pursue in light of cost and reliability for offshore applications. Also the number of rotor blades or even multi-rotor concepts would be interesting in this aspect (as discussed by Jamieson [12]).

2.3 Design criteria

For reliable wind turbine design, load simulations are carried out according different standards and guidelines. These all have the same general design criteria; in brief they can be summarized as a set of design load cases (DLC) including environmental conditions (e.g. wind, wave, current and ice) and fault conditions (e.g. electrical network loss, control system fault and yaw error) in combination with different simulation categories (power production, start up, normal and emergency shut down, parked and transport conditions). The different DLC are calculated in one or more of the following limit states; fatigue (FLS), ultimate (ULS), accidental (ALS) and serviceability (SLS), and given certain specific safety factors. For more details, the reader is referred to the specific standard or guideline, e.g., 'Guideline for the certification of offshore wind turbines' (GL Wind 2004) from Germanischer Lloyd [35], 'Design of offshore wind turbine structures' (DNV-OS-J101) from Det Norske Veritas [36] or 'Wind turbines - Part 3: Design requirements for offshore wind turbines' (IEC:2009 61400-3) from International Electrotechnical Commission [37]. Which standard or guideline to follow is often project specific.

It should be mentioned that for complex dynamic structures, such as wind turbines, FLS (not ULS) is often the governing design load case.

2.4 Fatigue assessment

Fatigue assessment is carried out based on the structural response from full wind turbine simulations. There are two ways to carry out full wind turbine simulations, in the frequency domain and in the time domain, with the former being the faster simulation tool. Although in the last design phase of a wind turbine, time domain simulations are required as the wind turbine is a highly complex system and the frequency domain simulations lack the possibility to take into account all non-linear effects of the wind turbine operation.

The time domain fatigue assessment is sketched in Figure 2.5. In short, the load time history (Figure 2.5b) is used for the rainflow count (Figure 2.5c) to obtain a stress range histogram (Figure 2.5d), which thereafter is compared to the Palmgren Miners' SN-curve to obtain the fatigue life of the structure (Figure 2.5e).

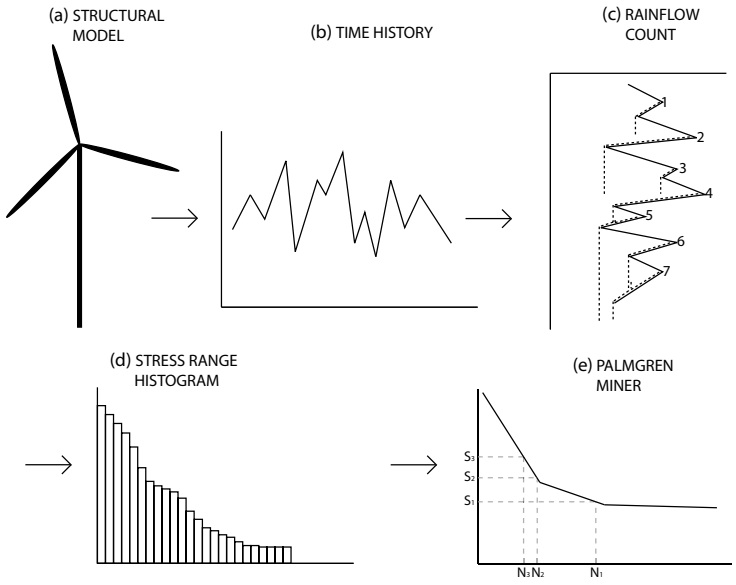

Figure 2.5: Schematic flow of fatigue assessment.

2.4.1 Rainflow count

The starting point of a rainflow count is the time series of the load that is to be investigated. The time series is rotated so that the time axis is pointing vertically downwards, Figure 2.5c. Peaks and valleys refer to the peaks and valleys of the horizontally rotated time series.

With the time axis pointing vertically downwards, the peaks can be taken as rooftops with water falling down from them (Figure 2.5c). A rain drop starts falling from a peak and continues down the next roof as long as the next peak is lower than where the raindrop originated from (e.g. starting from position 4, Figure 2.5c). If the next peak is higher the raindrop stops (position 1). The raindrop also stops if the drop merges with an already passing raindrop (position 5). One carries out this procedure until all peaks are looked at. Thereafter the same procedure is used for the valleys.

The amplitude of each load starts at the respective peak or valley and follows the raindrop until it stops. The amplitudes from each of the peaks and valleys make up half cycles in their respective cycle range (with a sufficiently long time series, the half cycles from the peaks and valleys make up full load cycles). The number of half load cycles are counted into a number of n bins (each bin covering a range of amplitudes). These n bins make up a histogram of amplitudes (Figure 2.5d) which is used in the fatigue assessment.

2.4.2 Damage equivalent load, DEL

Fatigue assessment using damage equivalent load (DEL) is a convenient way to compare fatigue loading from different simulations when the detailed geometry or material properties are unknown. It uses the S-N (stress versus number of cycles) curve (Figure 2.5e) and for each stress range, i, it calculates the damage from that range, that say number of cycles for the particular range, n_i, divided by the total number of cycles to failure at that range, N_i. The sum of each individual damage makes up the DEL (Equation 2.1). Total material failure occurs as DEL = 1.

$$DEL = \sum \frac{n_i}{N_i} \leq 1, \tag{2.1}$$

2.5 Turbulence and energy spectra

Turbulence contributes highly to the fatigue loading of wind turbines [38], and in real life it is present nearly everywhere. Turbulence is hard to predict with its' random, irregular and chaotic rotations originating from surface friction, temperature differences and mixing of fluid flows to mention some. In a lot of experiments

the flow is kept laminar to isolate the phenomena of interest. For the purity of the experiment this is ok, but the behaviour of the flow will often differ when it is changed into a turbulent flow. In the following, turbulence will be discussed in the context of flow around a circular cylinder (wind turbine tower). For cylinders placed in a fluid flow, the separation point will shift downstream the cylinder wall giving a different wake behaviour as the flow changes from laminar to turbulent (Figure 2.6c and d).

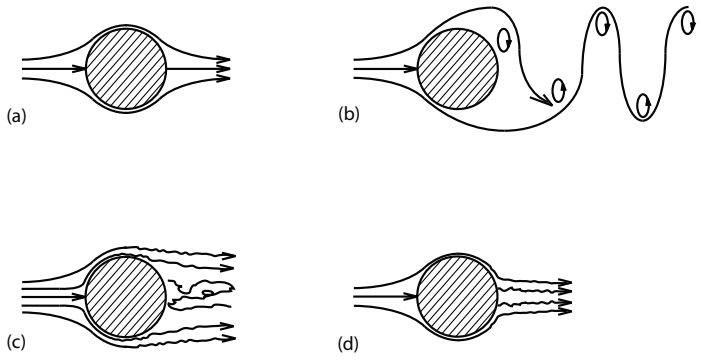

Figure 2.6: Flow around a cylinder at increasing Reynolds number; (a) attached laminar flow, (b) laminar vortex street, (c) turbulent boundary layer, and (d) turbulent boundary layer with late separation.

The transition between laminar and turbulent flow is dependent on the Reynolds number, *Re*, a non-dimensional number defined as the ratio of inertial forces to viscous forces [39]:

$$Re = \frac{inertial forces}{viscous forces} = \frac{VD}{\nu}, \tag{2.2}$$

where V is the mean velocity (m/s), D is the objects characteristic length (m) and ν is the kinematic viscosity given as μ/ρ (dynamic viscosity over density of the fluid), which for air is $1.46{\cdot}10^{-5}$.

Zdravkovich [40] categorized different flow regimes around circular cylinders depending on the Reynolds number. Above Re $\approx$ 5 (based on several earlier experiments) the flow start to separate and develop von Karman vortex streets (Figure 2.6b). These vortices are shed at a certain frequency f (Hz), described by the non-dimensional Strouhal number, *St* (Equation 2.3). For a vast region (10^2<Re<10^5) the Strouhal number is approximately constant (for a cylinder, 0.2, Figure 2.7b) and the vortex shedding frequency can be easily calculated (having one unknown) as long as the structure and flow are not in the lock-in regime [39]. But as the

Reynolds number goes into the super critical Reynolds number regions (corresponding to a sudden drop in drag coefficient, Figure 2.7a), the Strouhal number also changes and becomes dependent of the surface roughness. This is the region in where the laminar to turbulent transition in the boundary layer occurs, and is also the region in where the vortex shedding frequencies can be defined as the dominant frequency in a spectrum [41].

$$St = \frac{fD}{V}, \tag{2.3}$$

where D is the objects characteristic length (m) and V the free stream velocity (m/s).

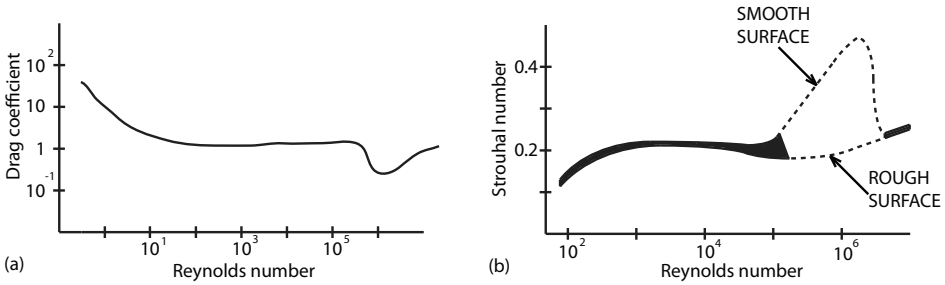

Figure 2.7: Drag coefficient and Strouhal number versus Reynolds number, (a) and (b), respectively.

For closely spaced cylinders (i.e. <3D), the vortex shedding frequency differs from that of a single cylinder. This phenomena has been extensively reported, refer e.g. Ishigai et al. [42], Zdravkovich [43], Meneghini et al. [44], Gao et al. [45] and Blevins [39].

2.5.1 Turbulence intensity and vorticity

Turbulence intensity, TI, is a measure of how much the flow changes from the mean at one point in space as a function of time, mathematically:

$$TI = \frac{\sigma}{V}, \tag{2.4}$$

where σ is the standard deviation of the wind speed and V is the mean wind speed.

2.5.2 Kolmogorovs' energy spectra

Energy spectra describe the distribution of energy, here discussed in the context of a turbulent flow, at different frequencies.

Turbulent motion (or flow) can be thought of as eddies of different size, each with a characteristic length-, velocity- and time scale. These large eddies are unstable and will break into smaller eddies, which further will break into yet smaller eddies. The kinetic energy, k, of the small eddies are eventually dissipated (ϵ) into heat due to the viscous shear stresses. This can be visualized through the Kolmogorovs' energy spectrum, which describes how energy is transferred from larger to smaller eddies. The Kolmogorovs' energy spectra clearly shows three regions (Figure 2.8); the integral length scale (left), the Taylor micro scale (middle) and the Kolmogorovs' dissipation scale (right).

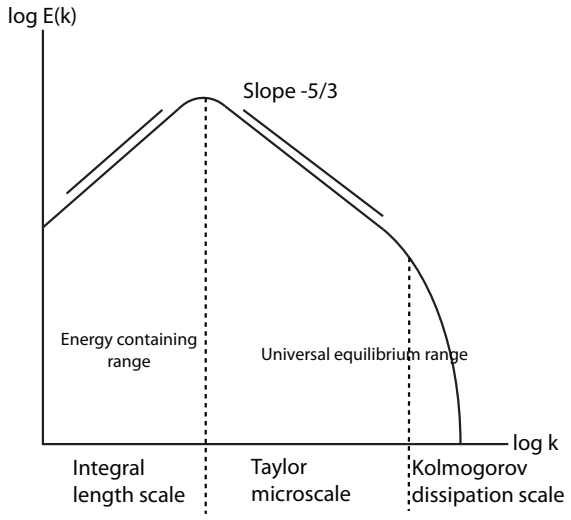

Figure 2.8: Kolmogorov's energy spectrum.

The largest eddies are found in the (case specific) energy containing range and the vortex shedding frequency of, e.g., a cylinder will show as a peak in this region. The Taylor micro scale region is dominated by isotropy, i.e., the turbulence is independent of orientation in space, and the turbulence in this region is applicable to all problems, independent of case specific interference. Independency and universal equilibrium also applies to the Kolmogorovs' dissipation scale (where in the end only 'noise' is left).

2.6 Physical tower shadow

The physical tower shadow gives the full and real tower shadow, including velocity deficit and turbulence. Such physical representations (of, e.g., the tower shadow) are often used in research through model scale experiments. These model scale experiments can not be used directly to 'explain' the behaviour in full scale models, but they are much cheaper to carry out and the information can be used to enlight trends on a comparative basis.

For information on the flow field in a tower shadow wake, a constant temperature hot-wire anemometry with a high frequency response will capture the fluctuating and complex flow behind the tower. The result is detailed information about the turbulent statistics in and the shape of the wake, which can be used for validation of parameters in steady tower shadow models.

The reliability of an experiment can further be evaluated comparing the results with the -5/3 slope in the universal equilibrium range of the Kolmogorovs' energy spectrum (Figure 2.8).

2.7 Empirical tower shadow

2.7.1 Steady wake models

Steady wake models are used to describe the mean velocity deficit behind structures. For wind turbines such models can be used both to describe the rotor wake and the tower shadow wake. These wake models have in common that they describe the velocity deficit behind the structure as a decaying Gaussian or cosine square shaped profile. Different rotor wake models can be found in, e.g., Sørensen et al. [46] (including amongst others the commercially applied Ainslie model [47]) and Krogstad and Eriksen [48].

In the following, steady wake models will be discussed in the context of wind turbine tower shadow and tower dam effects (latter for upwind rotors). These simple algebraic equations often include some flow dependent parameters for the downwind tower shadow, i.e., wake width, velocity deficit, drag coefficient or less physical factors to complete the equations.

Compared to CFD simulations (refer section 2.8) these wake models are simpler and less computational demanding. They are able to describe the averaged mean velocity field, but are not able to include the turbulent motion and vortices originating from the tower geometry. For full wind turbine simulations, these wake models are combined with an unsteady turbulent inflow, to account for the turbulent behaviour of the wind (refer 2.7.2).

For upwind mounted rotors the potential flow field is used to describe the velocity field upfront a tower of diameter D through x- and y-velocities (Equation 2.5 and

2.6, for x- and y-directions, refer Figure 2.9), with the velocity magnitude reading $V{=}\sqrt{V_x^2 + V_y^2}$. V_0 is the free stream wind velocity.

$$V_x = V_0 \left(1 - \frac{x^2 - y^2}{(x^2 + y^2)^2} \left(\frac{D}{2}\right)^2\right) \tag{2.5}$$

$$V_y = \frac{-2xy}{(x^2 + y^2)^2} \left(\frac{D}{2}\right)^2 V_0 \tag{2.6}$$

For downwind mounted rotors, Powles', Blevins', Schlichtings' and the JET wake models can be used, further outlined in the following.

Powles' model

In 1983 Powles [49] suggested a tower shadow model for downwind mounted rotors. From experiments he found that a cosine squared model predicted the tower shadow fairly accurately in the region 3-6 tower diameters downstream the tower centre (Figure 2.9).

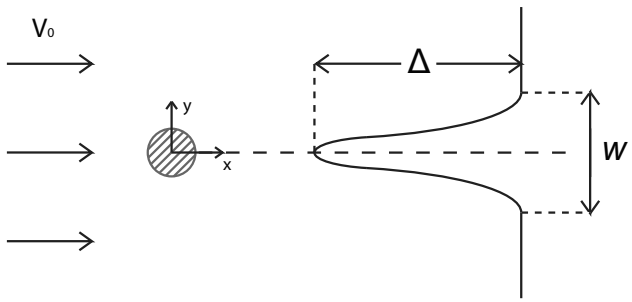

Figure 2.9: Tower top view with incoming wind velocity, V_0 (left). Cosine shaped velocity deficit using Powles model and its wake width (w) and velocity deficit (Δ) parameters (right), x- and y-directions originating in the tower centre.

Powles' model, is among others, implemented in the commercial software Bladed (from GL Garrad Hassan; Bristol, UK), where Powles' model is used in the vicinity of the tower (cosine term within ± 60 degrees) with potential flow for the remaining transversal domain [50]:

$$V = V_0 \left(1 - \Delta cos^2 \left(\frac{y}{wD}\pi\right)\right), \tag{2.7}$$

where V is the velocity at transversal position y, V_0 the free stream velocity, Δ the velocity deficit at the wake centre and w the wake width parameter (w=$2\,W/D$).

Also AeroDyn from the National Renewable Energy Laboratory (NREL) [51] is based on the Powles' model (Equation 2.8) in combination with the potential flow model (Equation 2.9 and 2.10). The difference is that this approach accounts for the presence of the tower with a speed-up on the sides of the tower through the tower's drag coefficient, C_d [52]. The drag coefficient is also present for the tower shadow downstream the tower, where it together with $\sqrt{d}$ is used to describe the velocity deficit. $\sqrt{d}$ is also taken to be the wake width, with d ($d = \sqrt{x^2 + y^2}$, for x- and y-directions, refer Figure 2.9) being the dimensionless radial distance from the tower centre to the point of interest.

$$V_x = \left(1 - \frac{C_d}{\sqrt{d}} cos^2\left(\frac{\pi}{2}\frac{y}{\sqrt{d}}\right)\right) V_0 \tag{2.8}$$

$$V_x = \left(1 - \frac{x_c^2 - y^2}{\left(x_c^2 + y^2\right)^2}\left(\frac{D}{2}\right)^2 + \frac{C_d}{2\pi}\frac{x_c}{x_c^2 + y^2}\left(\frac{D}{2}\right)\right) V_0 \tag{2.9}$$

Equation 2.8 is used instead of Equation 2.9 whenever $|y| \leq \sqrt{d}$.

$$V_y = \left(\frac{-2x_c y}{\left(x_c^2 + y^2\right)^2}\left(\frac{D}{2}\right)^2 + \frac{C_d}{2\pi}\frac{y}{x_c^2 + y^2}\left(\frac{D}{2}\right)\right) V_0, \tag{2.10}$$

with x_c=x+$0.1D/2$. The velocity magnitude is calculated as V=$\sqrt{V_x^2 + V_y^2}$.

Blevins' model

Blevins' model [39] has some similar features to the Powles' model, but originated in fluid dynamics to describe the wake behind a cylinder. The major difference between Powles' model and Blevins' model is the way Blevins' model describes a virtual origin of the wake, x_0. In addition both the wake width and velocity deficit depends on the drag coefficient, C_d, which makes the mean velocity deficit look like:

$$b = 0.23\left[C_d D(x + x_0)\right]^{1/2}, c = 1.02 V_0 \left(\frac{C_d D}{(x + x_0)}\right)^{1/2}, \tag{2.11}$$

$$V(x,y) = V_0 \left(1 - ce^{-0.69y^2/b^2}\right), \tag{2.12}$$

where D is the member diameter and b is the length from the centreline to the position where 50 percent of the centreline velocity deficit (c) is reached (refer Figure 2.9 for x-direction).

Schlichtings' model

Schlichting and Gerstens' [53] wake model originates from boundary layer theory with the idea of a frictional surface in the interior of the flow. The model is Reynolds number dependent and makes use of three variables to describe the flow; the objects drag coefficient (C_d), the objects' length (D, originally a flat plate) and the fluid viscosity (ν):

$$V(x,y) = V_0 \frac{C_d}{4\sqrt{\pi}} \sqrt{\frac{V_0 D}{\nu}} \left(\frac{x}{D}\right)^{-1/2} exp\left(-\frac{y^2 V_0}{4x\nu}\right), \tag{2.13}$$

where x and y are the longitudinal and transversal positions (Figure 2.9) at where the velocity (V) is calculated. It should be noted that Equation 2.13 is restricted to x $> 3D$.

JET wake model

The intention of the JET wake model was to represent a quasi steady reference for the time varying CFD simulated wake. The model is based on the boundary layer solution for a jet flowing into a fluid at rest [54], with the axial (V_x) and lateral (V_y) velocity components (refer Figure 2.9) being:

$$V_x(x,\eta) = \frac{\sqrt{3}}{2} \sqrt{\frac{K\sigma}{x}} \left(1 - tanh^2(\eta)\right), \tag{2.14}$$

$$V_y(x,\eta) = \frac{\sqrt{3}}{4} \sqrt{\frac{K}{x\sigma}} \left(2\eta\left(1 - tanh^2(\eta)\right) - tanh(\eta)\right), \tag{2.15}$$

where $\eta{=}\sigma y/x$, $\sigma{=}7.67$ and x and y are normalized with respect to the tower radius (Cartesian coordinates, with origin at tower cross section). K is the kinematic momentum; $K{=}J_m/\rho$, where ρ is the mass density and J_m is the momentum deficit behind the tower, defined as:

$$J_m = \frac{U_0^2 D}{2} \frac{\rho}{\pi} \left[\frac{1}{8} + \frac{16}{3\pi} \right] C_d^2 \tag{2.16}$$

All these mean velocity deficit models (wake models) are applicable for single cylindrical structures, e.g., a monopile tower for a wind turbine. For more complex tower geometries, e.g., truss towers, these models are not able to include the interacting flow behaviour from the closely spaced cylinders, which has been shown to play a significant role in the overall flow picture (refer section 2.5).

Still, a method for representing the mean velocity deficit behind the truss tower has been suggested used in Bladed, which currently is the only commercial software that has an available wake model for a truss tower. This method uses Powles' model (with potential flow in the outer velocity field) for each single cylinder (with diameter d) and adjusts the model for each cylinder with respect to the longitudinal distance x (refer Figure 2.9) from a reference plane, x_r. Hence the Δ and w are scaled for each single cylinder through the square-root-law [50]:

$$\Delta(x) = \frac{\Delta_r}{\sqrt{x/(x_r d)}}, \tag{2.17}$$

$$w(x) = w_r \cdot \sqrt{x/(x_r d)}, \tag{2.18}$$

and further superposed linearly, giving the total velocity field:

$$V = \Sigma_{i=1}^{n} V_i + (1-n)V_0, \tag{2.19}$$

where V_i (i=1,2,...,n) is the velocity field induced by the i-th member of the truss tower. In the PhD work, this method was also implemented for Blevins' and Schlichtings' models.

2.7.2 Turbulence models

As discussed in section 2.5, turbulence is hard to predict with its' random, irregular and chaotic motions. Still, models exist, that try to simplify these very irregular motions of flow. These models are important when evaluating fatigue loads on wind turbines. Here the focus is on a few models that represent the turbulent nature of the incoming wind (and which are implemented in commercial software) for full wind turbine simulations.

A grid is chosen across the wind turbine domain, and a separate wind speed time history is generated for each of these grid cells in such a way that each cell has the correct turbulence spectrum, and each pair of grid cells has the correct cross-spectral or coherence characteristics.

The most used and referred turbulence models for wind turbines are the von Karman (Equation 2.20) [55] and the Kaimal (Equation 2.21) [56] models:

$$\frac{fS_k(f)}{\sigma_k^2} = \frac{4fL_{1k}/\overline{v}}{\left((1+70.8fL_{1k}/\overline{v})^2\right)^{5/6}}, \tag{2.20}$$

$$\frac{fS_k(f)}{\sigma_k^2} = \frac{4fL_{2k}/\overline{v}}{(1+6fL_{2k}/\overline{v})^{5/3}}, \tag{2.21}$$

where f is the frequency, σ_k is the standard deviation, $S_k(f)$ the frequency spectrum, L_{1k} and L_{2k} the two length scales, respectively and $\overline{v}$ the mean velocity. Both models are funded on atmospheric turbulence, largely based on flat land sites and both tend to the asymptotic Kolmogorov dissipation limit of $f^{-5/3}$ at high frequencies (refer section 2.5.2). From the latter follows that the length scales are related by the ratio L_{2k}=2.329L_{1k} [57].

Petersen et al. [58] report that the Kaimal model provides a better empirical description of the observed spectra in the atmosphere than the von Karman model. But that above 150m altitude the von Karman spectra also gives a good representation of the atmospheric turbulence. Below 150m the von Karman spectra has some deficiencies, which have been sought improved through modifications of the von Karman spectra in works by, e.g., Harris [59], ESDU [60] and Thresher et al. [61].

The Mann uniform shear turbulence model [62] has become widely used in recent years. Similar to the above mentioned models, it is based on the von Karman spectra, which is further rapidly distorted by a uniform, mean velocity shear, and accounts for non-linear effects through a spectral tensor based on the three parameters; length scale (L), eddy lifetime constant (Γ) and a spectral multiplier in the inertial sub range ($\alpha\epsilon^{2/3}$). The model has been found to predict the coherence spectra better than the isotropic von Karman [63].

Also the Kaimal spectrum has been used as basis for other turbulence models, e.g., the spectra by Simiu and Scanlan [64] which takes other numerical constants than the Kaimal model, or the spectra proposed by Høystrup [65] which uses a different approach for the high frequency part (for better agreement closer to the ground).

For the different wind turbine standards, the present onshore IEC:2005 61400-1 standard [66] and offshore IEC:2009 61400-3 standard [37] recommend the Mann

uniform shear turbulence model or the Kaimal turbulence model (the former version of the IEC:1998 61400-1 standard [67] was based on Thresher et al.'s [61] exponential coherence model). The DNV's (Det Norske Veritas) offshore standard DNV-OS-J101 [36] also suggests the use of the Kaimal spectrum, while the turbulence model recommended in GL Wind 2004 from GL (Germanischer Lloyd) [35] is similar to the von Karman model, but includes shear effects through a turbulent scale parameter.

For other (less used) turbulence model and their comparison and performance, the reader is referred to the literature, e.g., Mann [62], Saranyasoontorn et al. [63] and Olesen et al. [68].

2.8 CFD tower shadow

A more sophisticated tower shadow (than those from steady wake models) is based on simulations using computational fluid dynamic (CFD) software. These numerical models are applicable to a vast variety of problems through their description of the unsteady behaviour of the flow. And with the increasing computer capacities over the past few years, these models have become both realizable and popular. In this PhD work, CFD simulations were used to investigate the flow field behind structures intended as wind turbine towers for offshore downwind mounted rotors.

The fundamentals of CFD are conservation of mass, momentum and energy [69]. It describes the detailed fluid motion at a given point in time and space through the Navier-Stokes equation (here assuming incompressible fluid, $\nabla \bullet \mathbf{u} = 0$):

$$\rho \frac{\partial \mathbf{u}}{\partial t} + \rho(\mathbf{u} \bullet \nabla)\mathbf{u} = -\nabla p + \mu \nabla^2 \mathbf{u} + \rho \mathbf{f}, \tag{2.22}$$

where ρ is the fluid density, $\mathbf{u}$ the fluid velocity, p the pressure, μ the dynamic viscosity in the viscous stress term $\mu\nabla^2\mathbf{u}$ and $\mathbf{f}$ the volumetric forces acting on the fluid.

The body of interest needs to be described with material properties (solid, fluid, both), flow regime (laminar or turbulent), boundary and convergence conditions, initial solution and solver monitors. The domain is discretized into many small cells (called the grid), where the applied mathematical conservation equations (mass, momentum and energy) are solved separately. A certain number of iterations is needed to make the solution converge (i.e. changes between cells are negligible according to the preset boundary and convergence condition). Thereafter quantities of interest can be extracted, such as lift, drag, flow separation and flow patterns.

The non-linearities of Equation 2.22 are causing a turbulent behaviour acting as stresses throughout the flow. As these stresses are unknown, their equations can be derived, but only to reveal additional unknowns. This problem, solving one

unknown at the cost of introducing more unknowns, is referred to as the closure problem, and indicates (through the extensive amount of equations) why it is demanding to explicitly solve the Navier-Stokes equation.

2.8.1 Turbulence models

Turbulence models are computational procedures that closes the Navier-Stokes equations without necessarily resolving the detailed time-dependent turbulent fluctuations. Different categories of turbulence models exist, which to choose depends on the problem that is to be solved and the level of accuracy that is required for the results (normally it all comes at the cost of computational time). The most heavy method resolves all length scales through (explicit) direct numerical simulations (DNS) [70] [71] (Figure 2.10), while the large eddy simulations (LES) resolve the eddies down to the dissipation region and models the smaller eddies [72]. Reynolds-Averaged Navier-Stokes (RANS) resolves the large eddies (in the energy containing range) and models all smaller eddies. Solving the time-averaged model equations for the eddies is based on statistical measures of the mean flow and closure coefficients (which could be obtained through the fully resolved DNS).

The probability density function (PDF) should also be mentioned, although it has not, to the authors knowledge, yet been implemented in any commercial software codes. It is derived from the Navier-Stokes equations with a mix of closed and modelled forms. For more details the reader is referred to literature by Pope, e.g., [71] and [73].

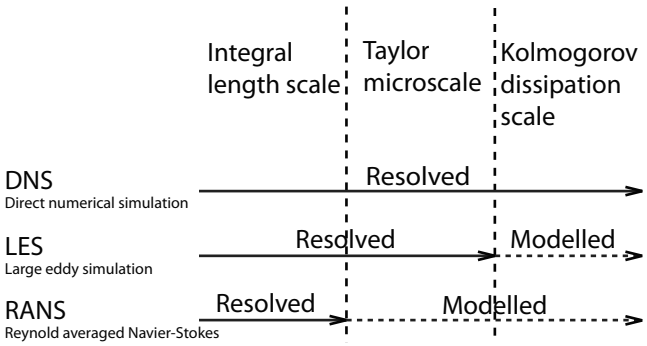

Figure 2.10: Resolved and modelled regions for different turbulence models.

Reynolds Averaged Navier-Stokes, RANS

The velocity **u** in the Navier-Stokes equation (Equation 2.22) can be decomposed into the mean velocity **U** and its fluctuations (**u'**):

$$\mathbf{u} \equiv \mathbf{U} + \mathbf{u'} \tag{2.23}$$

This decomposition is the idea behind the RANS model:

$$\rho\frac{\partial \mathbf{U}}{\partial t} + \rho(\mathbf{U} \bullet \nabla)\mathbf{U} + \rho\nabla\left(\mathbf{u}^{'} \bullet \mathbf{u}^{'}\right) = -\nabla p + \mu\nabla^2\mathbf{U} + \rho\mathbf{f}, \tag{2.24}$$

where ρ is the fluid density, p the pressure and $\mathbf{f}$ the body forces.

$\mathbf{u}^{'}\bullet\mathbf{u}^{'}$ (or more often written as $\langle u_i u_j \rangle$) is known as the Reynolds stresses. These are the unknown quantities in the RANS equation and are obtained through turbulent-viscosity models (Equation 2.26), either solved as an algebraic relation or as modelled transport equations. The Reynolds stresses may also be solved explicitly as in the *Reynolds-stress model*.

The RANS models (except the *Reynolds-stress model*) are based on the Boussinesq assumption (also known as the eddy-viscosity or turbulent-viscosity assumption) which assumes that the Reynolds stress tensor (τ_{ij}) can be given as the product of the mean strain-rate tensor (S_{ij}) and the eddy viscosity (μ_T) (Equation 2.25), where the latter is assumed to be a scalar isotropic quantity. This further implies that the Reynolds stress tensor coincide with the mean strain-rate tensor.

$$\tau_{ij} = \mu_T S_{ij}, \tag{2.25}$$

According to the Boussinesq assumption the Reynolds stresses are given as:

$$\langle u_i u_j \rangle = \frac{2}{3}k\delta_{ij} - \nu_T\left(\frac{\partial \langle U_i \rangle}{\partial x_j} + \frac{\partial \langle U_j \rangle}{\partial x_i}\right), \tag{2.26}$$

where k is the turbulent kinetic energy, δ_{ij} is the Kronecker delta, ν_T the turbulent viscosity and $\partial \langle U_i \rangle / \partial x_j + \partial \langle U_j \rangle / \partial x_i$ is the mean strain-rate tensor (also known as S_{ij}).

The Reynolds stress equation is complete and can be solved when the turbulent viscosity field $\nu_T(\mathbf{x},\mathrm{t})$ is known [74]:

$$\nu_T = u^* \ell^*, \tag{2.27}$$

where u^* and ℓ^* are the velocity and length of the eddies respectively. u^* and ℓ^* are solved in different ways, depending on the type of RANS model used.

The different RANS categories are the zero-, one-, two- and six equation models as well as the non-linear equation model. The number of equations denotes the number of additional partial differential equations that are to be solved.

The *zero-equation model* only calculates the mean flow properties and turbulent shear stress, and is thereby not applicable to cases where the turbulent length scales varies (e.g. separation or circulation) [75] [76]. Due to the models restrictions and today's computer capacities, algebraic models are not widely used in commercial software today.

All *one equation models* have in common that the turbulent viscosity model (Equation 2.27) is solved using one equation and the remaining unknowns are specified with closure coefficients. This model works for attached wall-bounded flows and flows with mild separation and recirculation, but not for massively separated flows, free shear flows or decaying turbulence [71] [77] [78] [79].

Compared to the zero- and one equation models, the *two equation model* is complete as no flow-dependent specifications are needed. The two transport equations represent the turbulent properties of the flow and has the benefit of including history effects through the convection and diffusion of turbulent energy.

Most *two equation models* use the same way of deriving the turbulent kinetic energy, k (Equation 2.28), and the turbulent viscosity field, ν_T (Equation 2.29), while the second transport equation varies.

$$\frac{\partial k}{\partial t} = \nabla \bullet \left(\frac{\nu_T}{\sigma_k} \nabla k \right) + P - \epsilon, \tag{2.28}$$

with ν_T as in Equation 2.29, ϵ=$\mathrm{C}_D k^{3/2}/\ell_m$, P is the production rate of turbulent kinetic energy, the Boussinesq assumption still apply and the specifications of ℓ_m, the mixing length.

Two well known models are the k-ϵ and k-ω models (further looked into below), while the kL [80], ω [81], ω^2 [82] and τ [83] are less known and the reader will for these be referred to the cited literature.

k-ϵ model - This is the most widely used complete turbulence model, incorporated in most commercial CFD codes. It was first introduced in 1972 by Jones and Launder [84]. The simplicity of the model makes it applicable to a lot of problems (e.g. heat transfer, combustion and multi phase flows) and leads to stable calculations that converge relatively easily. But the model is not well reproducing swirling and rotating flows, strong separation, axi-symmetric jets, certain unconfined flows and

fully developed flows in non-circular ducts. Turbulent kinetic energy, k, is solved in the same way as for the one equation model (Equation 2.28), and the rate of dissipation of turbulent kinetic energy, ϵ, as in Equation 2.30, with ν_T:

$$\nu_T = C_\mu k^2/\epsilon, \tag{2.29}$$

$$\frac{\partial \epsilon}{\partial t} = \nabla \bullet \left(\frac{\nu_T}{\sigma_\epsilon} \nabla \epsilon \right) + C_{\epsilon 1} \frac{P\epsilon}{k} - C_{\epsilon 2} \frac{\epsilon^2}{k}, \tag{2.30}$$

and constants C_μ=0.09, $C_{\epsilon 1}$=1.44, $C_{\epsilon 2}$=1.92, σ_k=1.0 and σ_ϵ=1.3. These constants have become standard in CFD simulations and were first derived in Launder and Sharma [85].

<u>k-ω model</u> - The k-ω model is made to simulate the near-wall boundary conditions in a better way (than the k-ϵ model), where the ω term is an inverse time scale associated with the turbulence. The numerical behaviour is similar to that of the k-ϵ models, and in Equation 2.31, the k-ω model is written based on the ϵ model, taking σ_k=σ_ϵ=σ_ω [71]. The original ω equation was provided by Wilcox [70] in 1993.

$$\frac{\partial \omega}{\partial t} = \nabla \bullet \left(\frac{\nu}{\sigma_\omega} \nabla \omega \right) + (C_{\epsilon 1} - 1) \frac{P\omega}{k} - (C_{\epsilon 2} - 1)\, \omega^2 + \frac{2\nu_T}{\sigma_\omega k} \nabla \omega \bullet \nabla k, \tag{2.31}$$

Written in this way, it is easy to see the difference between the ω and ϵ models, which arise from the additional last term in the equation. A disadvantage of the Wilcox model, is that it does not simulate the non-turbulent free-stream boundaries well.

With both the k-ϵ and k-ω models showing strengths and weaknesses with regards to each other, Menter [86] proposed a blending function where the Wilcox's [70] k-ω model is applied in the near-wall boundary, while the Launder and Sharma's [85] k-ϵ model is applied in the remaining domain. The model of Menter is also known as the k-ω SST (shear-stress transport) turbulence model.

The *Reynolds-stress model*, RSM (or six equation model) put forward by Lauder [87] closes the RANS equations solving additional transport equations for the six independent Reynolds stresses, $\langle u_i u_j \rangle$ (instead of one k equation), together with the ϵ equation. RSM excludes the need for the isotropic eddy viscosity assumption, which is one of the main limitations of the RANS models. RSM therefore gives good results also for largely separated flows (e.g. cyclones). But as mentioned earlier, the more detailed RSM model comes with the requisite of more cpu.

Non-linear models, e.g., by Speziale [88] and Yoshizawa [89] perform better for cases where the normal Reynolds stresses play an important role (in traditional RANS models all normal stresses are assumed to be equal).

Turbulence intensity output from RANS

I want to emphasize that the total turbulence intensity from RANS simulations originates from two parts; one part from the unsteady motions (including the mean velocity deficit and vortex shedding) and one part from the high frequency turbulent kinetic energy fluctuations within each element cell, the so called sub-grid parametrization. This feature of the RANS simulated turbulence intensity is actively used in my PhD work. The total turbulence intensity in the grid cell is found combining these two parts. A thorough derivation of the turbulence intensity from the RANS simulations is given in appendix B.

2.8.2 Challenges using CFD

The accuracy of the CFD solution is dependent on the provided initial and boundary conditions, as well as the mesh across the domain. Special care should be taken at the walls, where viscous stresses dominate the flow picture (in contrast to free shear flows). Coarse grids may lack to converge and could affect the solution accuracy, while a very fine grid (very many and small cells) comes at the cost of increased computational time. A large domain also increases the computational time, but the domain must be large enough to avoid boundary interference with the model that is to be investigated. A quality measure of the mesh is often given by y^+, the non-dimensional distance describing the ratio between the turbulent and laminar influences in a cell, and is part of the important validation of the model. In the viscous sub layer the distance should be $y^+ < 5$ for engineering applications [90].

The LES and RANS models need closure coefficients to solve the Navier-Stokes equations. These are often build into the CFD software, but could still be optimized for a more accurate end result (compared to physical experiments) [91]. Although, due to the stochastic nature of CFD, replicates of an experimental set-up would reveal slightly different results.

2.9 Software implementation

Software for modelling the dynamic response of offshore wind turbines (referred throughout the text as *full wind turbine simulations*) are FAST [92], Hawc2 [93], 3Dfloat [94], FEDEM WindPower [95], Bladed [50], WindSim [96] and ASHES [97] to mention a few.

These dynamic response software are based on time-domain simulations using aero-hydro-servo-elastic codes. The aerodynamics are mostly solved through the blade element momentum (BEM) method [57]. The hydrodynamics through Airy theory and the Morison's equation [98], and the control system called from external dynamic link libraries. The structural dynamics are modelled with the finite-element method (FEM) or its multibody generalization, latter often under further reduction of the dynamical degrees-of-freedom (e.g. modal analysis). For an overview of software implementations, refer e.g. Jonkman and Musial [99] and Popko et al. [100].

Software such as MSC ADAMS, MBS SIMPACK and FOCUS6 can also incorporate more advanced aerodynamic formulations (e.g. CFD and free vortex wake models) and structural FEM models.

2.9.1 Tower shadow model implementation

The tower shadow model in aero-hydro-servo-elastic software are mostly steady tower shadow models based on a cosine shaped velocity deficit, with Powles' model and varieties thereof being the most popular (refer section 2.7.1).

Blind comparison studies, such as the NREL *Unsteady Aerodynamics Experiment, UAE* [101] are used to validate new and modified software. Coton et al. [102] and Munduate et al. [103] compared their software tool (HAWTDAWG) with results from *UAE*, and reported that the accuracy of their tower shadow model [104] was largely depending on the velocity deficit parameters. For a good fit with *UAE*, their velocity deficit parameter was found to be somewhat larger than suggested by Snyder and Wentz [105], emphasizing the sensitivity of the tower shadow profile to the flow environment (laminar or turbulent) [104] [106]. Also Thresher et al. [107] found discrepancies in the blade response from a physical experiment and a simplified tower shadow description.

CFD simulations benefit by a more accurate representation (provided a validated CFD model) of the tower shadow, than provided by the steady wake models. Additionally, it is cheaper, less time consuming and easier to implement in full scale, compared to full scale physical experiments. Still, CFD simulations are time consuming and more computational expensive than steady wake models.

For wind turbine engineering application, CFD simulations are currently not suited for the extensive load case simulations given in the standards (refer section 2.3), but can be used for improving and fitting models (same way as physical experiments). An extensive amount of work is done on wind turbine rotors and blades, e.g., Krogstad and Eriksen [48], Krogstad and Lund [108], Hansen et al. [109] and Vermeer et al. [110], where the latter three conclude that the most accurate CFD model is the k-ω SST turbulence model.

For wakes behind structures intended as wind turbine towers, few CFD studies are reported. CFD simulations of cylinders can be used to some extent, but the

Reynolds numbers of the simulations are often very low compared to what is found for wind turbine towers. If comparing the flow around an operating, pitched rotor blade with the flow around a wind turbine tower, the latter will experience larger degree of flow separation. This favours, e.g., the *six equation model* (which is able to account for largely separated flows). But as it is much more computational expensive and more demanding with respect to initialization, the two equation turbulence models are also used for flows around cylinders [30] [111].

With the accuracy of the steady tower shadow models being dependent on the models' parameters [102] [103], they need to be carefully chosen for reliable tower shadow profiles. Fitting the steady wake model parameters with mean velocity deficits of the CFD simulations is an option. E.g., for the JET wake model by Madsen et al. [54] (refer section 2.7.1), this would be achieved by obtaining the drag coefficient (C_d) from the CFD simulations, which is the only parameter needed to solve the JET wake model.

In the present PhD work a similar method is suggested, but with the benefit of being independent of tower geometry (monopile, truss, fairing, etc.). CFD simulations are here used to fit the parameters for the steady tower shadow models of Powles, Blevin and Schlichting (refer section 2.7.1). Further, the method incorporates the turbulent motions (originating from the vortices and the additional turbulence due to the tower structure) through calibrating the turbulence intensity of the inflow (used with the Powles model in the software Bladed, by GL Garrad Hassan; Bristol, UK). This method will also benefit by limiting the time consuming CFD simulations, to short case studies of the specific towers.

Chapter 3

Investigations

This chapter summarize the findings in the papers of the PhD work. The papers highlight different parts of the answers to the research question (put forward in chapter 1), reading:

How does the tower shadow, caused by different tower geometries, affect the fatigue loading and power production in a downwind mounted rotor?

The different papers have sought to find ways to decrease and accurately describe this tower shadow impact on the blade fatigue loading. This has been done using three different tower geometries; the conventional monopile tower, one full height truss tower (from sea bed to nacelle) and one monopile tower using a fairing around sections of the tower, Figure 3.1. And, by describing the tower shadow using steady wake models, CFD simulations and model scale experiments.

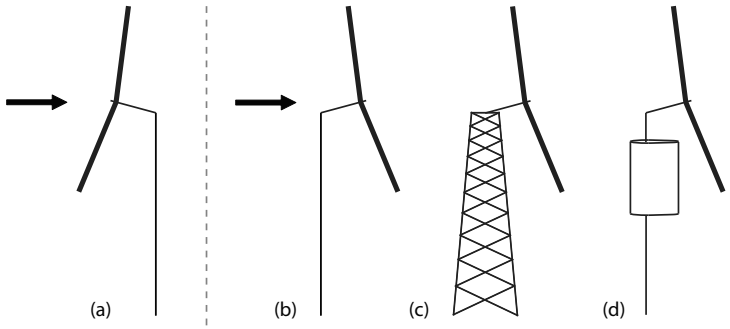

Figure 3.1: Tower and rotor configurations studied in the thesis; (a) upwind mounted rotor with monopile tower, (b) downwind mounted rotor with monopile tower, (c) downwind mounted rotor with truss tower, and (d) downwind mounted rotor with fairing tower.

All tower shadow simulations and full wind turbine simulations were run at 12 m/s wind speeds (close to rated wind speed for the investigated 5 MW wind turbine). Fatigue assessments were carried out for one design load case only; using a wind speed of 12 m/s, assuming 20 years operation and an uptime of 8760 hours per year (full year). This is a non-physical case set-up, but it works well for the purpose of comparison, and is thought to be the most critical fatigue load case under operational conditions for the blade root flapwise moment.

The full wind turbine simulations are based on the three bladed NREL 5-MW reference turbine [112], where some of the simulations are run with changes in shaft tilt and cone angles, Table 3.1. The rotor is also changed into a downwind position and the tower (in addition to the monopile geometry) also takes shape as a truss and fairing tower (refer Table 3.2 for tower properties).

Table 3.1: Applied wind turbine changes in the different papers compared to the NREL 5-MW reference turbine*.

	Rotor orientation	Shaft tilt [degrees]**	Cone angle [degrees]**	Tower geometry
Paper 1	up- and downwind	2.0	2.0	monopile and truss
Paper 2	downwind	-	-	monopile and truss
Paper 3	downwind	-	-	monopile and truss
Paper 4	downwind	-	-	monopile and truss
Paper 5	downwind	2.0	2.0	monopile and truss
Paper 6	up- and downwind	5.0	2.5	monopile and fairing
Paper 7	up- and downwind	2.0	2.0	monopile and truss

* The upwind NREL 5-MW reference has 5.0 and 2.5 degrees shaft tilt and cone, respectively and is mounted on a monopile tower.
** Changes only to the downwind rotor configurations.

The blade stiffness and weights were reduced in some of the downwind mounted rotor simulations. The aerodynamic blade shape was kept constant (same as NREL 5-MW reference blade), while the blade stiffness (edge, flap and torsional stiffness) and weight were reduced by 10, 15 and 20 percent, making up a total of 10 combinations of different blade stiffness and weights (including the NREL reference blade).

The steady wake (here tower shadow) models of Powles, Blevins and Schlichting were used in the pure tower shadow studies, together with CFD simulations and a model scale experiment (papers 2, 3 and 4). Fitting the parameters of the steady wake models (with data from CFD simulations and experiments) are crucial for a reliable tower shadow representation and accurate full wind turbine simulation results. A benefit of the steady wake models is that they are faster and less computational expensive than running experiments or CFD simulations.

The software used in the full wind turbine simulations was Bladed (Versions 3.82 and 4.2, GL Garrad Hassan; Bristol, UK). The software was used with its' original

Table 3.2: Physical 3D (three dimensional) and 2D CFD (two dimensional) properties for the monopile and the truss towers.

Parameter	Monopile tower	Truss tower (main leg/brace)
3D physical tower properties:*		
Diameter [m]	3.87-7.00	0.90/0.36
Number of sections	-	10
Tower height [m]	120	120
Top distance main legs [m]	-	4.00/-
Bottom distance main legs [m]	-	28.0/-
Angle against horizontal [^{0}]	-	84.3/50.0
2D CFD tower properties:		
Leg spacing [m]	-	10.80
Diameter [m]	4.00	0.90/0.36

*Model scale towers scaled by factor 157.5.

features, except for the tower shadow model and the turbulent wind field, which in papers 5, 6 and 7 were combined and implemented through an external wind file (disabling the tower shadow model in the software), assembled in MatLab (Version R2012a, The MathWorks Inc., US). The tower shadow models for the full wind turbine analysis were limited to the potential flow simulations, Powles' model and results from CFD simulations, Table 3.3.

Table 3.3: Tower shadow models used in the different papers.

Paper	Experiment	Potential flow	Powles' model	Blevins' model	Schlichtings' model	CFD
Paper 1	-	X	X	-	-	-
Paper 2	X	-	X	-	-	-
Paper 3	-	X	X*	-	-	X
Paper 4	-	X	X	X	X	X
Paper 5	-	-	X	-	-	X
Paper 6	-	X	X	-	-	-
Paper 7	-	X	X	-	-	X

*Run through the software's Bladed and AeroDyn, latter with a correction term due to Bak et al. for the tower dam effect [52].

In the following, short summaries of each of the papers are given individually. For full length papers, the reader is referred to appendix A.

3.1 Paper 1 - Blade response on offshore bottom fixed wind turbines with downwind rotors

Full wind turbine simulations were run to get an understanding of the blade root (flapwise) bending moment (RFM) for upwind versus downwind rotors and to see if the power production would be affected by changing the rotor position from the conventional upwind position to a downwind position. In addition to the 12 m/s wind speed, this paper also included wind speeds of 8 m/s and 16 m/s.

The highest RFM (averaged across the azimuth), was found at approximately rated wind speed (12 m/s, Figure 3.2a). The lower mean RFM at 16 m/s (versus 12 m/s, refer full length paper in appendix A) originates from the pitching of the blades above rated wind speed, which will turn the flapwise blade orientation away from the incoming thrust force (being the main contributor to the RFM).

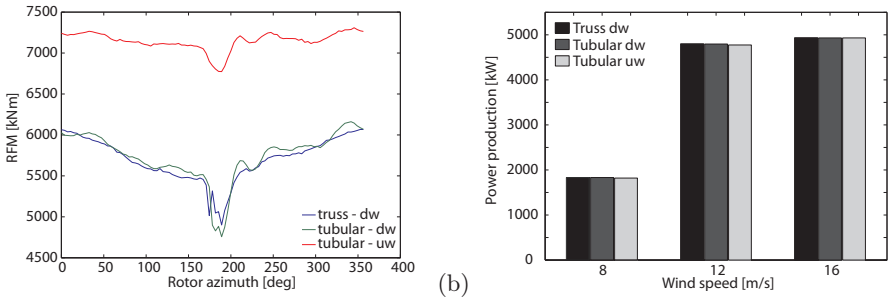

Figure 3.2: Mean results for the upwind (uw) and downwind (dw) monopile (tubular) tower and dw truss tower; (a) azimuthal averaging of the blade root bending moment (RFM) close to rated wind speed, and (b) power production at three different wind speeds - below rated (8 m/s), close to rated (12 m/s) and above rated (16 m/s) wind speed.

A benefit for the downwind mounted rotors, is that the cone angle (away from the tower) helps decrease the mean RFM (compared to the upwind mounted rotor), as the centrifugal force act in the opposite direction of the thrust force, counteracting parts of the bending moment originating from the thrust force (in the upwind position, these contributions adds together).

Contrary, a weakness for the blades on the downwind mounted rotors compared to those on upwind mounted rotors, is the stronger influence from the tower, seen as larger dips in the curves at about 180 degrees rotor azimuth (corresponding to the blade pointing directly downwards), Figure 3.2a. The same dip (but less pronounced) is also found in the curve for the upwind mounted rotor (180 degrees rotor azimuth), indicating that also the upwind mounted rotor is influenced by the presence of the tower. The blades mounted both upwind and downwind the monopile tower show a fluctuating behaviour in RFM as the blade goes out of the tower influenced zone. This effect is less pronounced for the blade mounted downwind the truss tower. How the dips at 180 degrees azimuth and the fluctuating

behaviour as going out of the tower influenced zone will affect the blade fatigue loading, need to be further investigated.

An important economic finding is that the downwind rotors give the same power production (within all three wind speeds) as the upwind mounted rotors, Figure 3.2b.

3.2 Paper 2 - Tower shadow - experiment comparing wake behind tubular and truss towers

For detailed information on the tower shadow profiles, a wind tunnel experiment with model scale towers was first executed. Hot-wire measurements [113] were used to obtain wind energy spectra, mean velocity deficits and turbulence intensities in the tower shadow region behind the monopile (tubular) and truss model scale towers. Thereafter the steady Powles' model was fitted with its' parameters, minimizing the root-mean square (RMS) error of the velocity profiles from the Powles' model (only considering main truss legs, excluding braces) and the experiment.

The largest mean velocity deficit behind the towers is found at the centreline for the monopile tower, while the truss tower show smaller, but multiple velocity deficits across the tower influenced region (originating from the different truss members), Figure 3.3a.

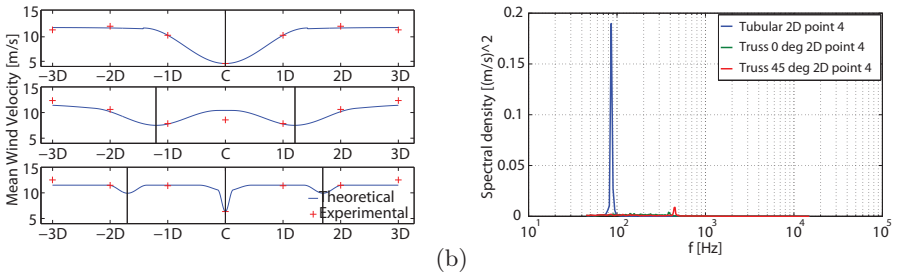

(a) (b)

Figure 3.3: Monopile tower and truss tower, latter at 0 and 45 degree angles towards the incoming wind direction; (a) mean velocity profiles at X-brace positions obtained from the experiment and the fitted Powles' model, and (b) velocity spectra at transversal position 2D (D = 25 mm).

The fitted Powles' model recaptured the experimental results for the monopile tower fairly well, while larger deviations were found for the truss tower. This indicates that the braces do influence the flow and need to be included in the steady multi-member (i.e. truss tower) wake models.

The truss tower showed a lower turbulence intensities (refer full length paper in appendix A) and lower spectral peaks (by two orders of magnitude, both at the

centreline and at transversal position 2D, D = 25mm) than the monopile tower, Figure 3.3b.

The distance from the tower members to the position where the measurements were carried out (measured in relative diameters for the monopile, truss leg and truss brace, respectively) seem to influence the measured TI, where, e.g., no effect on TI is found for braces at large distances.

The peaks in the spectra and the velocity deficits could harm the blades on downwind mounted rotors as they pass through the tower influenced region. From this point of view, the truss tower seem to be beneficial with smaller spectral peaks and smaller velocity deficits.

3.3 Paper 3 - Numerical tower shadow modeling for a downwind wind turbine truss tower

The two full wind turbine simulation software codes, AeroDyn and Bladed, are both implemented with varieties of Powles' tower shadow model. The two parameters in Powles' model (velocity deficit and wake width), were first fitted by minimizing the RMS error between the velocity profile (using Powles' model) and the CFD simulations. The parameters were then used in the AeroDyn and Bladed software codes and their respective velocity profiles were compared with those obtained from the CFD simulations.

The CFD simulations were first validated in the respective Reynolds number region for a single cylinder, comparing the pressure coefficient around the cylinder wall with results in Ong et al. [114] and the y^+ factor (for details on the CFD computations, refer full length paper in appendix A).

Large deviations with the CFD velocity profile was found for the monopile in the AeroDyn representation, Figure 3.4a. The Bladed model fitted the CFD profile better, but did not recapture the speed up on the sides of the tower. For the truss tower, Bladed gave a good fit with the CFD simulations, although with slightly larger deviations than for the monopile tower (no truss tower model available in AeroDyn).

To obtain good fits for the steady wake parameters for the monopile tower, the parameters needed to be fitted in two separate regions, i.e., the near wake region (1D-3D downstream, D = 4.0 m) and far wake region (> 3D downstream), respectively (Figure 3.4b, top). For the truss towers, the velocity deficit parameter fitted nicely in the intermediate range (2D-5D), but the wake width parameter should, in the 2D-5D range, be increased to 1.75 (Figure 3.4b, bottom).

The velocity density spectra 2D downstream the centreline, showed a more pronounced peak (about one order of magnitude) for the monopile tower than the truss tower, while at transversal distance 1D, the peaks had evened out (refer full length paper in appendix A).

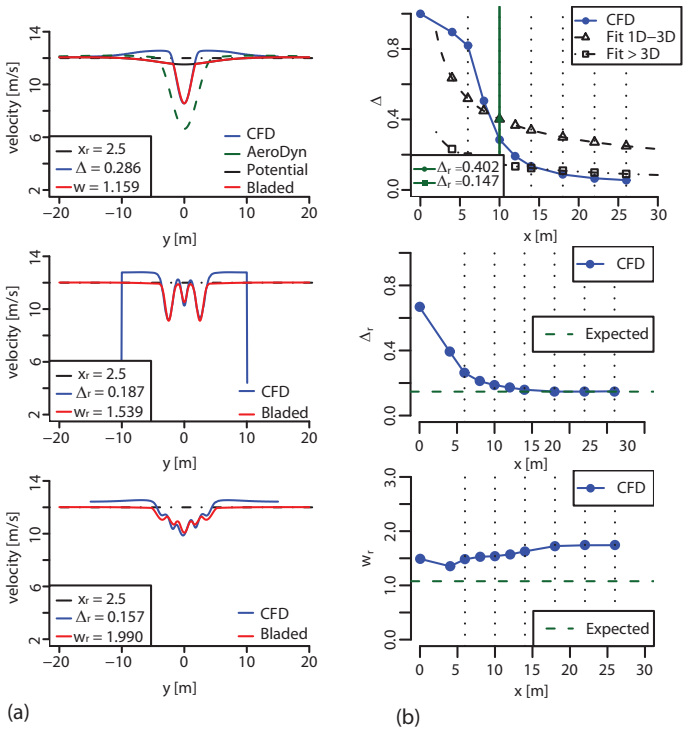

Figure 3.4: (a) Mean velocity profiles for the monopile (top), X-braced truss tower at 0 degree angle (middle) and X-braced truss tower at 45 degrees angle (bottom) for the CFD and Powles' models (implemented through Bladed and AeroDyn, respectively, latter only for the monopile profile), and (b) root-mean square (RMS) residuals for fitting the steady wake models with the mean velocity profiles from the CFD simulations, velocity deficits for monopile (top) and truss tower at 0 degrees (middle), and wake width for truss tower at 0 degrees (bottom).

Although the Powles' model parameters were correctly chosen, the velocity profiles deviated (by different amounts) from the CFD simulations, implying the difficulty of fitting steady parametrized models with profiles obtained from unsteady CFD simulations. The best steady wake model of the two, is the Bladed representation.

3.4 Paper 4 - Numerical analysis of turbulent flow past a truss tower for offshore downwind turbines

Downwind wind turbines are normally simulated with a tower shadow represented by a steady parametric wake model. As the accuracy of the wind turbine simulations largely depend on the choice of these steady model parameters, they are here fitted by minimizing the root-mean square (RMS) error between the results from the steady tower shadow model and the averaged velocity profile obtained from the CFD simulations.

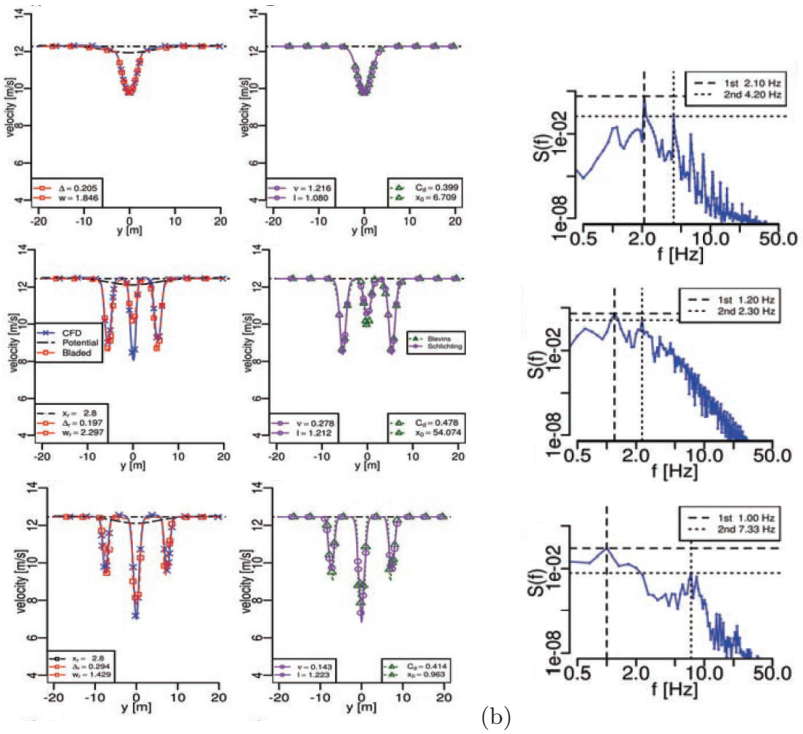

(a) (b)

Figure 3.5: (a) Mean velocity profiles at 2.8D (D = 4.0 m) for the monopile (top), X-braced truss tower at 0 degree angle (middle) and the K-braced truss tower at 45 degrees angle (bottom) for the CFD, Powles', Blevins' and Schlichtings' models, and (b) velocity spectra at the centreline 2.8D behind the monopile tower (top and middle) and K-braced truss tower (bottom), middle and bottom plots including additional turbulent inflow.

All three steady parametric wake models (Powles', Blevins' and Schlichtings') predict the velocity profile behind the monopile tower well (Figure 3.5a), which is also mirrored in the small RMS residuals of the parameter fits (refer full paper in appendix A). But all steady wake models have difficulties predicting the mean velocity profiles behind the truss tower. Especially seen behind the central dip of the X-braced truss tower at 0 degrees, where the CFD simulation shows a deeper velocity deficit than captured by the steady wake models, Figure 3.5a (middle).

The smaller deficit behind the X-braced truss tower for the steady wake models is due to the simple superposition of the flow fields from the individual trusses, where the steady wake model do not account for the interacting effects between the truss tower members.

For the spectral analysis, introducing additional turbulent inflow, renders the spectral peaks from the vortex shedding less pronounced, Figure 3.5b (top versus middle). Also the vortex shedding frequencies are slightly shifted, but without significantly changing the magnitude of the peaks. Compared to the monopile tower, the spectral peak for the truss tower in about an order of magnitude less (Figure 3.5b, bottom).

For a downwind mounted rotor, the steady wake models' underprediction of the velocity profiles behind the truss tower could impact the blade fatigue life. With the lower spectral peak magnitude of the truss tower, such a tower might be beneficial (compared to a monopile tower) for a downwind mounted rotor.

3.5 Paper 5 - Resolution of tower shadow models for downwind mounted rotors and its effects on the blade fatigue

This study was conducted to investigate the transversal and longitudinal grid resolution. The grid resolution can influence the result accuracy and thereby the result reliability, here measured as blade fatigue loading. Also reducing the grid resolution would benefit from a decrease in the time consuming wind turbine simulations.

The recommended grid resolution (for the wind field including the tower shadow described by results from CFD simulations) is 25Hz (longitudinal), with 300 points across the 150m transversal domain (vertical resolution kept constant with 20 grid points across the 200m vertical domain).

This grid resolution was used to carry out blade fatigue analysis using a detailed tower shadow model simulated by two dimensional CFD, including both static and dynamic effects. The two dimensional CFD simulations were converted into three dimensional space according *Step 1* (refer section 3.8).

The study investigate the possibility of approximating the dynamic effects of the tower shadow in the time dependent CFD simulations with averaged methods

(listed in Table 3.4), which would decrease the time consuming CFD simulations to short studies of the relevant tower geometries.

Table 3.4: Wind field components.

Wind field component	Description of wind field component
0	Mean wind speed
1	Mean velocity deficit
2	Unsteady motions (CFD)
3A	Turbulence (velocity spectrum)
3B	Turbulence (velocity spectrum) with different turbulence intensity, TI (averaged) for each lateral point
3B*	Same as case 3B with increased TI (including case 2)
3C	Turbulence (velocity spectrum) with different TI for each lateral point and time step

To a close approximation the blade fatigue assessment using the truss tower can be simplified using the mean velocity deficit together with an averaging of the turbulence from the k-ω sub-grid parametrization, while the monopile tower underestimate the blade fatigue loading by three percent using the same averaging (Figure 3.6).

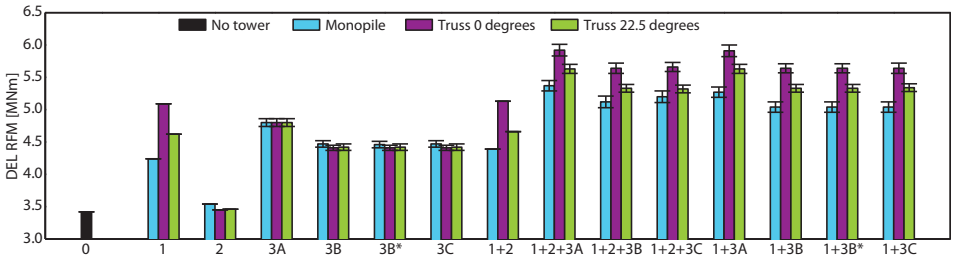

Figure 3.6: Damage equivalent load (DEL) on blade root bending moment (RFM) behind the monopile tower and the truss tower at 0 and 22.5 degree angles towards the incoming wind direction. Complexity of tower shadow wind field increasing from left to right. Error bars showing standard deviation of the mean (details on wind field complexity components, refer Table 3.4).

3.6 Paper 6 - The simultaneous effect of a fairing tower and increased blade flexibility on a downwind mounted rotor

The idea of using a fairing tower geometry to depress the tower shadow impact on a downwind mounted rotor was investigated. Compared to a monopile tower, the rotor overhang needs to be increased for such a tower, to avoid blade-tower

collision. A reduction in rotor overhang was obtained using a strut instead of a full airfoil fairing around the tower [115], Figure 3.7a. To further reduce the rotor overhang (as the blades are tilted and coned away from the tower), the fairing was applied to different sections of the tower, ranging from the position on the tower where only the blade tip would pass (reducing the rotor overhang), to the position covering the entire tower for the length of the blade, Figure 3.7b.

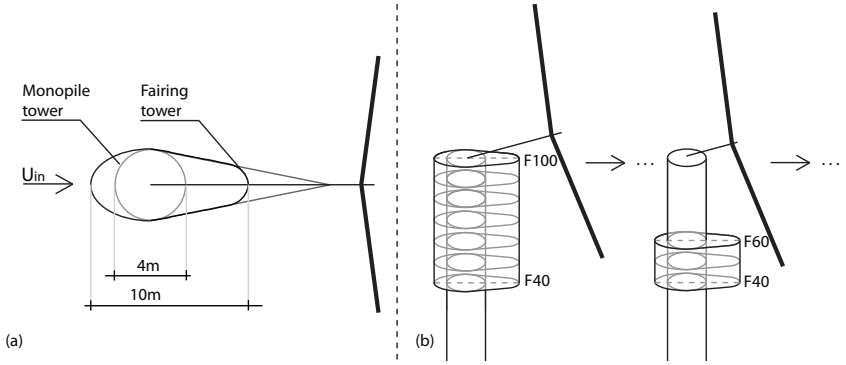

Figure 3.7: (a) Top view of the wind turbine with the monopile in the centre and the tower fairing, aligned with the free stream wind velocity, U_{in}, and (b) side view with the fairing taken off for some of the sections, with the rotor overhang reduced accordingly.

With the steady Powles' model parameters for the fairing found in Wilmshurst et al. [29], the turbulent wind file and the tower shadow were combined in a MatLab script, and called in Bladed for full wind turbine simulations (tower shadow model in Bladed disabled). Blade and tower fatigue loads, as well as mean tower bending loads were calculated.

The downwind mounted rotors allow for more compliant blades, as the blades are less prone to strike the tower during wind gusts, fault conditions and emergency stops. Hence, the downwind mounted rotors were simulated with different blade stiffness and weights, with a total of ten combinations (refer introductory section of chapter 3).

For fairing lengths covering the tower for the entire length of the blade and for the tower with a monopile geometry for the upper 20m of the tower, the blades with adjusted stiffness and weight performed up to five percent better than the conventional upwind mounted rotor, Figure 3.8a. The tower fatigue loads for fairing lengths F40-90 and F40-100 were lower than for the NREL reference (Figure 3.8b), but contrary was found for the mean tower bending moment (Figure 3.8c).

The optimal downwind turbine with a fairing tower therefore needs to be designed with a compromise between fatigue and ultimate loads.

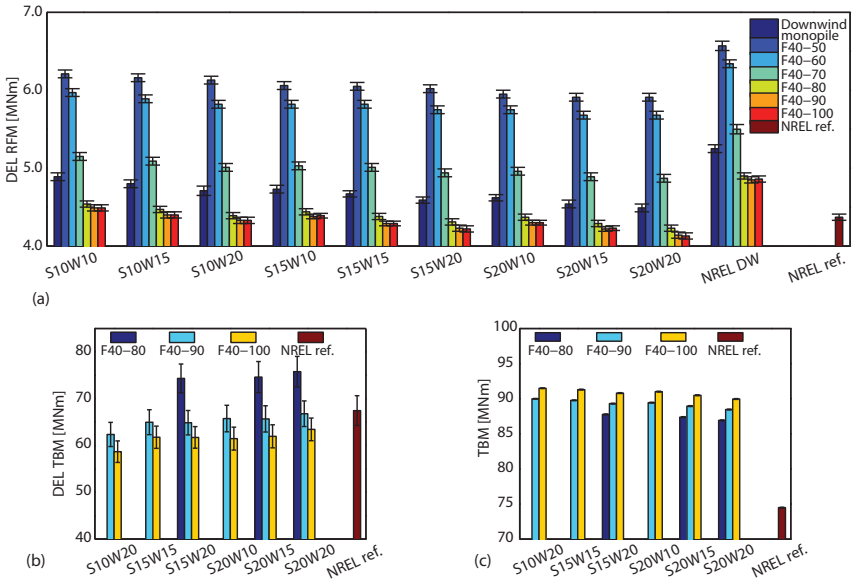

Figure 3.8: (a) Damage equivalent loads (DEL) on blade root bending moment (RFM) for different fairing lengths (F40-FXX) and adjusted blade properties. SxxWyy: xx percent reduction in stiffness (S), yy percent reduction in weight (W), (b) DEL on tower base bottom moment (TBM), and (c) mean TBM for the cases where DEL RFM is lower than for the NREL reference. The conventional NREL reference is included for comparison.

3.7 Paper 7 - A calibration method for downwind wake models accounting for the unsteady behaviour of the wind turbine tower shadow behind monopile and truss towers

A method for fitting a steady wake model and calibrating the turbulence intensity with short CFD simulations of the relevant tower geometries is suggested. This improves the reliability of the steady tower shadow model, and the method is directly applicable in commercially available software for full wind turbine simulations. The method was used in a study on upwind and downwind mounted rotors (on monopile and truss towers) using two blade stiffness and weights.

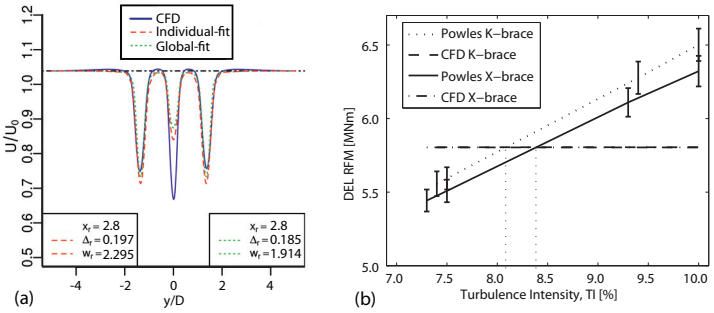

Figure 3.9: (a) Normalized mean velocity deficit for the CFD simulations and the Powles model (fitted with both individually and globally parameters), and (b) damage equivalent loads (DEL) on blade root bending moments (RFM) at different turbulence intensities (TI) for the globally fitted Powles' model and constant TI for the CFD simulations. All results for the truss tower at 0 degrees, (a) only at X-brace position.

The method is thoroughly outlined in section 3.8. The strength of the method is that any discrepancy in the velocity profile between the fitted steady wake model and the CFD simulations (Figure 3.9a) will be accounted for in the calibration of the turbulence intensity, Figure 3.9b. Additionally also the unsteady motions and the turbulence from the sub-grid parametrization are accounted for in the calibration of the turbulence intensity (used with the steady wake model). The blade fatigue loading measured with the method gave a maximum deviation of ± 3 percent (compared to results using the CFD simulated tower shadow).

The largest velocity deficit (based on the CFD simulations) was found behind the K-braced truss tower at 0 degrees (refer figure in full length paper, appendix A) and can be explained from the interaction between the closely spaced main leg and brace. Also the two K-braces are arranged in tandem for the truss tower at 0 degree angle, and the flow field behind the first K-brace seems to be insufficiently recovered as reaching the second K-brace (as large discrepancies are seen between the mean velocity deficit based on the CFD simulations and the steady wake model, where the latter cannot account for the interaction between the truss tower

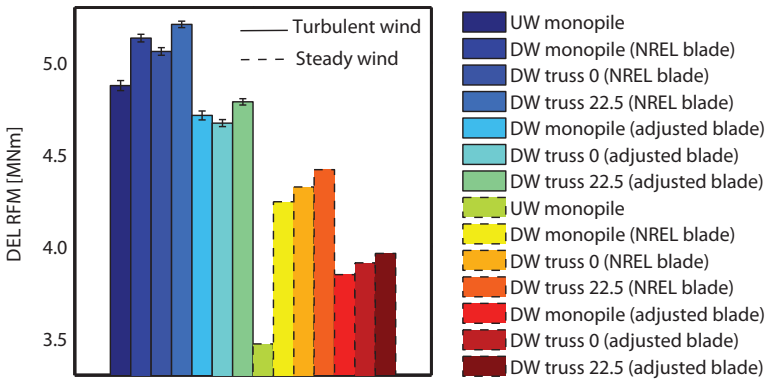

Figure 3.10: Damage equivalent loads (DEL) on blade root flapwise moment (RFM) for upwind (UW) and downwind (DW) mounted rotors on a monopile tower and a truss tower, latter both aligned at 0 and 22.5 degrees with respect to the inflow direction. Downwind rotors are run with two different blade flexibilities and weights.

members). For the truss tower at 22.5 degrees angle, fewer truss tower members were arranged in tandem, giving an increased velocity recovery (with a wider and more shallow velocity profile).

Results based on the suggested method, showed that changing the rotor configuration from an upwind to a downwind position, increased the blade fatigue loads (Figure 3.10). Introducing the 15 percent more flexible and 15 percent lighter blade, decreased the same values compared to the upwind mounted rotor (given turbulent wind). The lowest blade fatigue loads for the turbulent wind case were found for the blades mounted downwind the truss tower at 0 degree angle towards the incoming wind direction, while the largest fatigue loads were found for the blades mounted downwind the truss tower at 22.5 degrees. This suggests that the turbulent inflow disturbs the velocity profile of the tower shadow, with a larger averaging for the narrow (and deeper) velocity deficits downstream the truss tower at 0 degree angle, compared to the wider (and more shallow) deficit downstream the truss tower at 22.5 degrees. This disturbance from the turbulent inflow also helps explain that the lowest blade fatigue loads were found behind the monopile tower in the steady wind cases, but changed as imposing a turbulent inflow.

3.8 Calibration method for Powles' model parameters and the turbulence intensity

With the importance of a reliable tower shadow model for downwind rotor configurations, a method using short two dimensional CFD simulations for calibrating the steady Powles' model and the turbulence intensities for wakes behind monopile and

truss towers is suggested. The benefit of this method is an enhanced reliability and accuracy of the steady wake model, where the turbulence intensity is calibrated to account for any deviation in the fitting of the steady wake model, as well as accounting for the unsteady motions and sub-grid turbulence that are present in the CFD simulations. The method is directly applicable to the commercial software Bladed, where the tapered tower geometries are accounted for, which reduces the time consuming CFD simulations to short studies of a few cross-sections of the relevant tower geometries. Ansys Fluent (Version 12.1.4; Ansys Inc., Canonsburg, USA) was used for the numerical CFD simulations, with the meshing performed with Gambit (Version 2.4.6; Ansys Inc., Canonsburg, USA).

First the mesh of the two dimensional CFD simulations needs to be converted into a three dimensional grid. This was accomplished by reusing the two dimensional time series at different vertical positions (with a random offset in the time series), refer Figure 3.11, *Step 1*. The turbulence spectra extracted in Bladed has a maximum resolution of 50 transversal points (software limitation). As the CFD simulations were found to produce satisfying results at a resolution corresponding to 300 points across the transversal domain, a linear interpolation is used to increase the number of grid-cells (without increasing resolution) to match the 300 points in the CFD simulations and to enable combining the grids of the turbulence spectra and the CFD simulations. Ideally the CFD simulations would be run with turbulent inflow, but due to computational limitations, the CFD simulations were calculated with a constant inflow and the turbulent inflow accounted for later.

The velocity deficit and wake width parameters of the steady Powles' model are fitted by minimizing the root-mean square (RMS) error between the results from the Powles' tower shadow model and the mean velocity deficit profile from the CFD simulations, simultaneously with the Nelder-Mead simplex search algorithm [116]. The initial parameters were chosen randomly between 0.0 and 1.0 for Δ_r and between 0.25 and 10.0 for w_r (refer papers in appendix A for the exact ranges of each study) and further optimized ten times with a few hundred iterations each.

Calibrating the turbulence intensity (TI) is done in three steps, using three different methods to obtain the tower shadow profiles. The different methods are used in full wind turbine simulations in the commercial software Bladed, and damage equivalent loads (DEL) of the blade root bending moment (RFM) are calculated and used in the calibration.

In *Step 1* (Figure 3.11) the tower shadow is described using the time varying CFD results (with unsteady motions and turbulence from the sub-grid parametrization). The turbulence spectra and the tower shadow model are combined in a MatLab script (Version R2012a), where the turbulence from the sub-grid parametrization is multiplied with the time series of the turbulence spectra (normalized with unit standard deviation), and further the velocity time series (with the unsteady motions) is superposed. The final wind field is again normalized to unit standard deviation before being imported to the Bladed software for full wind turbine simulations. The TI is calculated for this new wind field (including the tower shadow)

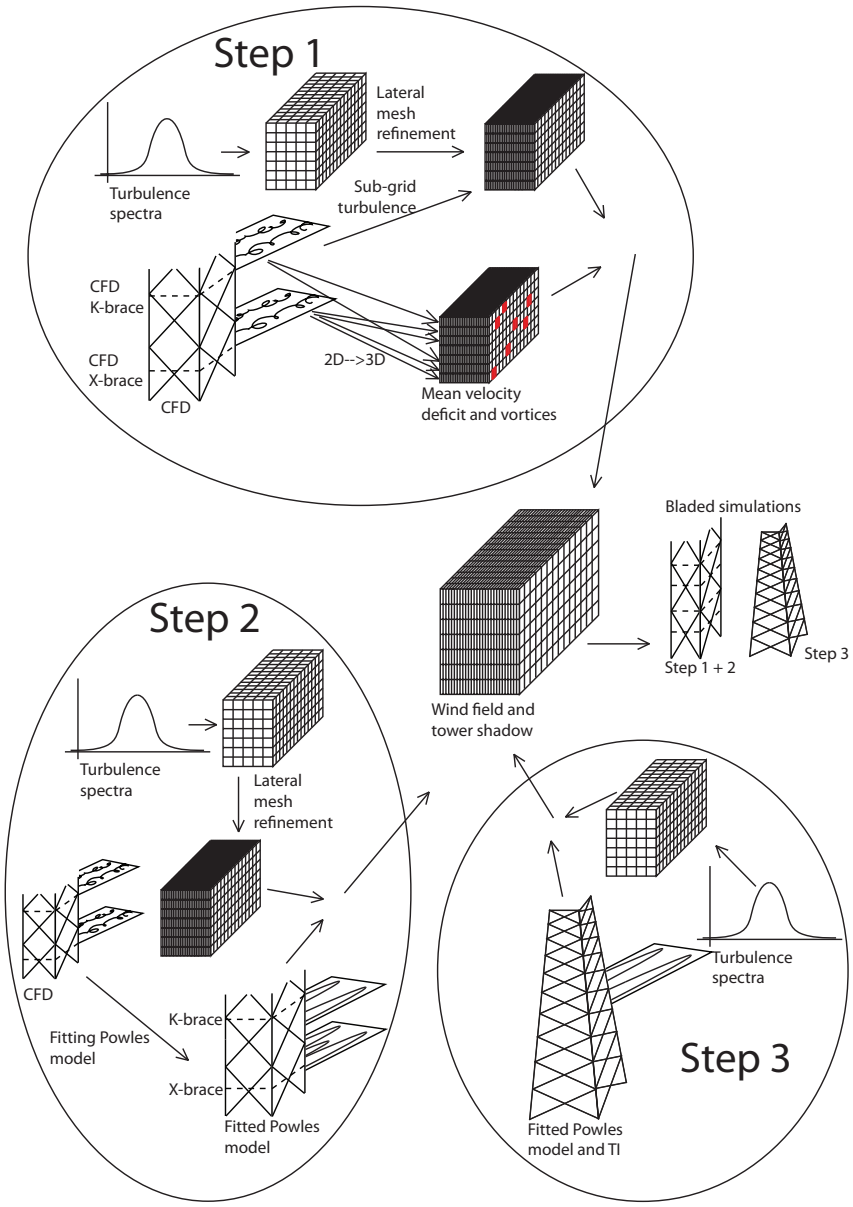

Figure 3.11: Steps for calibrating the turbulence intensity (TI); *Step 1*: wind field and TI from turbulence spectra and CFD tower shadow model, *Step 2*: two trial values for the TI and wind field from the turbulence spectra with the fitted Powles' model, and *Step 3*: wind field from the turbulence spectra and tower shadow from the fitted Powles' model and calibrated TI from *Step 2*, physical tower geometries used in *Step 3*.

and the value is used in the Bladed simulations.

Step 2 calibrates the TI to be used with the fitted Powles' model. Due to the findings of the linear trend-line between the TI's and DEL RFM, two different trial values for the TI are sufficient (range 5 to 15 percent). The wind field from the combined turbulence spectra and tower shadow is assembled in MatLab, simply adding their contributions. Plotting the DEL RFM versus TI with the linear regression line between the results, the calibrated TI is found as the regression line intersects with the plotted DEL RFM from *Step 1* (Figure 3.9). *Step 1* and *Step 2* are based on non-tapered tower geometries with the tower shadows included in the turbulent wind field (Figure 3.11).

The final, *Step 3* runs directly in the software Bladed (with no MatLab script for the wind field) using the turbulence spectra with 50 transversal grid points and the physical tower geometries (Figure 3.11, *Step 3*). The fitted parameters for the Powles' model and the turbulence intensities are those used and found from *Step 2*. For details on the tower properties, refer Table 3.2.

Chapter 4

Conclusions and suggestions for further work

Wind turbines have been studied in the context of reducing the cost of energy through a concept of a downwind mounted rotor. This concluding section summarize the findings of the PhD study in light of the research questions in section 1.2 and suggests some relevant further works.

4.1 Conclusions

The details of the wind field behind a tower at the position of a downwind mounted rotor was investigated in papers 2-4. Both as a model scale physical experiment and through full scale two dimensional CFD simulations. Normally the tower shadow in full wind turbine simulations is expressed through a steady parametric wake model. As the accuracy and reliability of the results from downwind wind turbine simulations depend on the steady wake model parameters, these were fitted for the models of Powles, Blevins and Schlichting with the experiment (only Powles' model) and the CFD simulations.

Constant values for the velocity deficit and wake width parameters of Powles' model (paper 3 and 4) can be used in the range from 2D-5D (D = 4.0 m) downstream the tower centre. This is a promising finding, as 2D-5D is the range in where the blades will pass, which means that the same parameter values are valid for all members of the truss tower.

Even with the steady wake parameters correctly chosen, the steady wake models were still not fully able to reproduce the actual flow field behind the towers, including speed up on the sides of the towers and for the more complex truss tower configurations also underestimating the central wakes with as much as 20 percent.

An option to avoid such discrepancies in the tower shadow representation in full wind turbine simulations would be to use the tower shadow obtained by CFD simulations, as done in paper 5. Results from this paper revealed that the main contribution to blade fatigue loading (from the different CFD 'components') came

from the mean velocity deficit and the turbulence in the incoming wind, with minor contributions from the unsteady motions and turbulence due to the presence of the tower structure.

Based on these findings, a method was proposed (paper 7) where the unsteady motions and turbulence could be approximated and accounted for through a calibration of the turbulence intensity. Thereafter the mean velocity deficit was described by the steady wake model, where the discrepancy between the mean velocity profiles (obtained from the steady wake model and the CFD simulation) also was accounted for through calibration of the turbulence intensity. The method is general and can be used with any steady wake model. A benefit is that the method is directly applicable in the commercial software Bladed (when using Powles' steady wake model), where the required input values are the parameters of the Powles' model and the turbulence intensity. The method limits the time consuming CFD simulations to short pre-processing studies of the relevant tower geometries to obtain the mean velocity profiles and a statistic sample of the unsteady motions and turbulence, while remaining the tower shadow accuracy (maximum deviation of ± 3 percent measured as blade fatigue loading). Thereafter the extensive amount of design load cases (according to wind turbine standards) can be run with the less time consuming steady wake model.

The result accuracy of the blade fatigue loads was also found to be dependent on the tower shadow resolution (investigated in paper 5). Where a coarse grid resolution (decreasing simulation time) was found to be conservative in the blade fatigue load estimation. On the other hand, the finer grid resolution could potentially decrease wind turbine costs.

Now; comparing the blade fatigue loads on upwind and downwind mounted rotors. The downwind mounted rotors with softer and lighter blades showed a 0.5-5.0 percent reduction in blade fatigue loads compared to the upwind mounted rotor (with the original blade stiffness and weight).

Among the downwind rotors, the blades behind the truss tower at 0 degree angle towards the incoming wind direction had a slightly lower blade fatigue loading in the turbulent wind cases than behind the monopile tower, by one to two percent. With an opposite finding in the steady wind cases (by approximately two percent). This seem to indicate that the more narrow velocity deficits behind the truss tower demolish due to the turbulent mixing (as the velocity deficits is larger for the truss tower).

The blades behind the fairing tower performed better by 7-8 percent compared to the blades behind the monopile tower, where a more suppressed tower shadow was found (paper 6). The 20 percent more flexible and 20 percent lighter blades further had a five percent lower blade fatigue loading compared to the conventional upwind mounted rotor on a monopile tower. With the downside of a fairing tower being the increased rotor overhang and thereby the increased mean tower base bending moment, the length of fairing and rotor overhang needs to be designed

with a compromise between these loads.

Based on the findings of this work, I recommend that simulations with downwind mounted rotors are run with the suggested pre-processing step of fitting and calibrating the parameters of the steady wake model and the turbulence intensity with CFD simulations to obtain an accurate tower shadow model and thereby reliable simulation results. And further that care should be taken when choosing the grid resolution of the wind field (including the tower shadow) as also the grid resolution influences the accuracy and reliability of the simulated results. If using downwind mounted rotors with fixed, non-symmetric tower geometries, results from this study encourage that care should be taken for the positioning of the tower with respect to the prevailing wind direction, as it will influence the blade fatigue loading.

4.2 Suggestions for further work

As I summarize the work carried out during my period as a PhD candidate, I see some interesting directions in which to pursue the work:

- A shortcoming of the studies is the limited number of design load cases used. The main focus throughout the thesis was the blade fatigue loading about rated wind speed, as it was assumed to be the most critical design load case for the blade flapwise bending moment under operational conditions. Running a more representative ensemble of design load cases would be advisable. Also investigating the load performance of other components that would be affected by the changed rotor configuration should be included.
- A weakness of the truss tower simulations is that the truss tower eigenfrequency is close to that of the blade. The potential influence this could have on the blade fatigue life should be investigated.
- Using the suggested method (in paper 7) to validate the steady wake parameters for the fairing tower, both with the fairing at zero degree (aligned) and slightly misaligned with the incoming wind direction.
- Running the two dimensional CFD simulations and fitting the parameters of the steady wake models (as described in the suggested method) for the truss tower using more closely spaced main legs, as well as looking at cross sections where the braces are situated at positions between the referred X-brace and K-brace position (where one can assume less interacting effects between the truss tower members) to investigate if the values for the steady wake model parameters will change.
- Implementing full three dimensional CFD simulations of the tower geometries in the suggested method would be valuable as also three dimensional effects could affect the tower shadow representation.

- Implementing a turbulence spectra to the CFD simulation inflow (in the suggested method) to investigate if the increased mixing of the flow will influence the wind field (including tower shadow) downstream the towers.
- Optimizing the fairing length.
- Optimizing the blades for downwind mounted rotors to a larger extent than simply modifying the blade stiffness and weights.

Appendix A - Appended papers

Paper 1
M. Reiso, and G. Moe. *Blade response on offshore bottom fixed wind turbines with downwind rotors.* In Proceedings of the 29th International Conference on Ocean, Offshore and Arctic Engineering (OMAE2010), Shanghai, pages 1-6, 2010.

Paper 2
M. Reiso, M. Muskulus, and G. Moe. *Tower shadow - experiment comparing wake behind tubular and truss towers.* In Proceedings of the 21st International Offshore (Ocean) and Polar Engineering Conference (ISOPE2011), Maui, HI, pages 335-341, 2011.

Paper 3
T.R. Hagen, M. Reiso, and M. Muskulus. *Numerical tower shadow modeling for a downwind wind turbine truss tower.* In Proceedings of the 30th International Conference on Ocean, Offshore and Arctic Engineering (OMAE2011), Rotterdam, pages 1-12, 2011.

Paper 4
T.R. Hagen, M. Reiso, and M. Muskulus. *Numerical analysis of turbulent flow past a truss tower for offshore downwind turbines.* In Proceedings of the 21st International Offshore (Ocean) and Polar Engineering Conference (ISOPE2011), Maui, HI, pages 319-326, 2011.

Paper 5
M. Reiso, and M. Muskulus. *Resolution of tower shadow models for downwind mounted rotors and its effect on the blade fatigue.* Submitted to: Journal of Physics: The Science of Making Torque from Wind, Conference Series XX (2012), IOP Publishing, 2012.

Paper 6
M. Reiso, and M. Muskulus. *The simultaneous effect of a fairing tower and increased blade flexibility on a downwind mounted rotor.* Journal of Renewable and Sustainable Energy 5, 033106 (2013); doi: 10.1063/1.4803749.

Paper 7

M. Reiso, T.R. Hagen, and M. Muskulus. *A calibration method for downwind wake models accounting for the unsteady behaviour of the wind turbine tower shadow behind monopile and truss towers.* Submitted to: Journal of Wind Engineering and Industrial Aerodynamics.

Paper 1

Blade response on offshore bottom fixed wind turbines with downwind rotors

By Marit Reiso and Geir Moe

In Proceedings of the 29th International Conference on Ocean, Offshore and Arctic Engineering (OMAE2010), Shanghai, pages 1-6, 2010.

Is not included due to copyright

Paper 2

Tower shadow - experiment comparing wake behind tubular and truss towers

By Marit Reiso, Michael Muskulus and Geir Moe

In Proceedings of the 21st International Offshore (Ocean) and Polar Engineering Conference (ISOPE2011), Maui, HI, pages 335-341, 2011.

Proceedings of the Twenty-first (2011) International Offshore and Polar Engineering Conference
Maui, Hawaii, USA, June 19-24, 2011

ISBN 978-1-880653-96-8 (Set); ISSN 1098-6189 (Set); www.isope.org

Tower Shadow - Experiment Comparing Wake Behind Tubular and Truss Towers

Marit Reiso, Michael Muskulus and Geir Moe
Norwegian University of Science and Technology (NTNU)
Trondheim, Norway

ABSTRACT

This work presents the results from an experiment run in the wind tunnel at the Norwegian University of Science and Technology (NTNU) for both a tubular and truss tower and compares the velocities in the tower shadow for these two alternatives. The findings are that the truss tower wake has lower energy spectra and turbulence intensities and a higher mean wind velocity than for the tubular tower case. This indicates that the loads caused by the tower shadow of the truss tower will be smaller.

KEY WORDS: Wind turbine; truss tower; downwind; tower shadow; vortex shedding; wind tunnel experiment; theoretical model.

INTRODUCTION

From the start of the modern wind turbine era up until today the growth in wind turbine size has been tremendous, ranging from the smaller kW size into today's MW size. In addition to increasing power output, the larger wind turbines also have a substantially larger weight. As the weight scales to the cube and the extracted power only scales to the square it is obvious that this growth to continuously increasing size cannot continue (Moe, 2007).

Instead of using the same technology and up-scaling it to larger size, as has been the trend during recent years, one could rather look at other layouts and other component designs. One alternative approach could be to use a downwind rotor.

One benefit of using of a downwind rotor is that the blades do not run the same risk of striking the tower during bending as when they are mounted upwind of the tower. Hence softer blades which both are more compliant in gusts and impact loads can be used (Lee and Flay, 1999). Acceptance of lower blade stiffness can mean lower weight and cost. Further, lower weight can lower the loads transferred onto the wind turbine nacelle and tower, which in turn will affect the whole system design towards a more cost efficient wind turbine.

As can be expected a downwind mounted rotor will give rise to larger and more fluctuating tower interferences than its upwind counterpart. Using a truss tower instead of the traditional tubular tower the shadow effect and hence the cyclic fatigue loading on the downwind rotor could be reduced. In addition, according to Long and Moe (2007), a truss tower can save up to 50 % of the material compared to a tubular tower. This estimate is for an upwind rotor configuration. Looking at a downwind rotor configuration the material savings could be even more if the blades are specially designed. The blades will become lighter for downwind rotors and hence further reduce the loading on the tower.

Tower interference has been investigated by many researchers. Chattot (2006) shows that even for upwind wind turbines the tower interference is an important factor in the unsteady working conditions of the blades. This becomes even more important when looking at downwind rotors (Glasgow, Miller and Corrigan, 1981).

Thresher, Wright and Hershberg (1986) compared a numerical model with experiments for a downwind rotor. They looked at the response on the blade as it passed through the tower shadow region and found that the numerical results were significantly higher than the experimental measurements, indicating that their pie-shaped tower shadow model was too simplistic to capture what actually happened in the tower shadow region.

Powles (1983) introduced a semi-empirical model with a cosine bell shaped function for the tower wake behind a single cylinder,

$$U = U_0\left(1 - \Delta\cos^2\left(\frac{y}{2W}\pi\right)\right) \tag{1}$$

where U_0 is the free stream velocity, Δ is the velocity deficit at the centre of the wake, y the distance from the centreline normal to the incoming wind direction, and W the tower shadow width parameter. Powles' approach has been implemented in a series of software codes specifically designed for wind turbines such as GH Bladed from GL Garrad Hassan (Bossanyi, 2009) and AeroDyn (in a modified and extended form) from National Renewable Energy Laboratory (Moriarty and Hansen, 2005). A major issue with Eq. (1) is that it describes the deficit of the wind field behind the tower only for a single cylinder, but it is not clear how to apply it in the case of a multimember truss towers. The velocity deficit Δ and tower shadow width W are usually unknown and need to be estimated. In addition, the irregularities and vortex shedding features of the flow field behind the cylinders are not included in Powles' model.

Ruud Hagen, Reiso and Muskulus (2011) did a 2D numerical analysis of the flow around a multimember tower comparing Powles' model

with computational fluid dynamics (CFD) simulations and found that it was replicating fairly well the results from the CFD model, except from the speed-up close to the wall of the truss members, which was generally underrepresented.

To the authors knowledge no physical experimental work has been conducted for a truss tower arrangement using the spacing between the legs as relevant for a tower used for offshore wind turbines. The spacing here is smaller than what is the case for offshore oil and gas platforms and is at the same time larger than what is reported in e.g. Blevins (1990, chapter 5). Most research in fluid dynamics studies closely spaced cylinder configurations, and in addition the present physical experiment includes tower cross bracings, i.e., three-dimensional effects.

For downwind wind turbines it is important to know the characteristics of the wind field behind the tower. In the present work a comparison between a tubular and truss tower has been looked at. Energy spectra, mean wind velocities and the shape of the velocity field behind the towers, as well as inferred vortex shedding frequencies, are reported. Also a comparison between the results from the wind tunnel experiment and Powles' semi-empirical model (referred to as the theoretical model) is included.

METHODS

An experiment was carried out to determine the wind forces that will act on a rotor mounted on the downwind side of the tower. The experiment was limited to the tower effects, excluding any effects from the rotation of the blade. Also an implementation of the tower shadow model combining Powles' approach and a potential flow model was realized for comparison with the experimental results.

Experiment

The experiment was carried out using both a model for a tubular and truss tower (Figure 2).

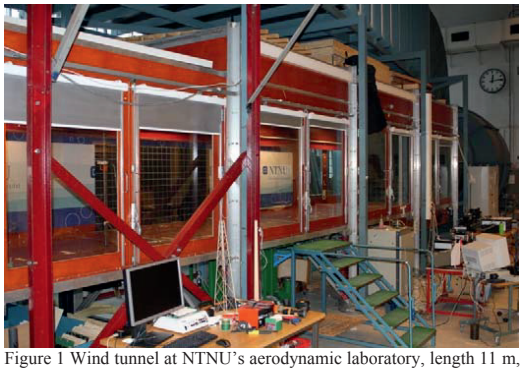

Figure 1 Wind tunnel at NTNU's aerodynamic laboratory, length 11 m, height 1.9 m and width 2.7 m.

The towers were scaled down from the NREL Offshore 5-MW Reference Turbine (Jonkman et al., 2009) by a factor of 157.5. The truss tower was modelled so that the eigenfrequency of the tower was the same as for the tubular tower, more details about the full scale truss tower can be found in Long et al. (2009). The scaling factor was chosen based on geometric similarity and the largest rotor diameter that could be mounted in the wind tunnel at NTNU's aerodynamic laboratory without getting appreciable blockage effects. The model scale truss and tubular tower geometric properties can be found in Table 1.

Table 1 Truss and tubular tower properties – model scale.

Parameter	Truss tower	Tubular tower
Main leg diameter [mm]	6	25
Brace diameter [mm]	2	-
Number of sections	10	-
Tower height [mm]	762	762

The wind tunnel is of a closed return type with length 11m, height 1.9m and width 2.7m (Figure 1). Measurements were carried out around a wind speed of 11.4 m/s, which correspond to the rated wind speed of the NREL Offshore 5-MW Reference Turbine. The free stream turbulence level in the tunnel is 0.4 %.

The truss tower has four sides and was placed at two different angles to the wind, both at 0 degrees (normal to the tower side) and 45 degrees angle to cover different rotor positions. Measurements were carried out at the following grid positions: C, the centreline behind the tower, and at 1D, 2D and 3D to the side of the tower, each with 5 vertical measuring points (Figure 4), in which D=2.5 cm is equal to the tubular tower diameter. In addition the free stream wind velocity U_∞ was recorded.

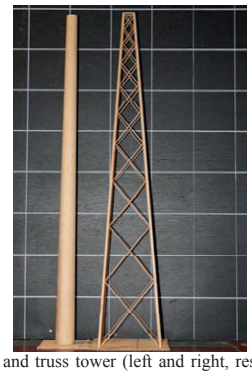

Figure 2 Tubular and truss tower (left and right, respectively) used in the wind tunnel experiment.

Both the tubular and truss towers were placed at a distance upfront of the measuring-point, corresponding to the distance between the tower and rotor plane (see experimental setup in Figure 3).

A hot-wire anemometer was used to measure the mean and turbulent wind velocity behind the two towers (Bruun, 1995). The hot-wire had a calibration temperature of 300 degrees Celsius and dimensions 1 mm and 5 µm for length and diameter, respectively. The sampling frequency was 30 kHz. The mean wind velocity, necessary to calibrate the hot-wire probe, was obtained from an in-situ calibration with a pitot-static tube.

Wind energy spectra were calculated for the different tower configurations based on the time series from the hot-wire measurements by Fast Fourier Transform. Also mean wind velocities and turbulence intensities, TI, defined as standard deviation divided by

mean velocity, are reported.

Theoretical Tower Shadow Model

At the moment more or less the only commercial software that allows for taking tower shadow effects for a multimember tower into account is GL Garrad Hassan's Bladed (Bossanyi, 2009), and hence we employed this approach, or more precisely, the combined model (Powles' approach and the potential flow solution) here.

Powles' wake model is written as

$$U = U_0\left(1-\Delta\cos^2\left(\frac{y}{wD}\pi\right)\right) \tag{2}$$

In contrast to Eq. (1) $w=2W/D$ is a dimensionless parameter for the wake width in terms of D, the diameter of the cylindrical member.

The parameters w and Δ were obtained by minimizing the root mean square (RMS), based on the deviation between the 7 experimental values for each of the towers and the velocity calculated using Eqs.2~6, for the tubular and truss towers at a fixed reference length of 2D downstream of the towers. The parameter search was initialized with a number of initial parameter values to avoid getting stuck in a local minimum. For the tubular tower these were uniformly distributed between 0.25 and 5.0 for w and between 0.4 and 0.9 for Δ. For the truss tower at 0 degrees angle the corresponding values were between 0.5 and 10, and 0.1 and 0.8. The truss tower at 45 degrees angle had initial values of 0.5-3.5 and 0.1-0.8 for the w and Δ, respectively.

For the truss towers the model (Eq. 2) was applied separately for each of the 4 legs in the tower (a simplification not including the braces), scaling the wake parameters used for each member by the scale-root law,

$$\Delta_x = \frac{\Delta_r}{\sqrt{\frac{x}{x_r D}}} \tag{3}$$

$$w_x = w_r\sqrt{\frac{x}{x_r D}} \tag{4}$$

and adding up the individual contributions to the total velocity deficit. Powles' model is thereby used within the region where $|y|\le wD/2$. This is a slight modification of the implementation in GH Bladed since with only 7 measuring points it is preferable to work with smoother curves (obtained using 1/2 period instead of 1/3 period of the cosine) for the numerical optimization of the parameters. For the remaining angles the potential flow solution is applied, expressed as x- and y-vectors of the velocity,

$$U_x = U_0\left(1+\frac{\left(y^2-x^2\right)}{\left(y^2+x^2\right)^2}\left(\frac{D}{2}\right)^2\right) \tag{5}$$

$$U_y = U_0\left(\frac{-2xy}{\left(y^2+x^2\right)^2}\left(\frac{D}{2}\right)^2\right) \tag{6}$$

The velocity magnitude then becomes $\sqrt{U_x^2+U_y^2}$. Combining Eqs.2~6 gives us the combined Bladed model used in the present theoretical calculations.

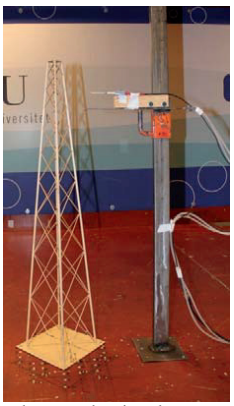

Figure 3 Experimental setup, showing the truss tower at 45 degrees angle at measurement point 1.

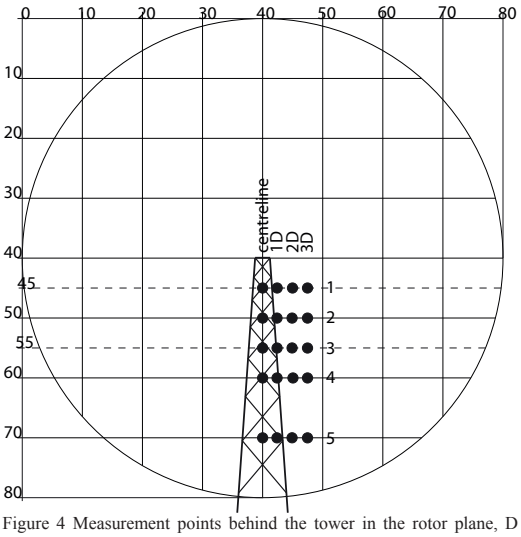

Figure 4 Measurement points behind the tower in the rotor plane, D being the tubular tower diameter.

It should be noted that Powles' model was not intended for multimember towers when it was introduced, and its extension in Bladed neglects possible interactions between different members in the truss tower, and simply adds up the individual effects on the flow.

The vortex shedding frequency is calculated from the Strouhal number, solving for the shedding frequency f in the formula

$$St = \left(\frac{fD}{U_0} \right) \tag{7}$$

St is the Strouhal number, f the vortex shedding frequency, D again the diameter of the cylinder, and U_0 the free stream velocity. For circular cylinders in the subcritical Reynolds number regime the Strouhal number is roughly 0.2. Vice versa, from the vortex shedding frequency the Strouhal number can be directly calculated and compared with values from the literature.

RESULTS AND DISCUSSION

The results from the experiments are reported in section *Spectral Analysis and Vortex Shedding*, where the wind energy spectra behind the different towers are compared and discussed. Thereafter the mean wind velocities and turbulence intensities obtained from the experiment and the theoretical model are compared and discussed in sections *Mean Wind Velocities* and *Turbulence Intensity*.

Spectral Analysis and Vortex Shedding

The energy spectra behind the tubular and truss towers were determined at a number of points behind the towers. The most interesting region is where the blade generates the highest power production, i.e. at one of the outermost positions on the blade, but not all the way out to the blade tip. In this experiment that will be close to point 4 (Figure 4).

In Figure 5, for frequencies above around $6 \cdot 10^2$ Hz the energy spectra fall off according to a power law (corresponding to a line in the double logarithmic plot). Their slopes correspond to what is expected from Kolmogorov's theoretical model for the inertial turbulence range, a subrange of the universal equilibrium range (Pope, 2010; chapter 6.5). This indicates that the measurements are generally trustworthy, exhibiting the spectral features typical of well-developed turbulence. Above these frequencies the energy spectra are dominated by dissipation and at the very high frequencies above the sampling frequency they are governed by noise. The lower frequency region is the energy containing range, i.e. dominated by processes related to the geometry of the towers. A pronounced peak is seen at about 86 Hz for the tubular tower, while no such behaviour is seen for any of the two truss tower configurations.

In Figure 6 the very high peak at 86 Hz as seen in Figure 5 appears even more formidable, since the ordinate scale is now linear. Any such peaks cannot be seen for the two truss tower setups on the centreline, C. They both exhibit an energy distribution more similar to that of the free stream wind velocity.

The same peak is found at 2D for the tubular tower with an even higher spectral energy (Figure 7) than in Figure 6. At 2D it is also possible to discern peaks for the truss tower both at 0 and 45 degrees angle. These peaks are at a much higher frequency, 383 and 453 Hz, respectively. Comparing the peaks from the tubular and truss towers, a much lower spectral energy is seen for the truss tower, in the range of 10^{-3} m^2/s^3 versus 10^{-1} m^2/s^3 for the tubular tower.

Such peaks can cause an impact like load that could be harmful to the blades on the downwind wind turbine, even though its duration is extremely short. Thus an investigation of the blade-tower interaction is needed. This part is not covered here, but will be left to future work. Still, the above is a promising finding as it indicates that the truss tower will induce a much smaller impact like load onto the blades than the tubular tower.

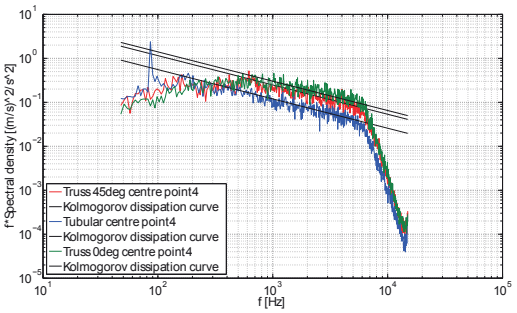

Figure 5 Velocity energy spectra on the centreline at point 4 for the tubular, truss 0 degrees and truss 45 degrees towers. Black lines: slope of Kolmogorov's dissipation spectrum.

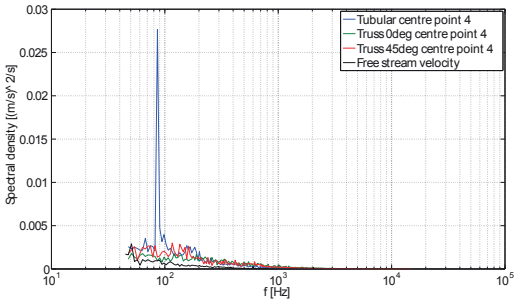

Figure 6 Wind energy spectra for the free stream wind velocity and behind the tubular and truss towers. Measurements are taken at the centreline, all at point 4.

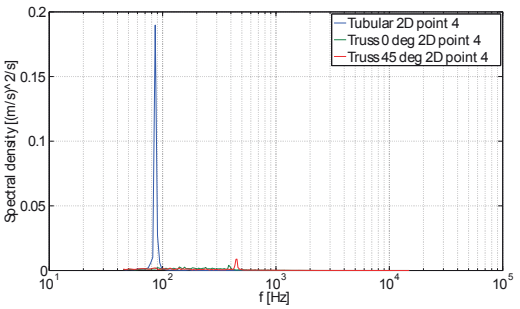

Figure 7 Wind energy spectra behind the tubular and truss towers. Measurements are taken at 2D, all at point 4.

The tubular tower exhibits a pronounced peak at about 86 Hz (Figure 6). With a diameter D = 0.025 m and free stream velocity U_∞ = 11.4 m/s the Strouhal number (calculated by Eq. 7) then becomes St = 0.19 at a Reynolds number Re = $2 \cdot 10^4$ (using a kinematic viscosity ν =

$1.5 \cdot 10^{-5}$), assuming that the frequency of 86 Hz corresponds to the vortex shedding process. This is the same Strouhal number as de Sampaio and Coutinho (2000) reported at a Reynolds number of $1.0 \cdot 10^{4}$. The same Strouhal number has also been reported for Reynolds numbers lower than $3 \cdot 10^{5}$ (Bearman, 1968; Roshko, 1960).

A peak at 383 Hz is identified in the energy spectrum (Figure 7) for the truss tower at 0 degrees at the transversal position 2D (from the centreline). Calculating the Strouhal number for a leg in the truss tower with D = 0.006 m gives St = 0.2, the corresponding Reynolds number being $4.6 \cdot 10^{3}$. The same Strouhal number is also obtained from the truss tower at 45 degrees angle.

The peak spectral energy differs by two orders of magnitude between the tubular and truss towers. The truss tower exhibits a much lower peak spectral energy compared to the tubular tower, which can be explained by the larger relative distance from the measuring point to the cylinders, measured in number of cylinder diameters. The tubular tower measurements were carried out at 2 tubular tower diameters downstream from the tubular tower, while for the truss tower the distance was 5-8 truss tower member diameters downstream from the tower. The larger relative distance for the truss tower allows for more wake development and dissipative mixing, and hence results in the lower energy seen at the vortex shedding frequencies of 383 Hz and 453 Hz. This is also seen by the way the peaks are distributed over a wider range of frequencies compared to the tubular tower with a more narrow peak at 86 Hz.

For the braces in the truss tower no distinct peak is readily identified in the energy spectra. Using a Strouhal number of 0.2 it is expected to find a peak at frequency 1140 Hz. The same reasoning as for the main legs in the truss tower explains the absence of such a peak. As the size of the bracing members is even smaller here, D = 0.002 m, no peak is seen in the energy spectra at this frequency.

The Strouhal number for the truss tower is comparable to a lot of other results published in the literature for single cylinders, indicating that the flow behind the structure is dominated by the vortex shedding process of the main truss members.

Mean Wind Velocities

A plot of the mean wind velocities focusing on the tower shadow area is shown in Figure 8. The data were sampled at one side of the tower and mirrored about the centreline, C. The wake width, w and the velocity deficit Δ parameters for the tubular and truss towers resulting in the minimum RMS values are given in Table 2.

Comparing the experimental values in Figure 8, the deficit in mean wind velocity is largest for the tubular tower, showing a minimum wind velocity reaching 4.6 m/s at C. The truss tower in position 45 degrees towards the wind direction shows the same unimodal dip at C with a smaller mean wind velocity deficit, down to 6.4 m/s. For the truss tower at 0 degrees it is not possible to compare the maximum deficit directly behind the legs, as no measuring points are located directly behind those. The measured deficit for the truss tower is 7.9 m/s measured at ±1D, while the legs are positioned at ±1.3D. From the best fit of the theoretical model, we estimate the minimum values for the double dips at 7.5 m/s. This corresponds to a reduction compared to the 11.4 m/s free stream velocity of 60 %, 44 % and 31 % for the tubular, truss 45 and truss 0 degrees angle towers respectively.

The values for the wake width w and the velocity deficit Δ (Table 2) are seen to match well with the dip at C (Figure 7A) for the tubular tower.

At the transversal position ±2D a speed-up of about 3 % compared to the theoretical calculation is seen for the experimental values but not in Powles' model, thereafter a 4 % decrease in wind velocity is seen for the experimental value at ±3D.

Table 2 Parameters w and Δ for tubular and truss towers.

Tower	w	Δ
Tubular tower	2.85	0.60
Truss tower 0 degrees	6.93	0.30
Truss tower 45 degrees	1.36	0.28

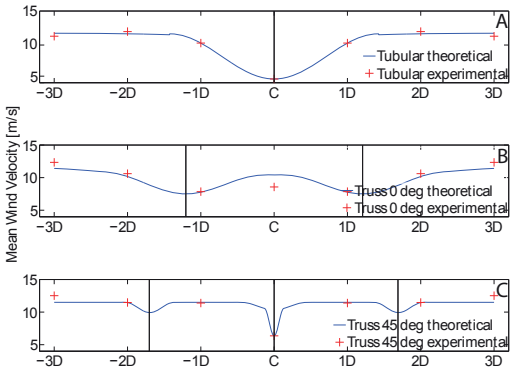

Figure 8 Mean wind velocity at different transversal distances from the tower at point 4, A – tubular tower, B – truss tower at 0 degrees and C – truss tower at 45 degrees angle. Vertical lines indicate the position of the main legs.

The best fit of Powles' model (more precisely, its multimember extension with the scaling law Eqs.3~4), used for the truss tower at 0 degrees angle (Figure 7B), is not as close to the experimental values as is seen for the tubular tower. At C the theoretical model predicts a velocity 18 % higher than the measured velocity at the same point. This can be caused, for example, by the simplification of not accounting for brace members in the theoretical model. At the same time a slight underprediction of the wind speed is seen for the theoretical model at ±2D and ±3D (4 % and 7 %) compared to the measured velocity.

At 45 degrees angle Powles' model exhibits better alignment with the measured values (Figure 7C) than for the truss tower at 0 degrees angle. Due to the limited number of measurement points there were again no measurements directly behind the tower legs between ±1D and ±2D, but as good alignment are seen for the points at C, and close to ±1D and ±2D, also the theoretically calculated dip behind the tower legs will be estimated more or less correctly. A discrepancy at ±3D shows an underprediction of the theoretical calculation of 8 % compared to the measured velocity.

The better alignment for the 45 degrees versus 0 degrees angle truss tower can indicate that the brace members will interfere with the wind velocity closer to the tower, while at a larger distance (as is the case for the truss 45 degrees tower) this seems not to play as significant a role. The magnitude of this effect has not been included here, but left for future studies.

For all three cases the experimental results show a somewhat higher mean wind velocity close to the wall of the cylinders with a wind velocity higher than the free stream velocity of 11.4 m/s. No such

speed-up is exhibited by the theoretical model. This could be partly due to Powles' model extending 1/2 period instead of 1/3 period to the side of the tower, which gave a smoother transition between Powles' model and the potential flow solution, but might also be due to genuine deficits of this approach. Ruud Hagen, Reiso and Muskulus (2011) also reported that the speed-up close to the wall of the cylinders were not well reproduced by the combined Powles' and potential flow model. This could mean that the impact like load that the wind velocity creates behind the tower would be slightly underpredicted.

Turbulence Intensity

Table 3 is divided into two parts, where the upper part gives the measured turbulence intensities TI, while the lower part scales the TI behind the towers, based on the free stream velocity TI (excluding the interaction of the brace members), thereby comparing the velocity fluctuations directly.

The TI is very high for the tubular tower directly behind the tower at the centreline, C, and also at 1D, 45 % and 30 % respectively, before it rapidly decreases and is closer to the TI of 0.4 % for the free stream velocity at ±3D (Table 3). The same trend is seen for the truss tower at 45 degrees angle towards the incoming wind direction, but the TI values are lower, except at ±2D where it shows a slightly higher TI than the tubular tower. The position of the legs of the towers (Figure 7A and Figure 7C) shows why the truss tower at 45 degrees has a higher TI at ±2D compared to the tubular tower, since the truss tower has its legs close to the ±2D position (refer black vertical lines). Still the TI for the truss tower at 45 degrees is only 2/3 of the tubular TI at C. This is most likely due to the smaller leg diameter for the truss tower.

For the truss tower at 0 degrees angle towards the incoming wind direction the pattern is slightly different, the TI is highest at ±1D and then is close to the TI for the free stream velocity at ±2D and ±3D. This is in accordance with the position of the legs, which are close to ±1D (Figure 7B). The reason why the TI is not close to the free stream velocity's at C is likely due to the mixing of free stream velocity with the small vortices from the braces and the vortex shedding from the rear legs, as the truss tower at 0 degrees does not have any main legs at C.

Table 3 Mean wind velocity and TI at C, 1D, 2D and 3D for point 4. Upper part obtained from experiment, lower part calculated from free stream velocity.

Position	C		±1D		±2D		±3D	
	U [m/s]	TI [%]	U [m/s]	TI [%]	U [m/s]	TI [%]	U [m/s]	TI [%]
Tubular tower, position 4	4.6	45.1	10.1	30.5	11.8	5.3	11.1	1.7
Truss tower 0 degrees, position 4	8.6	14.51	7.8	24.7	10.6	1.8	12.3	0.5
Truss tower 45 degrees, positions 4	6.4	30.2	11.4	19.3	11.5	8.4	12.5	0.5
Free stream velocity	11.4	0.4	-	-	-	-	-	-
	$TI = TI_{U\infty} \cdot U_\infty / U$ [%]		$TI = TI_{U\infty} \cdot U_\infty / U$ [%]		$TI = TI_{U\infty} \cdot U_\infty / U$ [%]		$TI = TI_{U\infty} \cdot U_\infty / U$ [%]	
Tubular tower, position 4	1.0		0.5		0.4		0.4	
Truss tower 0 degrees, position 4	0.5		0.6		0.4		0.4	
Truss tower 45 degrees, position 4	0.7		0.4		0.4		0.4	

The higher TI for the tubular tower, compared to the truss tower, especially at C and ±1D, can be explained by the relative distance at which the measurements were carried out behind the towers. As stated above the measurement points were about 2D and 5-8 relative diameters downstream of the tubular and truss towers, respectively, so the wake from the tubular tower is in a different regime than the truss tower.

Moving further to the side from C the TI decreases and at ±3D the TI is very close to the TI for the free stream velocity for all three tower setups. At the transversal position ±3D the measurements are so far to the side that they are outside the shadow of the structure and hence a TI close to that of the free stream velocity is as expected.

At ±1D the truss tower at 0 degrees shows a higher TI than at C both for the measured and the calculated TI. The measured value at ±1D has increased by 70 %, while the calculated TI has increased by 20 %. For the truss tower at 45 degrees angle the corresponding decrease is 36 % and 43 %, respectively. This indicates that the braces play a significant role in the TI behind the tower as the measurements are carried out close to the tower (as for the 0 degrees configuration), while it evens out as the distance from the braces increases (as for the truss tower at 45 degree angle). This is also in alignment with what was found for the mean wind velocity (see above).

At ±2D and ±3D the TI is the same as for the free stream velocity indicating that is does not seem to be namely affected by the tower structures for either the tubular or truss towers.

The TI is depending mostly on how far downstream from the tower members measurements are carried out, and no effect is found for truss tower braces at large distances. For the transversal displacement all three tower configurations have a TI close to the free stream velocity's TI at ±2D and ±3D.

CONCLUSIONS

We have compared the wind field behind different towers through physical experiments and by comparison with a theoretical model (a combined Powles and potential flow model).

The energy spectra for the tubular and truss towers differ significantly. The tubular tower shows a pronounced peak in the spectrum, while the truss towers do not exhibit such peaks, except from a smaller peak directly behind the truss legs. The energy in the truss tower peak is lower by two orders of magnitude compared to the tubular tower peak, indicating a more transparent tower and a higher dissipation behind the truss tower.

The theoretical model matches the experimental results from the tubular tower fairly well, but does not capture the speed-up on the side of the tower wall properly.

The higher mean wind velocity, lower spectral energy and lower TI for the truss tower results in a situation which might be advantageous from the viewpoint of downwind rotor fatigue.

ACKNOWLEDGMENT

Thanks to Professor Per-Åge Krogstad for his help and constructive discussions. Thanks to laboratory technicians Arnt Egil Kolstad and Olav Haldorsen at NTNU for their support and encouragement during my work. Thanks also to PhD candidate Pål Egil Eriksen for assistance in the laboratory. The work of Marit Reiso and Michael Muskulus was financed by the Norwegian Research Council (NFR), the latter under the RAVEN project (BIP), 193326.

REFERENCES

Bearman, PW (1969). "On Vortex Shedding from a Circular Cylinder in the Critical Reynolds Number Régime," *Journal of Fluid Mechanics*, Vol 37, No 3, pp 577-585.

Blevins, RD (1990). *Flow-Induced Vibration*, Van Nostrand Reinhold.

Bossanyi, EA (2009). *GH Bladed Theory Manual,* Technical Report 282/BR/009, Garrad Hassan and Partners Limited, Bristol, UK.

Bruun, HH (1995). *Hot-wire Anemometry: Principles and Signal Analysis,* Oxford University Press.

Chattot, JJ (2006). "Extension of a Helicoidal Vortex Model to Account for Blade Flexibility and Tower Interference," *Journal of Solar Energy Engineering*, Vol 128, pp 455-460.

Glasgow, JC, Miller, DR, and Corrigan, RD (1981). "Comparison of Upwind and Downwind Rotor Operations of the DOE/MASA 100-kW Mod-0 Wind Turbine," *In Proceedings of the 2nd DOE/NASA Wind Turbine Dynamics Workshop, Cleveland, Ohio.*

Jonkman, J, Butterfield, S, and Musial, W (2009). *Definition of a 5-MW Reference Wind Turbine for Offshore System Development.* NREL Technical Report NREL/TP-500-38060, National Renewable Energy Laboratory, Golden, CO, USA.

Lee, A, and Flay, R (1999). "Compliant Blades for Wind Turbines," *Ipenz Trasactions,* Vol 26, pp 7-12.

Long, H, Fischer, T, and Moe, G (2009). "Design Methodology and Optimization of Lattice Towers for Offshore Wind Turbines in 35m Water," *In Proceedings of EWEC, Marseilles.*

Long, H, and Moe, G (2007). "Truss Type Towers in Offshore Wind Turbines," *In Proceedings of European Offshore Wind Conference (EOW 2007), Berlin.*

Moe, G (2007). "What is the Optimum Size for a Wind Turbine?" *In Proc Int Conf Offshore Mech and Arct Eng, CD-ROM.*

Moriarty, PJ, and Hansen, AC (2005). *AeroDyn Theory Manual,* Technical Report NREL/EL-500-36881, National Renewable Energy Laboratory, Golden, USA.

Pope, SB (2010). *Turbulent Flows,* Cambridge University Press.

Powles, SRJ (1983). "The Effects of Tower Shadow on the Dynamics of a Horizontal-Axis Wind Turbine," *Wind Engineering,* Vol 7, No 1, pp 26-42.

Roshko, A (1960). "Experiments on the Flow Past a Circular Cylinder at Very High Reynolds Number," *Journal of Fluid Mechanics*, Vol 10, No 3, pp 345-356.

Ruud Hagen, T, Reiso, M, and Muskulus, M (2011). "Numerical Tower Shadow Modelling for a Downwind Wind Turbine Truss Tower," *Proc Ocean, Offshore and Arct Eng. in press.*

de Sampaio, PAB, and Coutinho, ALGA (2000). "Simulating Vortex Shedding at High Reynolds Numbers," *Proc the Tenth Intl Offshore and Polar Eng Conf, Seattle, USA, Vol 3, www.isope.org.*

Thresher, RW, Wright, AD, and Hershberg, EL (1986). "A Computer Analysis of Wind Turbine Blade Dynamic Loads," *Journal of Solar Energy Eng,* Vol 108, pp 17-25.

Zdravkovich, MM (1997). *Flow Around Circular Cylinders. Vol I: Fundamentals,* Oxford University Press.

Paper 3

Numerical Tower Shadow Modeling for a Downwind Wind Turbine Truss Tower

By Torbjørn Ruud Hagen, Marit Reiso and Michael Muskulus

In Proceedings of the 30th International Conference on Ocean, Offshore and Arctic Engineering (OMAE2011), Rotterdam, pages 1-12, 2011.

Is not included due to copyright

Paper 4

Numerical Analysis of Turbulent Flow Past a Truss Tower for Offshore Downwind Turbines

By Torbjørn Ruud Hagen, Marit Reiso and Michael Muskulus

In Proceedings of the 21st International Offshore (Ocean) and Polar Engineering Conference (ISOPE2011), Maui, HI, pages 319-326, 2011.

Proceedings of the Twenty-first (2011) International Offshore and Polar Engineering Conference
Maui, Hawaii, USA, June 19-24, 2011

ISBN 978-1-880653-96-8 (Set); ISSN 1098-6189 (Set); www.isope.org

Numerical Analysis of Turbulent Flow Past a Truss Tower for Offshore Downwind Turbines

Torbjørn Ruud Hagen, Marit Reiso, Michael Muskulus
Department of Civil and Transport Engineering, Norwegian University of Science and Technology
Trondheim, Norway

ABSTRACT

For a downwind wind turbine simulation a realistic tower shadow model is needed. The flow past two dimensional cross sections of both a monopile and a truss tower was simulated, and the tower shadow models of Powles, Blevins and Schlichting were compared with numerical results, assuming linear superposition of wake effects. It was found that all models have difficulties predicting the mean velocity profile. Spectral analysis showed about an order of magnitude less fluctuations for the truss towers, which might mean less fatigue. Under unsteady inflow from a von Karman spectrum, the flow is still dominated by fluctuations from vortex shedding.

KEY WORDS: truss tower; turbulence; computational fluid dynamics; offshore wind turbine; tower shadow; high Reynolds number flow.

INTRODUCTION

Wind turbines have seen a large increase in height recent years, and finding areas that have the accessibility needed for such large structures is a challenge. Moving wind turbines offshore is one option that will become more important in the future. Advantages, such as more stable wind fields and less surface roughness are available in an offshore environment, but since such installations are expensive, it is vital to reduce the cost. By replacing the usual monopile with a truss tower a significant reduction in material cost can be achieved (Long and Moe, 2007). Bottom-fixed offshore wind turbines are installed on substructures, such as gravity based foundations, tripod substructures, monopiles and truss tower structures (Breton and Moe, 2009), but also a full truss tower from the foundation to the nacelle is a possibility.

Since such a truss tower has a larger diameter than the corresponding monopile, tower clearance becomes an issue. Downwind turbines are an interesting option then, since the blades will experience counterbalancing centrifugal forces that will reduce the risk of them hitting the tower. Thereby, an additional reduction of material cost might be realized by making the blades softer. However, as the periodic velocity deficit due to the tower shadow potentially induces structural vibrations, which then cause fatigue damage, it is important to study the wind field behind such towers. As a truss tower is more transparent, it is hoped that these damages are smaller compared to the fatigue due to the tower shadow of a monopile.

There are several approaches to model the mean wind fields behind wind turbine towers. These steady tower shadow models make it possible to run complete wind turbine setup simulations. The models are, however, usually combined with an unsteady turbulent inflow. A popular choice has been Powles' model (Powles, 1983). This model assumes a cosine bell-shaped wind field behind a circular cylinder, representing a monopile tower, for each two-dimensional cross section. The wake is assumed to have its origin in the center of the cylinder and is represented by two parameters describing its width and maximum deficit, for a certain distance. In order to use this model for a multi-member structure, such as a truss tower, the first idea that comes to mind is to superpose the velocity deficit from each member of the tower (Bossanyi, 2009). Since each of the members is located at a different position, the two wake parameters then need to be scaled relative to their distance from the point of interest. Again, the simplest possibility is to assume that the wake width grows with the square root of the distance, and that the velocity deficit decreases with it[1]. Thereby, a complete model for a multi-member structure is obtained, depending on two parameters only.

Another approach for the cylinder wake was proposed by Blevins (1990). Again, this is a two-parameter model with one parameter describing the upstream virtual origin of the wake, and the second parameter being the drag coefficient of the member. The dependence on the distance is similar to the above square-root law, but the virtual origin allows for more flexibility, which could give a better model for the velocity deficit in the region of interest.

Finally, Schlichting developed a model for wakes arising from boundary layers on thin plates (Schlichting and Gersten, 2000), that is also applicable to extended bodies such as cylindrical members. Comparing these three models with numerical results is the first step in assessing the quality of current tower shadow models, and in finding a more accurate one.

In our analysis we simulated an unsteady turbulent flow past two dimensional cross sections of a monopile and a truss tower, represented by a circular cylinder and an ensemble of cylinders, respectively. The turbulent inflow was implemented with two different methods. The first method adds turbulence, specified by turbulence intensity and length scale, to the velocity inflow profile. A second method, used to obtain more realistic results, adds unsteady turbulent motion based on stochastic transient simulation from the von Karman spectrum. All

[1] This derives from modeling wake development as a diffusion process, and noticing that profiles for such a process exhibit this behavior.

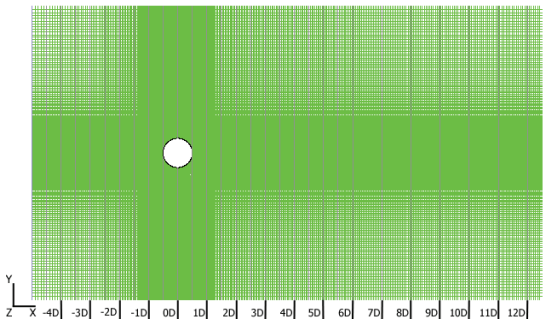

Fig 1: Domain for the numerical model of the monopile. Lines indicate positions where time series data was sampled.

three steady tower shadow models are compared with computational fluid dynamic (CFD) simulations. The Reynolds Averaged Navier-Stokes (RANS) equations with the k-omega Shear-Stress Transport (SST) viscosity model (Menter, 1994) were used for this study to keep the computational cost reasonable.

METHODS

A two dimensional unsteady turbulent flow past a cross section of a monopile and a truss tower wind turbine tower has been simulated. The cross section of the truss tower is represented as four main cylinders with additional smaller cylinders to represent the X-brace between the main cylinders. To evaluate the effect from different wind directions the truss tower was simulated at 0 degrees and 45 degrees, respectively, to the inflow direction. The flow past a cross section of the monopile, represented as a single cylinder, was compared with results from the literature to validate the numerical model. In all cases, velocities and turbulence intensity were recorded at a number of lines transverse to the free stream flow, resulting in time series data.

Numerical Model

The numerical model was implemented in the commercial software package ANSYS FLUENT (Version 12.1.4; ANSYS Inc., Cantonburg, USA). The truss tower was represented by four main cylinders with a diameter of 0.9m and the cylinders were separated by 10.8m corresponding to the height with the highest power production (42m above sea level). An intersection (x-brace) between the main cylinders was represented by eight additional smaller cylinders with diameter 0.36m. These small cylinders were placed at different locations to represent the cross section for slightly different heights (Fig. 2). In reality, the main cylinders are angled at 84.3 degrees and the brace members are angled at 50.0 degrees, which would make the cross sections an ensemble of ellipsoids. For simplicity, this was approximated here using only circular members. Another simplification is that the model is two dimensional. This means that three dimensional effects that occur due to, e.g., varying distances between the cylinders and finite height of the tower are not captured here.

The geometry was implemented using ANSYS GAMBIT (Version 2.4.6; ANSYS Inc., Cantonburg USA). Each cross section was inserted into a domain that spanned 40m along the y-direction and 70m along the x-direction (Fig. 1); the latter being the free stream flow direction. The sidewalls of the domain were implemented with periodic boundaries and the outflow boundary was implemented with the reference pressure of one atmosphere. To model the air, an

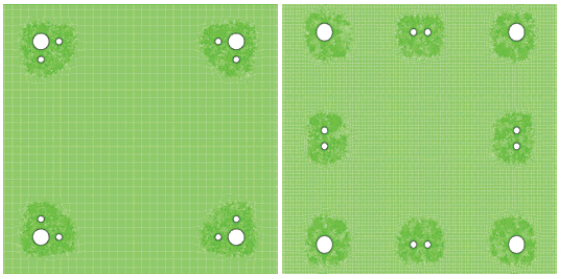

Fig 2: Detail geometry of the numerical model for the two truss tower cases at 0 degree position. Left: Cross section close to the beginning of the brace (Case 1). Right: Cross section close to the center of the brace (Case 2). The rest of the domain is the same as in Fig. 1.

incompressible fluid was considered with a density of ρ=1.225kg/m^3 and dynamic viscosity of μ=1.789x10^{-5}kg/ms. For each circular member a boundary layer, consisting of 30 layers with an inner element size of 0.0001m and a growth factor of 1.2 was added.

For computational efficiency we reduced the amount of unstructured mesh in the domain. By adding control surfaces, the unstructured mesh was concentrated around the cylinders in the structure. An unstructured mesh was needed everywhere around the cylinder due to no prior knowledge of the location of the separation point. The rest of the domain was implemented with a structured mesh (Fig. 1 and Fig. 2), to reduce the number of cells. For the monopile the total number of quadrilateral cells was close to 86 000 and was increased for the truss tower cases to approximately 310 000 cells. In addition to the truss geometry in Fig. 2, the same structure was also simulated at 45 degrees (not shown) to study the velocity deficit for a different wind direction.

Turbulent Inflow

The inflow boundary (on the left side of the domain) was implemented with a mean free stream velocity of 12m/s, which represents a typical power production speed for offshore wind turbines, e.g., the 5MW NREL (Jonkman et al., 2007) wind turbine. The flow enters the domain with turbulent fluctuations superposed on it, and two different methods were used. For all cases velocity fluctuations were imposed using the subgrid turbulence parameterization for the k-ω model with a turbulent intensity (ratio of mean-square velocity fluctuations to mean velocity) of 10 percent on a turbulence length scale of 1m, which is a typical scale of turbulent energy containing motions (eddies) behind a structural member with these diameters.

In addition, all cases were tested with additional fluctuations obtained by simulating from a von Karman spectrum, which was implemented with a user-defined function. The spectrum follows the form given in Burton et al. (2001, Eq. 2.24), with a length scale of 73.5m for the longitudinal turbulence, and a length scale of 37.25m for the lateral variations. Note that the turbulent length scale for subgrid turbulence within the domain is still 1m. The standard deviation was set to 1.6m/s for the x-velocity and 1.2m/s for the y-velocity. To save computational time and to avoid unwanted correlations due to the periodic boundary, lateral correlations were implemented by a simplified version of Rice's method (Shinozuka, 1972), in which the power coefficients of twenty neighboring grid cells (corresponding to about 4-6m distance) contribute to each time series, instead of by the usual diagonal mixing matrix across all grid cells (Veers, 1988). The correlations were wrapped around at the periodic boundary (the sides of the domain).

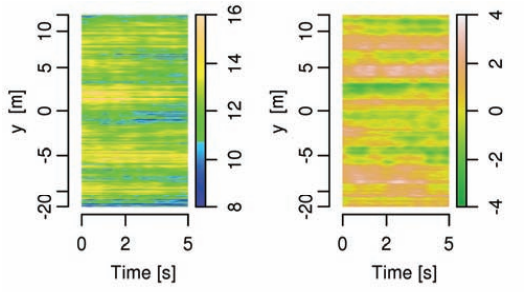

Fig. 3: Turbulent inflow imposed at the velocity inlet. Colors represent velocity magnitude (in m/s). Left: Velocity along x-direction. Right: Velocity along y-direction. Note that the y-axis is not scaled linearly to represent the differences in cell size.

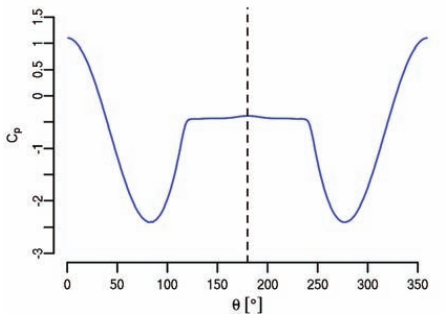

Fig. 4: Pressure coefficient around the circumference of the monopile.

The frequency band was discretized with 100 frequency components distributed between 0 and 10Hz. Phases were still realized for each grid cell and frequency component separately, and it was simulated directly from the spectral coefficients (Shinozuka, 1972, Eq. 24). This avoided numerical instabilities and led to a very efficient method suitable for long time-domain simulations.

Validation

Flow past cross section of the monopile was simulated with the k-ω SST model and validated in the supercritical Reynolds number regime ($Re=3.3\cdot10^6$). Figure 4 shows the pressure coefficient distribution around the circumference of the monopile, where =0° is the stagnation point, relative to the flow, in front of the cylinder. Comparing with the data of Ong et al. (2009), we see that the drop to C_p=-2.5 at =80° due to separation of the flow is predicted accurately by the k-ω SST model, both with respect to strength and position. Further around the cylinder, C_p rises to -0.5 at =120° where it stabilizes, also in excellent accordance with the literature. Experimental results by Warschauer and Leene (2009) confirm this pattern. Note that the Reynolds numbers for these earlier results is slightly higher, but since they lie in the same qualitative regime the results are comparable (Zdravkovich, 1997).

To check if the transitions near the wall were accurately predicted we employed the computational wall y^+ which is a nondimensional quantity that measures the length of the boundary layer in viscous length units (Pope, 2009; pg.269). For a flow in the supercritical

Fig 5: Vortex shedding behind the monopile. Colors represent vorticity magnitude.

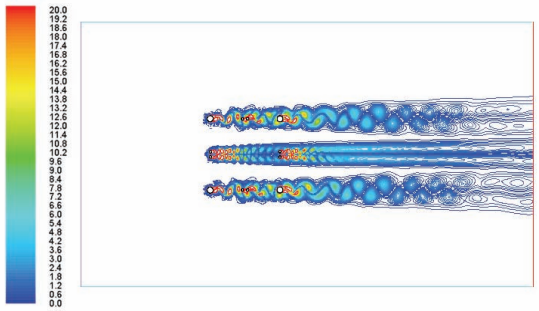

Fig 6: Vortex shedding behind the truss tower (Case 2). Colors represent vorticity magnitude.

Reynolds number regime y^+ should be less than 5. Our results were obtained with y^+_{max}=3.5 and should be accurate enough for industrial applications (Salim and Cheah, 2009). The model is also capable to capture the vortex shedding instability (Fig. 5-7) for low enough time-steps (dt<0.06), which is nontrivial in the high Reynolds number regime.

The drag coefficient was calculated to be 0.37 which is inside expected range of 0.21-0.6 in the supercritical regime and also in the lower range of (0.36-0.75) in the upper-transition regime (Ong et al. 2009). As our Reynolds number is just on the limit between these regimes, the drag coefficient seems very reasonable. Our simulations were also able to predict C_{Lrms} (which is the root mean square of the lift coefficient) equal to 0.12 which is also in the expected range for both the supercritical (0.03-0.15) and upper-transition regime (0.06-0.14). With the validation results inside the expected range we chose to proceed. Note that the drag coefficient was first calculated with a factor of ¼ wrong (due to size of the cylinder), this was detected and changed.

Analysis

A fixed time step of 0.005s was used with a second-order upwind scheme for both spatial and temporal integration, and after initialization of the flow (with a few thousand time steps) an additional 6000 time steps were simulated, corresponding to a physical flow time of 30s. After these, the additional von Karman turbulence was switched on and another 3000 time steps were obtained, of which the first 1000 were removed before the analysis, such that the turbulent flow had reached

the structure.

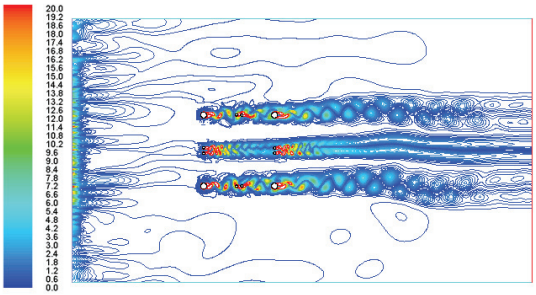

Fig. 7: Vortex shedding with turbulent von Karman inflow. Colors represent vorticity magnitude.

Rake lines with 401 points at 0.1m intervals were added transverse to the free stream flow, where total pressure, velocity magnitude, x-velocity, y-velocity, turbulent kinetic energy (k) and turbulent intensity were recorded. The monopile diameter D=4m was used as a reference for the location of the lines, these being measured from the middle of the structure (such that "3D behind" the truss tower refers to a distance of 12m behind its center). The data was output every time step for all half-integer multiples of D, and analyses were performed with the statistical computing environment R (R Development Core Team 2009), using the MASS library (Venables and Ripley, 2002) and custom written functions. Spectral analysis was done with the Fast Fourier Transform (FFT).

Tower Shadow Models

Powles' model. The multi-member extension of Powles' model, implemented in GL Garrad Hassan Bladed and used here, is a combination of the potential solution and Powles' empirical model (Bossanyi, 2009). The wake effect is modeled by (Powles, 1983):

$$V = V_0\left(1-\Delta\cos^2\left(\frac{y}{wd}\pi\right)\right), \tag{1}$$

where Δ is the velocity deficit at the middle of the wake, and w=W/2d is a dimensionless parameter dependent on the cylinder diameter d and the physical wake width W. This expression is applied for arguments of the cosine function within ±60 degrees. This means that the wake is cut off when the deficit falls to $\Delta/4$, and the potential solution is used for the wind field of the remaining locations. For multi-member towers (Eq. 1) is used to calculate the wake effect for each individual member relative to the current position, and then these effects are superposed linearly, resulting in:

$$V = \sum_{i=1}^{n} V_i + (1-n)V_0, \tag{2}$$

for the final velocity. Here V_i (i=1, 2,…, n) represents the velocity calculated for the i-th member, and V_0 is the free stream velocity. Additionally, the model imposes that V≥0.

To fit the model to a multi-member structure both $\Delta>1$ and w>0 in Eq. 1) have to be known for each member of the structure. In order to more easily compare these parameters with each other, a dimensionless (in terms of member diameter d) reference length x_r=2.825 at a typical distance for a downwind rotor was used. The change in wake characteristics was modeled with the square-root-law (Bossanyi et al., 2009):

$$\Delta(x) = \Delta_r / \sqrt{x/(x_r d)}, \quad w(x) = w_r \cdot \sqrt{x/(x_r d)} \tag{3}$$

Here the reference values Δ_r and w_r are used to scale Δ and w. Together with Eq. 2 one can then calculate the total velocity profile. However, interactions between members are not accounted for, and members that are close to each other (as in Fig. 2, left) could exhibit different wake behavior and render the model less valid. Considering the flow in the far wake regime, these close clusters could maybe be modeled as a single member, but this interesting possibility is not worked out further here.

The reference values Δ_r and w_r were each fitted by minimizing the root-mean square (RMS) error between the results from the tower shadow model and the average profile obtained from the computational fluid dynamic simulations, simultaneously with the Nelder-Mead simplex search algorithm (Nelder and Mead, 1965). The initial parameters were chosen randomly between 0.0 and 1.0 for Δ_r and 0.5 and 5.0 for w_r and further optimized ten times with a few hundred iterations each.

Blevins' model. Whereas Powles' model originated in the wind energy field, Blevins' model was conceived in fluid dynamics to describe the wake behind a cylinder (Blevins, 1990). Although a similar square-root law is the basis of this velocity wake model, a parameter describing the virtual origin of the wake, x_0, makes for the major difference. Moreover, both the wake width and the velocity deficit depend analytically on the second parameter, the drag coefficient C_d. The time-averaged velocity profiles are then given by:

$$\begin{aligned} b &= 0.23\left[C_d d\left(x+x_0\right)\right]^{1/2}, \\ c &= 1.02V_0\left(\frac{C_d d}{(x+x_0)}\right)^{1/2}, \\ V(x,y) &= V_0(1-ce^{-0.69y^2/b^2}), \end{aligned} \tag{5}$$

where d is the member diameter. The half-width b is the length from the centerline to the position where one-half of the centerline velocity deficit c is reached. Note that a misprint was corrected, following Fredheim (2006). As before, the parameter estimates were found by minimizing the RMS error between Blevins' model and the averaged profile from the simulations.

Schlichting's model. In the original formulation of this model the wake behind a thin flat plate of length *l* is described (Schlichting and Gersten, 2000). The velocity deficit is given as:

$$V(x,y) = V_0\frac{C_d}{4\sqrt{\pi}}\sqrt{\frac{V_0 l}{\nu}}\left(\frac{x}{l}\right)^{-\frac{1}{2}}\exp\left(-\frac{y^2 V_0}{4x\nu}\right) \tag{6}$$

Here C_d is the drag coefficient, the fluid viscosity is represented by ν, and *l* represents the length of the body. In practice, to use this model we assumed one of the three parameters ν, *l* and C_d known and adjusted the values of the other two. C_d was taken from the validation run to be 0.37. Note that Eq. 6 is Reynolds number dependent and for large Reynolds numbers as here the body length *l* will also need to be large. This will render the numerical fit unstable and hints at the possibility that it should not be applied in such a way. We therefore chose to adjust the fluid viscosity parameter ν and the body length *l,* again minimizing

the RMS error. Note that *l* can be interpreted as the virtual origin of the

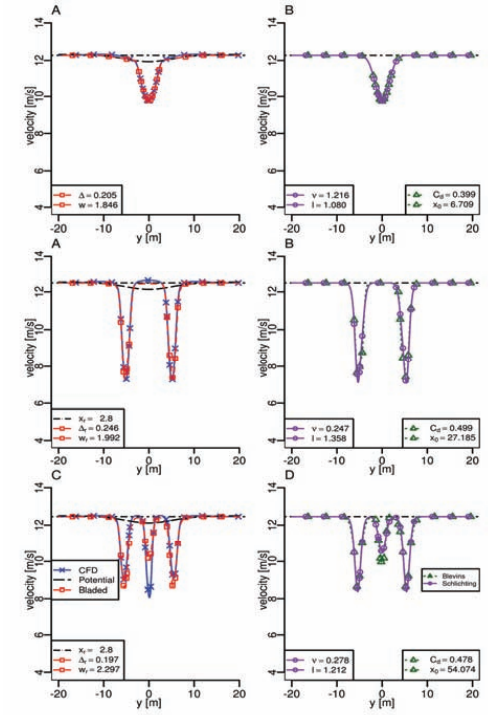

Fig.8: Mean velocity profile 3D behind the tower. Top row: Monopile. Middle row: Truss tower Case 1 at 0 degrees. Bottom row: Truss tower Case 2 at 0 degrees (points are not to be recognized as discrete values).

wake, similar to x_0 for Blevins' model. We used the same multi-member approach as for Powles' model (Eq. 2).

RESULTS

Simulating flows in the supercritical Reynolds number regime ($Re=3.3 \cdot 10^6$) with the RANS k-ω SST mode is a challenge. Generally, these flows are difficult to realize even in physical experiments. Numerically, the challenge lies in the calculation time and to accurately predict features in the boundary layer. However, with the correct initialization, the k-ω SST model was able to reproduce the main properties characterizing this flow regime.

As the blades of a downwind wind turbine would pass behind the tower at a distance of around 3D, results for this distance are particularly interesting, but we will also look further behind the towers. Mean profiles are shown for 3D and 6D, the parameter estimates of all three models are discussed, and spectra are considered. The von Karman turbulence is only considered for the spectra since relatively long time series are needed to obtain good estimates of the mean flow, whereas the spectral estimates, especially for higher frequencies, are more reliable.

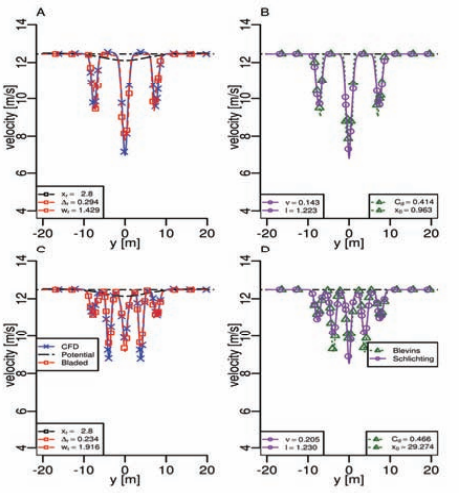

Fig.9: Mean velocity profile 3D behind the tower. Top row: Monopile. Middle row: Truss tower Case 1 at 45 degrees. Bottom row: Truss tower Case 2 at 45 degrees (points are not to be recognized as discrete values).

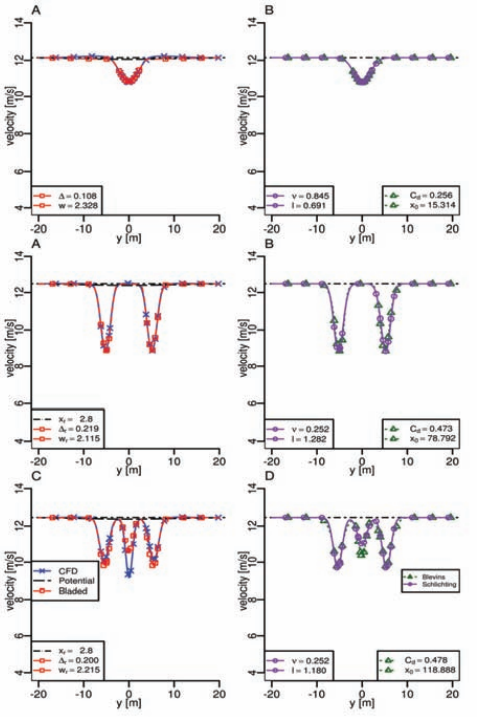

Fig.10: Mean velocity profile 6D behind the tower. Top row: Monopile. Middle row: Truss tower Case 1 at 0 degrees. Bottom row: Truss tower Case 2 at 0 degrees (points are not to be recognized as discrete values).

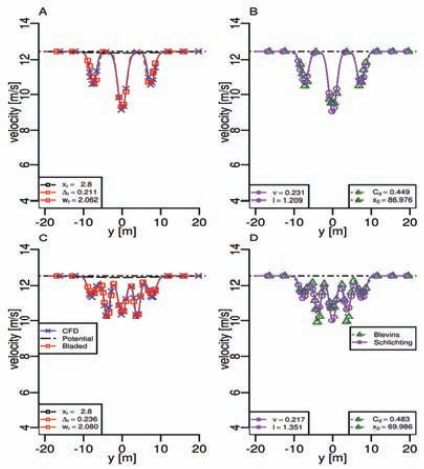

Fig.11: Mean velocity profile 6D behind the tower. Top row: Monopile. Middle row: Truss tower Case 1 at 45 degrees. Bottom row: Truss tower Case 2 at 45 degrees (points are not to be recognized as discrete values).

Mean Profiles

The first obvious difference between the CFD simulations and expectations is that the velocity does not reach the free stream velocity at the boundaries (Figs. 8-11). This is an artifact caused by the periodic boundary conditions, the limited size of the domain and total momentum conservation. However, it was impractical to enlarging the domain or to use pressure outlets, due to constraints on computational time and numerical stability.

We have dealt with this issue by considering the value of the velocity magnitude at the boundary to be the free stream velocity in the tower shadow models. The difference amounts to roughly 2 percent and might lead to a slight underestimation of the tower shadow effect on the same order.

With this adjustment all tower shadow models were able to reproduce the velocity deficit behind the monopile well (Fig. 8 and fig. 9, top row). At 3D distance the optimal parameters for Powles' model were a wake width of 1.8 diameters (Eq. 3) and a velocity deficit of 20 percent. Common choices encountered in the literature amount to 1.0 diameter and 40 percent deficit, but are mostly based on empirical measurements in the field. For Blevins' model the parameter C_d is in the physically meaningful range, between 0.21-0.6 (Ong et al., 2009), and the virtual wake origin of 6.7 diameters corresponds to the recommended value of roughly 6 diameters (Blevins, 1999). The parameters for Schlichtings' model have no direct physical interpretation here.

Behind the truss tower is where the models start to disagree. The wake for the first case (Fig. 8 and fig. 9, left middle row) is reasonably represented, although with almost a doubling in most parameters related to wake width. Since the legs of the tower are more than four times smaller than the monopile, the wake should be narrower than was found, if wake model predictions for single members can be simply added. This is compensated partially for the increased distance (3D for the monopile corresponding to about 7-18 diameters for the legs here, depending on position) and the growth of the wake over this distance. Still the wake width is larger than expected by a factor of about two,

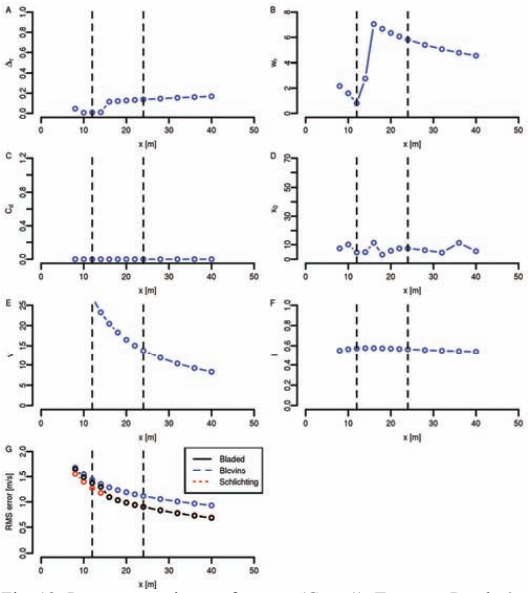

Fig. 12: Parameter estimates for truss (Case 1). Top row: Powles' model. Left: Wake width, Right: Velocity deficit. Second row: Blevins' model. Left: Drag coefficient, Right: Virtual wake origin. Third row: Schlichting's model. Left: Viscosity parameter, Right: Virtual body length. Bottom row: Residuals. Vertical lines indicate distances of 3D and 6D behind the structure.

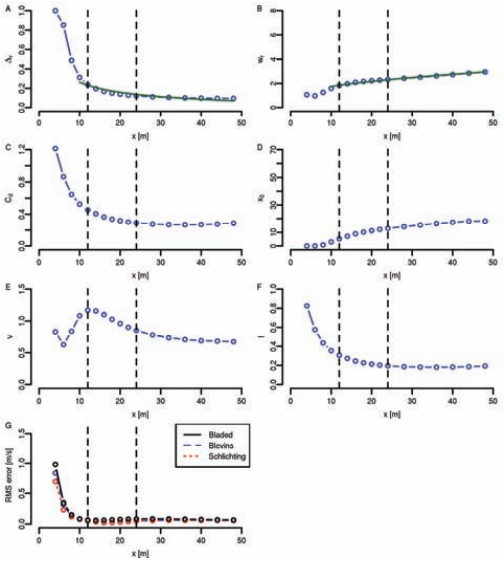

Fig. 13: Parameter estimates for the monopile. Top row: Powles' model. Left: Wake width, Right: Velocity deficit. Second row: Blevins' model. Left: Drag coefficient, Right: Virtual wake origin. Third row: Schlichting's model. Left: Viscosity parameter, Right: Virtual body length. Bottom row: Residuals. Vertical lines indicate distances of 3D and 6D behind the structure.

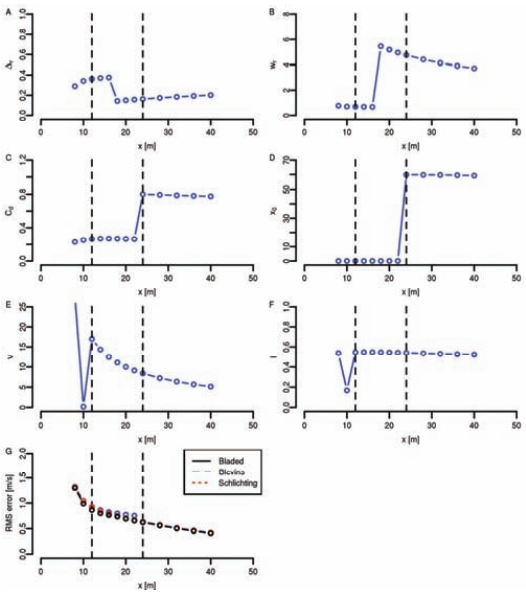

Fig. 14: Parameter estimates for truss (Case 2). The same quantities were plotted as in Fig. 12.

and slightly shallower. The same effect can be seen for Blevins model, with both C_d and x_0 increasing.

For truss tower case 2 a further problem arises, in that the central wake is larger than the wakes on the side, which is due to flow interaction effects. All tower shadow models underpredict this central wake by roughly 10 percent. Further downstream at 6D (Fig. 10 and fig. 11) the situation is similar. The wake is still wider than expected from superposition but not as pronounced as at the smaller distance. The velocity deficit is, interestingly, larger than expected, which indicates that the wake does not seem to decay as quickly as described by the square-root law (Eq. 3).

At 45 degrees, results are comparable (Fig. 9 and fig. 11). Again the wake width and the velocity deficit are larger than expected, and all tower shadow models underpredict the central wakes, by up to 50 percent.

Assessment of Tower Shadow Models

Fitting the tower shadow models at a number of distinct distances behind the structures, a more sophisticated assessment can be made. For the monopile, the parameter estimates were obtained at the actual distance, not scaled to the reference distance x_r, and should then exhibit the square-root behavior (Eq. 3). This is more or less the case (Fig. 13, top row) for distances that are not too small. Blevins' and Schlichting's models do not, however, use the reference distance and should exhibit constant parameters (i.e., straight horizontal lines). However, this is only the case far downstream (~6D). Their parameters therefore need to be adjusted with regard to the distance behind the cylinder.

For the truss tower, now also the parameters of Powles' model were scaled to a reference distance and should be constant with respect to the distance. This is roughly the case for the velocity deficit (Fig. 12, top left), but the wake width parameter depends on distance. A transition

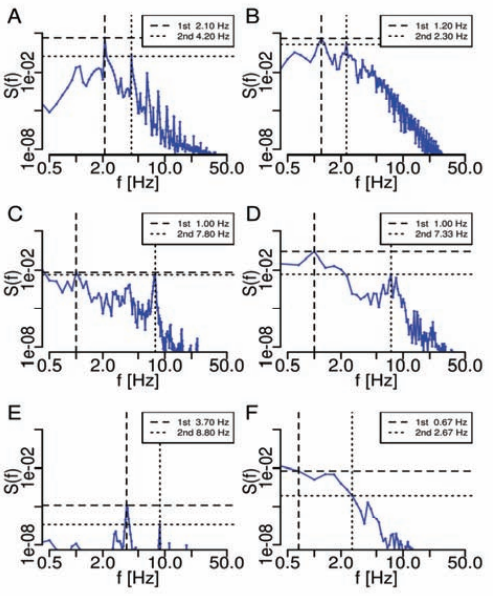

Fig.15: Power spectral densities for the velocity magnitude. Top row: 3D behind the monopile. Middle row: 3D behind the truss tower (Case 1). Bottom row: 3D in front of the truss tower (Case 1). Left: Turbulent intensity. Right: Additional von Karman turbulence.

can also be observed, at about 4D distance behind the tower. Before that, a wake width of 2 diameters and a low velocity deficit should be used, beyond that point; both the wake width and velocity deficit parameter should be taken much larger. This transition might be due to the existence of different flow regimes (for the near and the far wake). Note that the models are simplifications that try to generalize a complex flow situation. When several wakes from members with different diameters occur close to each other the global parameters have trouble adjusting due to this. Superposing the individual wakes in the models, almost the same profile can be obtained by (a) larger wakes with large central deficits, or (b) more concentrated wakes with lower central deficits. The same issue arises for the truss tower case 2 (Fig. 14, top row).

Blevins' model represents both structures with almost constant parameters, apart from a transition at about 6D for case 2, in which again an identifiability issue plays a role. Schlichting's model is the worst, since its parameter ν is distance-dependent. Note that the residuals are relatively large for all models (Fig. 12 and fig. 14, panel G), which is due to the interaction effects leading to underestimation of the central wake.

Spectral Analysis

The spectral density estimates at the centerline show that the truss towers exhibit roughly one order of magnitude less fluctuations than the monopile (Fig. 13, left column). The monopile spectrum is dominated by the vortex shedding frequency of about 2.1 Hz and its higher harmonics; for the truss tower, the vortex shedding frequency is much higher (around 7.8 Hz for the large members), and exhibits similar power than the low-frequency background around 1 Hz.

If turbulence from the von Karman spectrum is introduced into the simulations, there is a broadband increase in the relevant frequency band (0-10 Hz), which renders the spectral peaks from vortex processes less pronounced. Also the observed vortex shedding frequencies are slightly affected. However, the magnitude of the peaks is not significantly changed. Interestingly, for the truss tower case 1 (Fig. 15, middle right); low-frequency background from the turbulence contributes significantly to the variance, which might possibly be related to instabilities on a slow timescale, e.g., intermittency in vortex shedding behavior. However, much longer time series are necessary to conclude this with confidence. Also, the fluctuations from the parameterized turbulence would need to be accounted for in the spectra, to assess this properly.

The spectral density for the regular inflow (only parameterized turbulence, 3D in front of the truss tower) has a lower power, in the order of 10^{-5} (Fig. 15, bottom, left), compared with the von Karman inflow, exhibiting a power of 10^{-2} (Fig. 15, bottom, right). This power is due to small pressure fluctuations from the shedding process that slightly modify the flow field before the tower. The spectral density behind the structure is significantly higher for the von Karman inflow (Fig. 15, middle row), showing both the effects of vortex shedding and unsteady inflow.

DISCUSSION

Different steady tower shadow models (Powles', Blevins' and Schlichting's) have been tested to see if they were able to reproduce properties of the flow field behind a two dimensional cross section of a truss tower. By fitting model parameters, minimizing the root mean square error, parameter estimates where obtained for the multi-member tower that should more accurately represent its behavior in time-domain simulations. For example, in Powles' model the wake width should be taken at a value of about 2 diameters, and the velocity deficit at about 20 percent, at the reference length xr=2.825D, to represent the wake in the vicinity of this distance.

Concerning velocity profiles, the truss tower cases had difficulties reproducing the properties of the central wakes, exhibiting rather large residuals and underpredictions of up to 50 percent. It seems then that the simple idea (Eq. 2) to neglect wake interaction effects can have a significant influence on the magnitude of fluctuations that a passing blade will experience, thereby underpredicting loads and fatigue.

The simplifications in this study could bias the results and further studies would be desirable to ensure consistent results. There exist complex, unsteady three dimensional effects, discussed in (Williamson, 1996), that are not possible to capture with the two dimensional cross sections used in this study. A numerical study of this issue would be an interesting direction to pursue in the future.

CONCLUSIONS

A tower shadow model that is able to predict all features of a flow field behind a multi-member tower is difficult to realize. The complexity of such a wake not only depends on parameters that vary with wake region, but also on the actual geometry, and it is unlikely that a single model can capture all aspects of flows through such structures.

However, limiting to regular truss towers with typical braces; it could be possible to find an improved model. As a starting point, one might consider to represent nonlinear wake interaction effects in a parametric way. Together with longer time series with turbulent inflow with well-known spectral properties, further numerical research could give indications of how to realize this.

In the future we plan to study how this will affect the fatigue experienced by the wind turbine blades, to provide a more detailed study of the subjects discussed in this paper.

ACKNOWLEDGEMENTS

A travel grant from Statoil to attend the ISOPE conference is gratefully acknowledged. The work of MM was financed by the Norwegian Research Council under the RAVEN project (BIP no. 193326).

REFERENCES

Blevins, RD (1990). *Flow-Induced Vibrations,* Van Nostrand Reinhold, 450 pp.

Bossanyi, EA (2009). *GH Bladed theory manual,* Technical Report 282/BR/009, Garrad Hassan and Partners Limited, Bristol, 111 pp.

Breton, SP, and Moe, G (2009). "Status, plans and technologies for offshore wind turbines in Europe and North America," *Renewable Energy*, Vol 34, pp 646-654.

Fredheim, A (2006). *Current forces on net structures,* PhD thesis, Department of Marine Technology, NTNU, Trondheim.

Jonkman, J, Butterfield, S, Musial, W, and Scott, G (2007). *Definition of a 5-MW Reference Wind Turbine for Offshore System Development,* Technical Report NREL/TP-500-38060, National Renewable Energy Laboratory, Golden.

Long, H, and Moe, G (2007). "Truss type towers in offshore wind turbines", *Proceedings of European Offshore Wind Conference* (EOW 2007).

Menter, FR (1994), "Two-equation eddy-viscosity turbulence models for engineering applications," *AIAA J*, Vol 32, pp 1598-1605.

Nelder, JA, and Mead, R (1965). "A simplex method for function minimization", *Comput J*, Vol 7, pp 308-313.

Ong, MC, Utnes, T, Holmedal, LE, Myrhaug, D, and Pettersen, B (2009), "Numerical simulation of flow around a smooth circular cylinder at very high Reynolds numbers", *Marine Structures*, Vol 22, pp 142-153.

Pope, S (2000). *Turbulent flows,* Cambridge University Press, 771 pp.

Powles, SRJ (1983). "The effect of tower shadow in the dynamics of a horizontal-axis wind turbine," *Wind Engineering*, Vol 7, pp 26-42.

R Development Core Team (2009), "*R: A Language and Environment for Statistical Computing,"* R Foundation for Statistical Computing, Vienna. Software available at http://www.r-project.org/.

Salim, SM, and Cheah SC (2009). "Wall y+ strategy for dealing with wall-bounded turbulent flows", *Proc. Int. Multi-Conference Eng Comp Sci 2009* (IMECS 2009), Vol II.

Schlichting, H, and Gersten K (2000). *Boundary-Layer Theory,* Springer, 799 pp.

Shinozuka, M (1972). "Digital Simulation of Random Processes and its Application", *J Sound Vibration*, Vol 25, pp 111-128.

Veers, PS (1988), *Three-Dimensional Wind Simulations,* Technical Report SAND88-0152, Sandia National Laboratories, Albuquerque, 36 pp.

Venables, WN, and Ripley, BD (2002). *Modern applied statistic,* Springer, 501 pp.

Warschauer, KA, and Leene, JA (2009). "Experiments on mean and fluctuating pressures of circular cylinders at cross flow at very high Reynolds numbers,". *Proc. Int. Conf. Wind Effects Buildings Structures*, Tokyo, pp. 305-315.

Williamson, CHK (1996). "Vortex dynamics in the cylinder wake", *Annu Rev Fluid Mech*, Vol 28, pp 477-539.

Zdravkovich, MM (1997). *Flow around circular cylinders. Vol I: Fundamentals.* Oxford University Press.

Paper 5

Resolution of tower shadow models for downwind mounted rotors and its effects on the blade fatigue

By Marit Reiso and Michael Muskulus

Submitted to: Journal of Physics: The Science of Making Torque from Wind, Conference Series XX (2012), IOP Publishing.

Resolution of tower shadow models for downwind mounted rotors and its effects on the blade fatigue

M Reiso and M Muskulus
Department of Civil and Transport Engineering, Norwegian University of Science and Technology, Høgskoleringen 7a, 7491 Trondheim, Norway

E-mail: marit.reiso@ntnu.no

Abstract. A simulation study on the wind field resolution in computer load simulations has been conducted, both in transversal/vertical and longitudinal direction, to determine the effect on blade fatigue loading. Increasing the transversal/vertical resolution decreased the loading significantly, while only small changes to the load, at very low frequencies were found for increased longitudinal resolution. Next the influence of the tower shadow for a downwind mounted rotor was investigated, with respect to blade fatigue loading. The influence of different components to the total tower shadow effect was studied, both for a monopile and a truss tower, latter at inclination 0 and 22.5 degrees with respect to the incoming wind direction. Four components were considered, both individually and in combinations: mean wind speed, mean velocity deficit, unsteady motions from vortex shedding, and turbulence. The mean velocity deficit and turbulence were the main contributors to blade fatigue loading, and the unsteady motions can be neglected for the truss tower. For the monopile, neglecting the unsteady motions resulted in an underestimation of fatigue loading in the order of 3 percent.

1. Introduction

The classical wind turbine configuration, i.e., an upwind mounted rotor on a monopile tower, might be challenged by other configurations when going offshore where the installation costs are higher and the maintenance level is restricted due to access and weather windows. E.g. using a downwind mounted rotor has the advantage of reducing the root flapwise bending moment (RFM), as the blades cone away from the tower [1].

With a rotor mounted on the downwind side, the tower will introduce a shadow region onto the blade as it passes behind the tower. The tower shadow becomes more transparent if one uses a truss type tower instead of the traditional monopile tower. To simulate the effect of the tower shadow currently existing software approximates the wind field behind such a truss tower using a deterministic mean velocity deficit. Varieties of Powles' model [2] are the most commonly used to calculate the tower shadow. The drawback with Powles' model is that the user needs to choose the parameters for tower deficit and tower wake width. As these are often not known in advance it could cause discrepancies to the actual wind load if chosen incorrectly. Even if the parameters are chosen correctly it has been shown that Powles' model still is not fully able to reproduce the actual flow field behind the towers, including speed up on the sides of the towers and for the more complex truss tower configurations also underestimating the central wakes with as much as 20 percent [3] [4]. Latter indicating that the interaction between the truss tower members is also crucial to the total wake and Powles' model simply adds the contributions from each single truss tower member without

considering their interaction. As the blade experiences an impact like load due to the disturbance in the wind field caused by the tower structure as it passes behind the tower, an underestimation of this disturbance could have fatal consequences overestimating the lifetime of the wind turbine blade.

The tower shadow effect is really a dynamic phenomenon, but we currently only use static tower shadow models, i.e., for the mean velocity deficit. Here we also study different ways of extending these models to include more dynamical effects, and assess their importance for fatigue of rotor blades. These dynamic effects are included through time series obtained by computational fluid dynamic simulations, CFD, and are further imported through a turbulent wind file into the commercial software tool Bladed to study the unsteady motions behind such a support structure and how these affect the turbine. The present paper also shows that these effects can be approximated adjusting the turbulence intensity values (TI), through an up-scaling of the turbulent fluctuations present in the wind directly behind the towers.

In load simulations turbulent wind fluctuations are typically resolved at discrete points across the rotor disc. These typically have a lateral resolution of 2-5 m, which is thought to be sufficient as high-frequency turbulent fluctuations are averaged out spatially along the blade on a scale of about 10m. However, to the best of our knowledge this has not been studied systematically. Therefore a simulation study has been included herein to show how the blade loading is affected by changing the wind field resolution, both in transversal/vertical and longitudinal direction. Results are given as damage equivalent loads (to allow for comparisons, without a fully detailed assessment of fatigue lifetime) of root flapwise moments for the NREL Offshore 5-MW Baseline Wind Turbine [5].

The influence of the resolution of the velocity grid is studied here both for the one component Kaimal spectrum and for the total wind field obtained from CFD simulations of a full-height truss tower, as well as for a monopile tower [3] [4].

2. Material and methods

The study was conducted in two parts. The first part is a resolution study, performed with a typical turbulent wind field, and with an unsteady tower shadow model. The second part is a study of the impact of different wind field components on damage equivalent loading (DEL) on the RFM.

2.1. Wind turbine

The wind turbine used in the present study was based on the NREL Offshore 5-MW Baseline Wind Turbine [5]. The turbine was changed from an upwind to a downwind configuration, and some of the simulations were run using a truss tower instead of the conventional monopile tower; the truss tower is based on [6]. Shaft tilt and cone angles were adjusted from 5 and 2.5 degrees, to 2 degrees each.

Table 1. Parameters for the turbulent wind fields.

Turbulence model	One-dimensional Kaimal
Width of field [m]	150/130
Number of points across [-]	1503/750/300/100/50/40/30/20/10
Height of field [m]	200/150/130
Number of points in vertical	10/20/30/40/50
Length of field [m]	1800
Along wind spacing [m]	0.06/0.12/0.24/0.48/1/2/4/8/17/31.5/63.2/133
Mean wind speed [m/s]	12
Simulation time [s]	150
Longitudinal turbulence length scale:	
Longitudinal [m]	340.2
Transversal [m]	0.1
Vertical [m]	0.1
Longitudinal turbulence intensity [%]	10

2.2. Wind field

The one dimensional Kaimal model was used to generate a three dimensional wind field (Table 1).

For the tower shadow a numerical study was previously conducted, in which the detailed flow field behind a conventional monopile and a truss tower was investigated for two dimensional cross sections [4]. Results were output in the form of time series for a distance 3D (D=4m being the monopile diameter) behind the tower centres, corresponding to the approximate position where the rotor will pass. Two different configurations of the truss tower, aligned with the flow, and at an angle of 22.5 degrees (not shown), were considered, latter representing the more frequent positioning of the rotor behind the tower (not fully aligned at e.g. 0 degrees), Figure 1. Results included wind velocity and turbulent kinetic energy, and were obtained for 30 seconds flow time at 200 Hz resolution. This corresponds to 6000 time steps, of which the first 1000 were neglected. Only one wind speed (12 m/s) was considered.

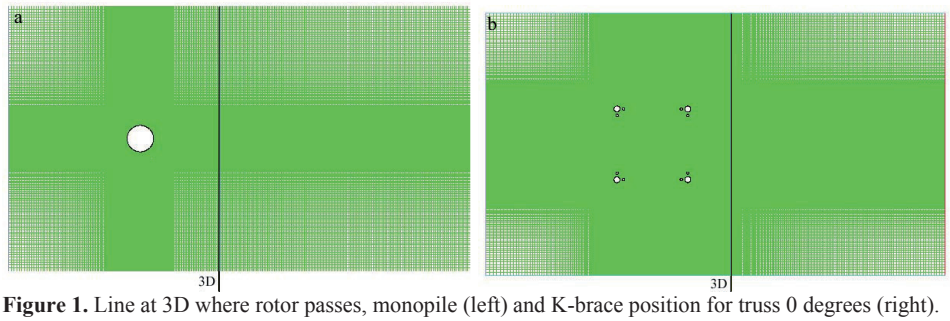

Figure 1. Line at 3D where rotor passes, monopile (left) and K-brace position for truss 0 degrees (right).

Wind turbine load simulations require three dimensional wind fields, this was achieved by reusing the two dimensional time series at different vertical positions (with random offsets in the time series). For the truss tower two different cross sections were combined (close to X- and K-brace position, Figure 2) and the cross section closest to each vertical grid position was used. The series were also looped in time. To avoid artificial increases in loading, the first and last values were compared to see if there would be a large change at the transition point, no such deviation was found and the time series were simply re-looped.

The domain of the CFD simulations extended 40m in transversal direction (corresponding to 401 grid points) with the tower placed in the centre. This domain was embedded in a larger domain of size 150m in the transversal direction (corresponding to 1503 grid points), to encompass the entire rotor (Figure 3). In the vertical direction ten discrete layers of the CFD simulations were used (at 10m spacing). Additional ten layers of pure turbulence were included to encompass the entire rotor in the vertical direction, total vertical domain spanning 200m (Figure 3).

The wind speed at the lateral boundaries of the computational domain was slightly higher than the free stream velocity of 12m/s, this was most likely an artifact due to the presence of periodic boundaries in the CFD simulations [4]. To correct for this, the observed offset from 12 m/s at the domain boundaries was subtracted from the velocities, to avoid artificial discontinuities when embedding into the larger domain. These offsets were 0.27 m/s, 0.47 m/s and 0.48 m/s for the monopile, and the truss towers at 0 and 22.5 degrees, respectively.

The combined wind fields including both the realization of the Kaimal spectrum and the tower shadow were assembled using MatLab (The MathWorks, Inc.; R2012a). As the highest transversal resolution that could be obtained for the Kaimal spectrum was 50 points across the domain, the spectrum was first interpolated to obtain a total of 1503 points across, using the *meshgrid* function in MatLab (above 50 grid points the interpolation systematically underestimates the fluctuations). Secondly stochastic realizations from the Kaimal spectrum (with unit standard deviation) were scaled by the standard deviation (derived from the local TI values resolved by the k-ω sub-grid

parameterization) for each point in time and space, where the boundary values from the k-ω sub-grid parameterization were used to extend the total CFD domain from 40 to 150m. Further the absolute value of the mean velocity deficit and unsteady motions were added across the central part of domain (Figure 3) before the total wind field was normalized and compiled into a wind file that could be used directly in the software Bladed (Version 4.2, GL Garrad Hassan; Bristol, UK). An exponential vertical wind shear component of 0.14 was used. Total simulation time was 150 seconds, where the first 30 seconds were used for initialization purposes and discarded from the output to remove the initial transient.

As the highest wind field resolution file (1503 transversal points, 20 vertical points and 200Hz longitudinal) exceeded the maximum array size MatLab could store in memory, the wind files were processed in six parts.

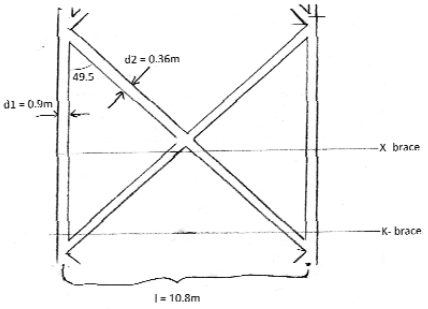

Figure 2. X- and K-brace positions shown on a side panel of the truss tower.

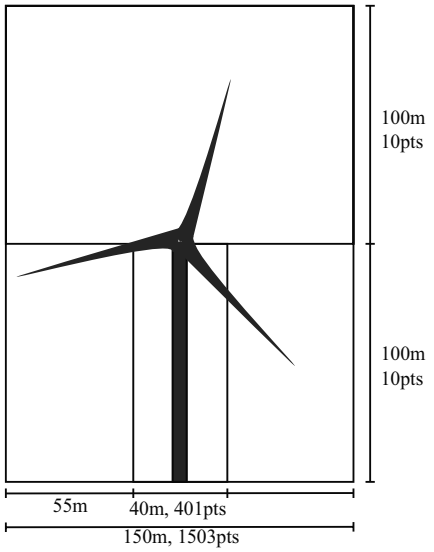

Figure 3. Wind field domain (fixed size) with maximum grid resolution, CFD domain at bottom centre (40m times 100m).

2.4. Resolution study

How both the spatial and temporal resolution changed within the resolution limitations of the software was investigated both for turbulent wind, and for the unsteady tower shadow.

Table 2. 12 longitudinal and five lateral/vertical resolutions combined to obtain 60 different turbulent resolution combinations.

Longitudinal [Hz]			
0.09	0.7	6	50
0.19	1	12	100
0.38	3	25	200
Number of grid points (transversal/vertical)			
10/10		40/40	
20/20		50/50	
30/30			

Table 3. Five longitudinal resolutions (transversal resolution fixed at 1503) and six transversal resolutions (using the longitudinal resolution result) were used for the wind field including the unsteady tower shadow.

Longitudinal [Hz]	
12	100
25	200
50	
Number of grid points (transversal)	
40	300
50	750
100	1503

2.4.1. Resolution of turbulent wind field. For this study five lateral and vertical resolutions and 12 longitudinal resolutions were combined to obtain a total of 60 cases (Table 2).
All simulations were run using a downwind rotor with no tower shadow effect. Linear interpolation between grid points was used to achieve a common output time step of 0.005s (corresponding to the 200Hz case) for all simulations. Four different turbulent seeds were used to obtain a better estimate. A domain size of both 150x150m and 130x130m were included.

2.4.2. Resolution of wind field including unsteady tower shadow. First the longitudinal resolution was assessed, using five different longitudinal resolutions with 16 different turbulent seeds (transversal resolution kept constant at 1503 points) and output time step of 0.005s. Results from the longitudinal resolution study were thereafter used with the six transversal resolutions (Table 3).

The resolution study for the tower shadow on the downwind rotors was based on the most complex flow pattern, including CFD mean velocity deficit, unsteady motion and k-ω sub-grid parameterization as well as the one component Kaimal spectrum.

2.5. Wind field component influence study
The second part of this paper separates the contributions of the complete wind field into four different components; mean wind speed, mean velocity deficit, unsteady motions and turbulence across the rotor plane to address their separate and interacting contribution to DEL varying in time and space on the RFM (Table 4).

In addition a simplified method for representing the tower shadow has been included, through an increase in the mean TI (3B*, Table 4). This would, if applicable limit the time consuming CFD simulations to short dynamic studies for the relevant tower structure.

The recommended resolutions found in the resolution study of the wind field including the unsteady tower shadow were used here.

Table 4. Wind field components.

Wind field component	Description of wind field component
0	Mean wind speed
1	Mean velocity deficit
2	Unsteady motions (CFD)
3A	Turbulence (Kaimal spectrum)
3B	Turbulence (Kaimal spectrum) with different turbulence intensity, TI (averaged) for each lateral point
3B*	Same as case 3B with increased TI (including case 2)
3C	Turbulence (Kaimal spectrum) with different TI for each lateral point and time step

3. Results and discussion

3.1. Resolution study
Time domain simulations are time consuming but although necessary for wind turbine analysis in the last design phase. The presented results show how decreasing simulation time through reducing grid resolution affects the load accuracy.

3.1.1. Resolution of turbulent wind field. The DEL on the RFM based on loads from the turbulent wind field (without tower shadow effects) show similar values across the different longitudinal resolutions for the same transversal resolutions (Figure 4), except at 0.09Hz (transversal grid point resolution 10x10), where a 3 percent lower mean DEL was found compared to the 200Hz case. Hence using a resolution of at least 1Hz is recommended for including the full effect from the turbulent wind.

The transversal resolution exhibits a different behaviour with the DEL progressively decreasing by 19 percent (from 10x10 to 50x50 transversal and vertical grid points). It was not possible to

investigate higher resolutions on the 150x150m domain, so results might still change somewhat for increasing resolutions. For the 130x130m domain the grid point resolution increased by 13 percent (compared to the 50x50 grid points on the 150x150m domain), while the average DEL only decreased by 2 percent. The blade is more severely fatigue loaded at the lower transversal grid resolutions, where the load is more constant across the blade length (Figure 4). A resolution of at least 50 points is recommended to include the effect from the turbulent wind. Preferably this should be increased but the software resolution had a limit of 50 grid points.

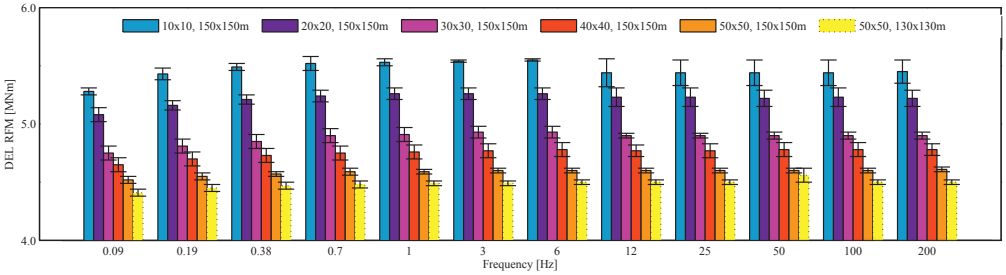

Figure 4. DEL on RFM with changing longitudinal and transversal resolutions for the wind field based on the one component Kaimal spectrum (no tower shadow present). Frequencies increase from 0.09Hz to 200Hz and grid point resolution from 10x10 to 50x50 points across domains of 150x150m and 130x130m.

3.1.2. Resolution of wind field including unsteady tower shadow. The longitudinal resolution does not change the DEL on the RFM by much; the maximum difference in mean DEL is 2 percent at 50Hz (with respect to the 200Hz case for the monopile). Although due to the increased complexity of the wind field a resolution of at least 25Hz is required to re-capture the DEL at 200Hz (Figure 5a, c, e).

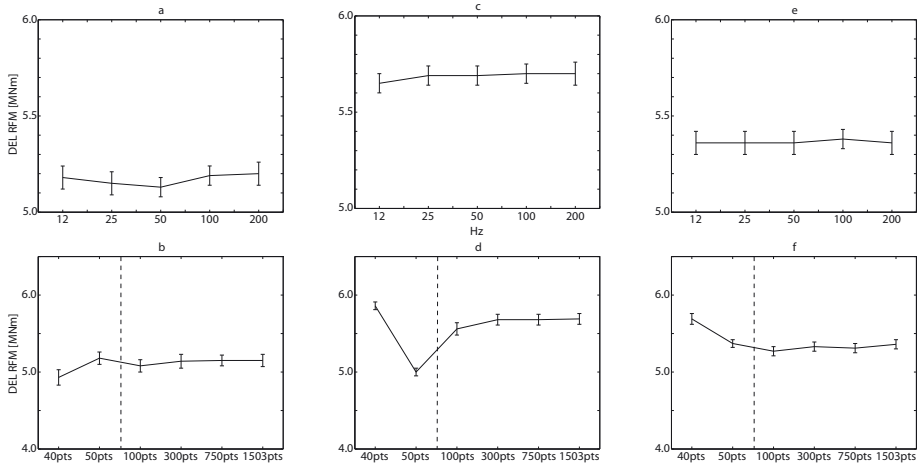

Figure 5. DEL for longitudinal (top) and lateral tower shadow resolutions (bottom). Left monopile tower, middle truss tower at 0 degrees and right truss tower at 22.5 degrees (dotted line show transition into interpolated turbulence).

The higher DEL at 40 versus 50 points in both truss tower setups is in agreement with the results from the turbulent wind field resolution (resolutions beyond 50 points is obtained through linear interpolation, making 50 points the highest turbulent resolution). The low transversal resolution at 50 points could be too coarse to fully represent the narrow truss tower members, which causes a significantly lower DEL for the truss tower at 0 degrees (Figure 5d). A transversal resolution of at

least 300 points across the domain is required to re-capture the DEL on the RFM at 200Hz (Figure 5b, d, f).

3.2. Wind field component influence study

All cases were run at a mean wind speed of 12m/s, which has been isolated in case 0 (Figure 6), showing a DEL on the RFM of 3.42MNm, arising mainly from oscillating gravity and centrifugal forces as the blade rotates on the rotor plane at a frequency of 1P (corresponding to 0.2Hz at 12.1rpm).

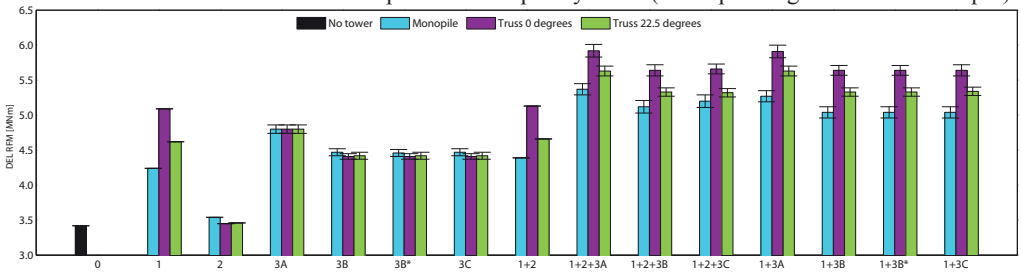

Figure 6. DEL on RFM behind monopile, truss 0 and truss 22.5 degree towers. Complexity of wind field increasing from left to right. All results presented at longitudinal resolution 25Hz and transversal and vertical grid resolutions 300 and 20 respectively, error bars showing standard deviation of the mean (details on wind field complexity components in Table 4).

Introducing a mean velocity deficit behind the tower increases the DEL in the range of 25 to 50 percent (from case 0) for the three tower setups (case 1, Figure 6). The truss tower at 0 degrees exhibits a 20 percent higher DEL than the monopile tower. This points in the direction of although more transparent, the truss tower covers a larger cross sectional area (11.7m versus 4m for the monopile) with deeper throughs which contributes more to the DEL than the solid monopile (Figure 7a, c). But at 22.5 degrees the truss tower covers an even larger cross sectional area (15.7m) exhibiting only a 9 percent higher DEL compared to the monopile. So the DEL on the RFM is higher for the truss tower aligned at 0 degrees than for the staggered trusses at 22.5 degrees (off by 10 percent), Figure 7c, e, as the aligned trusses magnify the deficit from each of the legs, while the staggered arrangement smoothens the deficit.

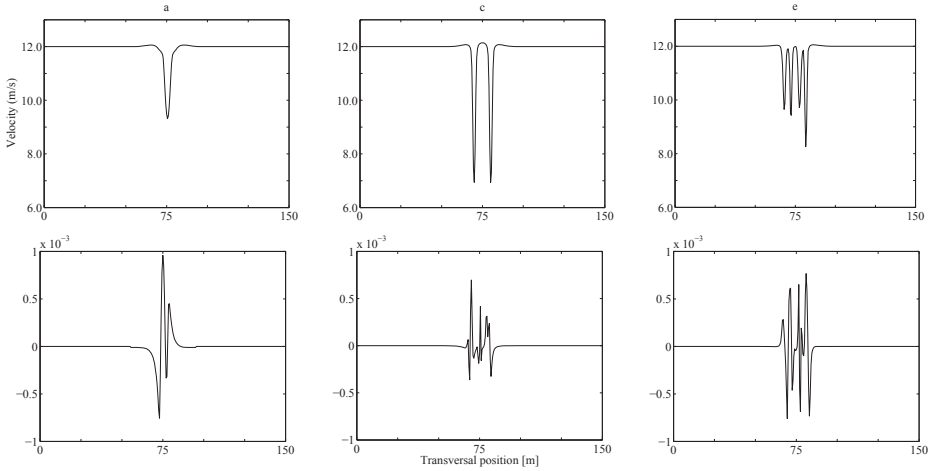

Figure 7. Mean velocity deficit (top) and time averaged unsteady motions (bottom) for monopile (left), truss 0 (middle) and truss 22.5 degrees (right).

For the unsteady motion (case 2) the picture is different from case 1, with the DEL being only 1 and 4 percent higher than in case 0 for the truss and monopile towers respectively. This means that the

vortex sheddings arising from the tower structures are not that important when it comes to the fatigue loading on the blades. From Figure 7b, d, f one would expect to see a larger effect on the DEL from the unsteady motions than what is present in Figure 6 (case 2). This means that the influenced area is too small compared to the total rotor plane and the passing frequency of the blade. Combined case 1+2 also reflects this, with case 1+2 only accounting for additional 1 and 3 percent DEL for the truss and monopile towers, respectively (compared to case 1).

Case 3A represents the turbulent wind field (no tower shadow present) and results in a DEL of 4.80MNm for all three tower configurations, corresponding to a 40 percent increase in DEL compared to the mean wind speed (case 0). Including the turbulence from the k-ω sub-grid parameterization (case 3C) the mean DEL decreased by 8 and 7 percent for the truss and monopile towers, respectively, similar finding also in case 3B and 3B*. This indicates a conservative approach for the tower shadow representation in commercial software methods (using 3A).

For the truss towers the full dynamic simulations (case 1+2+3C) can be approximated using the time averaged TI from the k-ω parameterization. While the monopile tower needs to include the unsteady motions to avoid a three percent underprediction of the DEL on the RFM.

The overall picture for the combined cases 1+3A/B/C and 1+2+3A/B/C is that the mean tower shadow deficit and the Kaimal spectrum are the main contributor to the DEL on the RFM, with the Kaimal spectrum increasing the averaged mean DEL by 13 and 4 percent (compared to case 1) for the monopile tower and truss tower at 22.5 degree, respectively, while a decrease of 6 percent was found for the truss tower at 0 degrees.

4. Conclusion

The turbulent wind field resolution study recommends longitudinal and transversal/vertical resolutions of at least 1Hz and 50 points across the domain to include the full effect of the turbulent wind. For the wind field including the tower shadow these resolutions increase to 25Hz and 300 points across the domain.

The most interesting result from the wind field component influence study was that the most complex case (1+2+3C) for the truss tower could be approximated using an averaging of the turbulence from the k-ω sub-grid parameterization, case 1+3B, while the same approximation for the monopile tower resulted in an underestimation of DEL of 3 percent.

Preferably one would like to run three dimensional CFD simulations both to get a correct shape of the tower (smaller diameter at top could cause different loading on the blade) at the different elevations (here looked at leg spacing of 10.8m corresponding to blade length position 1/3 from the blade root) and to be able to capture all three dimensional effects.

5. References

[1] Reiso M and Moe G 2010. *Blade response on offshore bottom fixed wind turbines with down-wind rotors.* In Proceedings of the ASME 29th International Conference on Ocean, Offshore and Arctic Engineering, 499-504.

[2] Powles SRJ 1983. The effect of tower shadow on the dynamics of a horizontal-axis wind turbine. *Wind Engineering*, **7** 26-42.

[3] Hagen T, Reiso M and Muskulus M 2011. *Numerical analysis of turbulent flow past a truss tower for offshore downwind turbines*. In Proceedings of the ISOPE 21st International Offshore and Polar Engineering Conference, 319-326.

[4] Hagen T, Reiso M and Muskulus M 2011. *Numerical tower shadow modeling for a downwind wind turbine truss tower*. In Proceedings of the ASME 30th International Conference on Ocean, Offshore and Arctic Engineering, 859-870.

[5] Jonkman J, Butterfield S, Musial W and Scott G 2009. *Definition of a 5-mw reference wind turbine for offshore system development*. NREL Technical Report NREL/TP-500-38060, National Renewable Energy Laboratory, Golden, CO.

[6] Long H, Fischer T, Moe G 2009. *Design methodology and optimization of lattice towers for offshore wind turbines in 35m water*. In Proceedings of EWEC, Marseilles.

Paper 6

The simultaneous effect of a fairing tower and increased blade flexibility on a downwind mounted rotor

By Marit Reiso and Michael Muskulus

J. Renewable Sustainable Energy 5, 033106 (2013); doi: 10.1063/1.4803749.

JOURNAL OF RENEWABLE AND SUSTAINABLE ENERGY **5**, 033106 (2013)

The simultaneous effect of a fairing tower and increased blade flexibility on a downwind mounted rotor

M. Reiso[a] and M. Muskulus
Department of Civil and Transport Engineering, Norwegian University of Science and Technology (NTNU), Trondheim 7491, Norway

(Received 3 January 2013; accepted 19 April 2013; published online 3 May 2013)

This is a parametric study on how blade and tower loads for a prototypical downwind offshore wind turbine are affected as the tower geometry and blade properties are changed. Downwind turbines have the potential to reduce the cost of energy, as blades can be more flexible and lighter, but the tower shadow induces additional structural vibrations. In order to reduce the latter, a fairing around the tower has been introduced. The length of the fairing is varied, adjusting the rotor overhang accordingly. Additionally, the blade weight and stiffness are adjusted. The blade and tower fatigue loads are, thereby, significantly decreased. In the first case, a maximum reduction of 8% and 28% (for the blade root bending and tower bottom moment, respectively) was achieved, compared to a downwind version of the National Renewable Energy Laboratory (NREL) 5 MW reference wind turbine on a monopile tower. Using softer and lighter blades resulted in loads even lower than for the conventional upwind rotor of the NREL turbine, up to 5% and 13% less for the blade and tower fatigue loads, respectively. The increased overhang increased the mean tower bending moments, suggesting that an optimal downwind turbine needs to be designed with a compromise between these fatigue and ultimate loads. The power production stayed approximately the same as that of a conventional wind turbine or was slightly higher. © *2013 AIP Publishing LLC*. [http://dx.doi.org/10.1063/1.4803749]

I. INTRODUCTION

Offshore wind turbines are becoming more common as land sites applicable for wind turbines are decreasing due to already developed areas. Offshore, the mean wind speeds are higher than onshore and larger wind turbines can be installed as transportation is less problematic. Using larger MW size wind turbines results in benefits from the "economy of scale," as fewer turbines are needed to obtain the same total power production. This is beneficial from a foundation point of view, as foundation costs increase significantly in the offshore environment.[1,2]

What has been the trend so far has been to use the same technology offshore as onshore, only up-scaled to larger size turbines, using a monopile tower with an upwind mounted rotor. By using geometric up-scaling, an increased blade length gives an energy capture that increases with the swept area (i.e., the square of the blade length), while the blade weight increases with the cube of the blade length.[3,4] Taking the actual development in blade design into account, the observed exponent is somewhat lower.[5] Still, there might be potential for further reduction of the cost of energy (COE) by using new technologies and alternative configurations.

Here we consider changing the rotor configuration from the conventional upwind design to a downwind mounted rotor, which for most normal operational conditions makes the downwind turbine much less affected by the risk of the blades striking the tower. Historically, relatively stiff two-bladed steel rotors with a hinged connection to the main shaft were used in downwind

[a]Author to whom correspondence should be addressed. Electronic mail: marit.reiso@ntnu.no

turbines,[6] as an alternative to traditional upwind designs. With the large self-weight of the rotor, a hinged connection to the main shaft was needed to relieve blade bending moments. Because of noise emission issues and stronger structural requirements on their towers, downwind rotors were eventually replaced by upwind three bladed rotors onshore. With today's technology, lighter composite blades are available, so the weight issue is not so critical anymore. In fact, for downwind machines the blades can be softer and more compliant compared to their upwind counterparts,[7] and the downwind design should be reconsidered.[8]

The main challenge for a downwind mounted rotor is the tower shadow that the blade is subjected to once per revolution, which induces increased fatigue loads onto the blade and the remaining structure. In order to be competitive with the upwind configuration, it is necessary to reduce the tower shadow effect, e.g., by using a different tower geometry. Hagen *et al.*,[9] Hagen *et al.*,[10] and Reiso *et al.*[11] showed promising results with a truss type tower instead of the conventional monopile tower. Blade fatigue loads were also found to decrease.[12]

Another way to reduce the blade loading is to use a fairing around the tower. Thereby, blade lift and drag coefficients and mean normal force can be decreased.[13,14] Experiments performed by Wilmshurst *et al.*[15] for teetered and cantilevered rotors showed that also fatigue loads are typically decreased. However, if using a fairing all the way up to the nacelle, the rotor overhang will have to be increased to avoid the rotor hitting the fairing at hub height.[13] This could increase tower costs due to increased mean tower bending moments. A compromise is to use a fairing mounted for parts of the tower (not all the way up to the nacelle).

In the present study, the effect of different lengths of fairing on wind turbine performance was evaluated. This was additionally studied in combination with softer and lighter blades of varying degrees.

II. MATERIAL AND METHODS

Numerical models of wind turbines were used to simulate the effect of the different variables on the forces acting on the tower and blades as well as the energy production. Different wind turbine towers were included and the blade stiffness and weight adjusted.

A. Wind turbine

The offshore 5-MW baseline wind turbine from National Renewable Energy Laboratory (NREL) was used in the simulations.[16] The rotor was changed into the downwind position, and the blade stiffness and weights were adjusted (see Sec. II D). For comparison, the original upwind NREL reference was included (further referred as the NREL reference).

B. Fairing

A fairing was applied around the monopile tower in order to change the aerodynamic properties of the wind field behind the tower. The fairing was not physically included in the simulation model (i.e., the structural model was implemented with the monopile tower), but its effect on the flow field was implemented in the wind velocity time series, used in the wind turbine simulations (see Sec. II E). A constant tower diameter of 4 m was used, both for simplicity as well as for avoiding dealing with Reynolds number dependence. Using the symmetric NACA 0030 airfoil (with a thickness of 4 m) resulted in a chord length of 13.3 m. The fairing was neglected in the structural model, because the focus of this study was to primarily study the influence of the fairing on the rotor loads. Although the structural model is, therefore, not completely realistic, it nevertheless gives a good indication of the changes in loading pattern at the tower bottom. Note that the eigenfrequencies of the tower are, therefore, the same for all cases, which facilitates the comparison of the loads.

For the fairing, the largest thickness was taken at 25% chord and the center of the monopile was, thereby, aligned at this position (Fig. 1). To avoid the blade hitting into the tower, the rotor overhang (using the fairing with chord length 13.3 m) would need to be 13.0 m (versus 5.0 m for the original NREL reference).

To decrease the rotor overhang, a strut instead of a full airfoil fairing around the tower was used, Fig. 1 (for wake behavior and how it was implemented in the wind velocity time series, see Sect. II C). Bairstow[17] has shown that for chord to thickness ratios from 2.5 to 3.5 the drag coefficient is roughly the same as for the full fairing (ratio of 3.3 for the NACA 0030 profile); the ratio for the strut was chosen to be 2.5 (keeping the drag coefficient unchanged). This gave a strut chord length of 10.0 m, reducing the rotor overhang from 13.0 m down to 9.7 m, with a maximum thickness still at the same absolute length from the leading edge (Fig. 1).

The fairing was taken off (using the original monopile tower instead) section by section; 10 m by 10 m starting from hub height (F40-100) down past the point on the tower where the rotor tips would pass (F40-50). As the blades were both coned (2.5°) and tilted (5.0°) away from the tower, the clearance between the tower and blade increased as going down the tower from hub height. This was taken into account when decreasing the rotor overhang for the shorter fairing lengths, Table I.

The fairing would rotate with the yaw bearing, to ensure alignment with the rotor plane, and was assumed to be aligned with the wind direction in the simulations. Simulations were carried out at a free stream wind velocity of 12 m/s, corresponding to the wind turbines' rated wind speed where the highest loading on the blade root in flapwise direction would occur. Above rated wind speed, the blades start pitching out of the wind, and hence also the largest wind loads transferred onto the tower (through the thrust force) will be found at about 12 m/s.[8]

C. Tower shadow

Mean velocity profiles were used to describe the tower dam and shadow effects for the upwind and downwind rotor configurations, respectively. For the NREL reference, these were derived by assuming potential flow,[18] which is the current standard in wind turbine simulations.

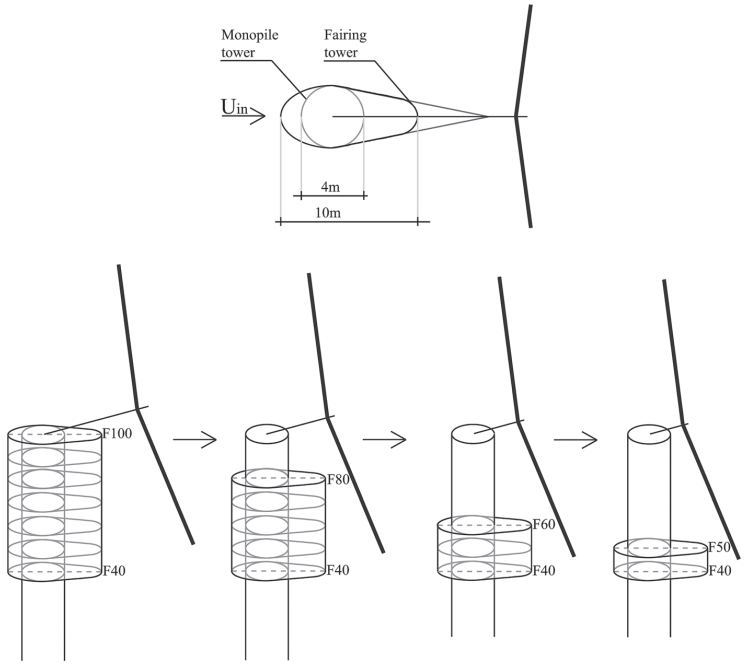

FIG. 1. Top: top view of the wind turbine with the monopile in the center and the tower fairing, aligned with the free stream wind velocity, U_{in}; bottom: side view with the fairing taken off for some of the sections, with the rotor overhang reduced accordingly.

TABLE I. Rotor overhangs for all 8 cases studied: all 6 fairing cases, and up- and downwind rotors without fairing (for comparison).

Tower	Fairing F40-50	Fairing F40-60	Fairing F40-70	Fairing F40-80	Fairing F40-90	Fairing F40-100	Monopile, up- and downwind
Rotor overhang	5.0 m	5.0 m	5.8 m	7.1 m	8.4 m	9.7 m	5.0 m

The tower shadow for the downwind rotor was implemented using Powles' semi-empirical model,[19]

$$V = V_0\left(1 - \Delta\cos^2\left(\frac{y}{2W}\pi\right)\right), \tag{1}$$

for the mean wind speed V at each lateral position y, relative to the free stream velocity V_0. The two parameters Δ and W denote the mean velocity deficit at the centerline and the tower shadow wake width, respectively.

In the JET wake model by Madsen *et al.*,[20] the mean wake deficit is calculated for a cylinder by combining potential flow with the boundary layer solution for a jet flowing into a fluid at rest. These calculations show that the drag coefficient fully determines the wake deficit, and this is assumed to be also approximately valid for an airfoil. Since Bairstow[17] showed that the drag coefficient is roughly the same for a shorter strut, the values of wake width and velocity deficit measured by Wilmshurst *et al.*[15] for the NACA 0030 airfoil were used, Table II. Thereby, it is assumed that the mean velocity deficit is the major contribution to the wind turbine fatigue damage, and that differences in unsteady and turbulent behavior originating from the tower geometry do not significantly affect the results.

It should be noted that the Reynolds number is a power lower ($\mathrm{Re} = 10^5$) for the experiment in Wilmshurst *et al.*[15] compared to the situation studied here ($\mathrm{Re} = 10^6$). The values of the tower shadow parameters are, therefore, only representative examples of what one can expect in terms of aerodynamic performance in this flow region.[21]

The position for which the tower shadow has been modeled is at three monopile diameter downstream from the tower center. This approximately corresponds to the blade position where the highest power production will occur (about 2/3 along the blade length), when the overhang, cone, and tilt angles are 5.0 m, 2.5°, and 5.0°, respectively. This was done for simplicity, and is a conservative approach that overestimates the loads by a maximum of 1%–2%.

D. Reduced blade stiffness and weight

For some of the simulations, mass per unit length, bending stiffness about both flapwise and edgewise directions as well as torsional stiffness of the blades were reduced (keeping the airfoil shape the same as for the NREL reference), similar to the approach used in Ahlström.[22]

Three different scenarios were studied, with a 10%, 15%, and 20% reduction in mass and stiffness with respect to the parameters of the NREL reference blade. This resulted in a total of 10 combinations, including the original NREL turbine blade. These are denoted by SxxWyy, where xx is the percentage reduction in stiffness (S) and yy is the percentage reduction in weight (W).

TABLE II. Tower shadow parameters for the monopile and fairing towers.

Parameter	Monopile tower	Fairing tower
Mean velocity deficit, Δ	0.5	0.15
Wake width, W	2	1
Reference position/width of tower	3	3

E. Wind file

The domain that the wind field covered, 150 m × 200 m, was discretized on a grid with 300 × 20 points in width and height, respectively, which has been found to be sufficient (including tower shadow effects) for capturing the main loading effects for a downwind mounted rotor.[23] The longitudinal resolution was 25 Hz. The simulation time was 150 s, instead of the usual 600 s (recommended in the relevant standards, with typical lateral resolutions of 32 × 32 points), to be within standard file size limits for these detailed wind field representations.

On top of the mean wind field, turbulent fluctuations were added from a one component Kaimal spectrum, Table III. In order to obtain more reliable results, 16 different realizations (random number seeds) were used. The resolution of the turbulence generator of GL GH Bladed was limited to 50 grid points across the transversal direction, and its output was therefore (linearly) interpolated on the larger grid. Such interpolation underestimates the true variation in the turbulent wind. However, these fluctuations are averaged out along the blade length to a large degree, and are also not crucial for the purpose of the study.

The turbulent wind field for each point in time and space was added to the results of the tower shadow models using an in-house MATLAB script (Math Works version R2012a).

F. Software

Wind turbine simulations were carried out using the commercial software Bladed (Version 4.2, GL Garrad Hassan Ltd; Bristol, UK). The 30 first seconds of the simulations were used for initialization purposes and discarded from the output to remove initial transients.

The tower shadow and tower dam effect (for the upwind rotor case) were included in Bladed by way of a "turbulent wind file," and not through the limited tower shadow models available in Bladed itself. This necessitated normalization to unit standard deviation, and using corresponding values for "turbulence intensity" in the software.

G. Post processing

Results are given as damage equivalent loads (DELs) for both the blade root flapwise bending moment (RFM) and the fore-aft tower base bending moment (TBM). For the rainflow counting, 128 bins were used with an inverse SN slope of 10 and 4 for the blades and towers, respectively. The equivalent frequency was 0.003169 Hz, corresponding to 2×10^6 cycles during the total lifetime of 20 years.

TABLE III. Wind field model parameters.

Width of wind field (m)	150
Number of lateral points (-)	50/300
Height of wind field (m)	200
Number of points in height (-)	20
Length of wind field (m)	1800
Longitudinal spacing (m)	0.48
Mean wind speed (m/s)	12.0
Simulation time (s)	150
Turbulence length scales:	
Longitudinal (m)	340.2
Transversal (m)	0.1
Vertical (m)	0.1
Turbulence intensity (%)	10

III. RESULTS

A. NREL blade

The fairing at the two outermost positions (F40-50 and F40-60, Fig. 2(a)) resulted in an increase of 20%–25% of the DEL RFM compared to the downwind monopile, while the longer fairing F40-70 shows a 5% increase in DEL RFM compared to the downwind monopile. For fairing lengths from F40-80 to F40-100, the DEL RFM is lower by 7%–8%, with no significant difference between fairing lengths of F40-90 and F40-100.

The same pattern was also found for the DEL TBM (Fig. 2(b)), with fairing lengths F40-50 and F40-60 exhibiting a 30%–40% higher DEL TBM, while the fairing at F40-70 shows no significant difference from the downwind monopile. Fairing lengths F40-80 to F40-100 result in a 20%–30% lower DEL TBM than found for the downwind monopile.

The reason for the increased DEL RFM and DEL TBM for the shorter fairings, F40-50 to F40-70 (compared to the monopile tower in the downwind configuration), is not known, but it can be hypothesized that the changes in impulse loading along the blade (much more pronounced changes in loading behind the monopile than behind the fairing during blade-tower passage) and their position are influential factors.

Still, all the downwind rotor configurations perform worse than the upwind NREL reference for the DEL RFM (Fig. 2(a)). This is slightly different for the DEL TBM, where fairing lengths of F40-90 and F40-100 exhibit an 11%–13% lower DEL TBM than the NREL reference. The different findings for the DEL RFM and DEL TBM with respect to the NREL reference are due to the increasing overhangs (i.e., the shaft length) for the enlarged fairing lengths

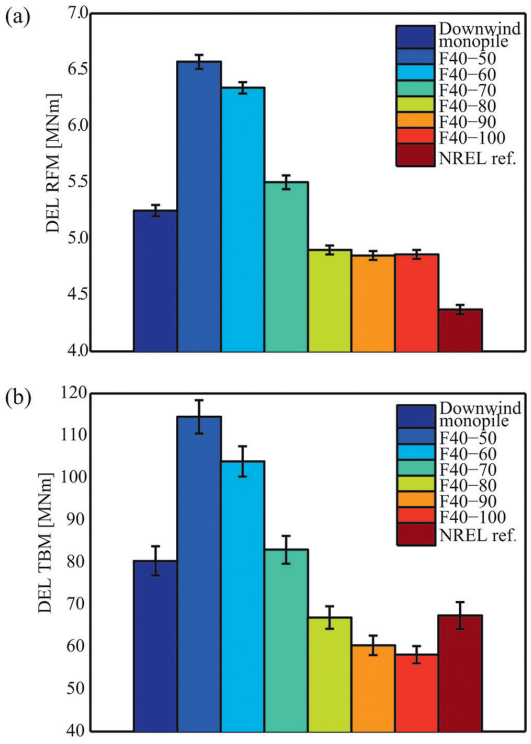

FIG. 2. DEL for (a) the blade RFM and (b) the TBM with respect to the different fairing lengths (F40-XX). The conventional NREL reference is included for comparison. These results are based on the original NREL blade.

and the mounting of the rotor, where the larger shaft length together with the downwind mounted rotor give a smaller aerodynamic impact onto the tower (DEL TBM) than from the more closely mounted upwind rotor (with the shorter shaft). For the DEL RFM, the tower shadow still impacts the downwind mounted rotors of the larger fairing lengths (with the larger overhangs) more than the tower dam effect experienced by the blades on the upwind mounted rotor.

B. Reduced blade stiffness and weight

The blade flapwise eigenfrequencies are kept constant within the blades with the same reduction in both blade stiffness and weight, i.e., S10W10, S15W15, and S20W20 (and hence equal to the NREL blade), Table IV, which also agrees with what Ahlström[22] reported. For the remaining combinations of blade stiffness and weight, the frequencies deviate by a maximum of 6% from the NREL eigenfrequency of 0.66 Hz. With a 3P frequency of 0.6 Hz, the lowest eigenfrequency of 0.62 Hz (for the S20W10 blade) is only 3% away from the 3P frequency, and also for the remaining adjusted blades, some resonance could occur and affect the results. The main factor is the combined effect of the flexibility and inertia of the blade, where the more flexible blade will deflect more to the impact-like load from the tower shadow, and will transfer less of the load to the blade root. Blade and tower loads will be discussed omitting the blade frequency influence.

The adjusted blade stiffness and weight classes (SxxWyy) show the same pattern within each SxxWyy class as the NREL blade for the downwind rotor with respect to the different fairing lengths. All adjusted blade classes show a significant decrease in the DEL RFM by 6%–15% compared to the downwind NREL blade (Fig. 3).

A 5% decrease in blade stiffness (from S10 to S15 and S15 to S20) decreased the mean DEL RFM by 1%–3%, while a 5% weight reduction (from W10 to W15 and W15 to W20) decreased the mean DEL RFM by 1%–2%.

For fairing lengths F40-80 and above, the DEL RFM was in the same range or significantly lower, compared to the conventional NREL reference, except for fairing F40-80 at S10W15 and S15W10 and all fairings at S10W10. Using a fairing tower in combination with a softer and lighter blade decreased the DEL RFM by as much as 5% compared to the NREL reference.

For the cases where the DEL RFM is lower than for the NREL reference, the DEL TBM is within the same range or lower, except for fairing length F40-80, where the DEL TBM is larger than for the NREL reference, by approximately 11% (Fig. 4(a)). This is likely from the same reason as explained for the DEL TBM with the NREL blades, where the downwind mounted rotor shaft length for fairing length F40-80 results in larger aerodynamic impact loads on the tower than the tower dam effect experienced by the upwind mounted rotor.

The lowest DEL TBM is found for the fairing F40-100 at S10W20, with a DEL TBM approximately 5% lower compared to the other SxxWyy classes and 13% lower than the NREL reference (Fig. 4(a)).

In contrast, for the mean and maximum TBM, all SxxWyy classes exhibit a 17%–23% higher mean TBM and 16%–19% higher maximum TBM than the NREL reference (Figs. 4(b) and 4(c), respectively). This is due to the downwind mounted rotor and the increased rotor overhang. These two effects (due to thrust force and rotor weight) give a positive contribution

TABLE IV. Blade flapwise eigenfrequencies (Hz) for the different blade stiffness (S) and weight (W) combinations.[a]

	S10	S15	S20
W10	0.66 Hz	0.64 Hz	0.62 Hz
W15	0.68 Hz	0.66 Hz	0.64 Hz
W20	0.70 Hz	0.68 Hz	0.66 Hz

[a]NREL blade eigenfrequency, 0.66Hz.

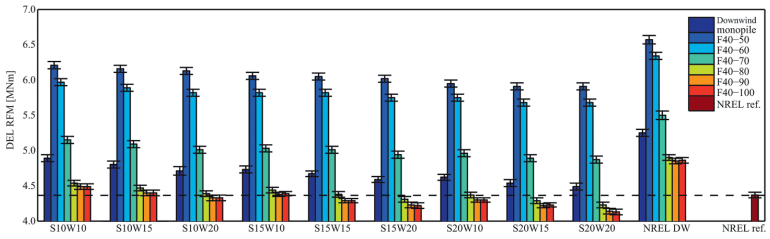

FIG. 3. DEL for the blade RFM with respect to the different fairing lengths (F40-XX) and adjusted blade properties. The conventional NREL reference is included for comparison. Blade stiffness and weight decreases from left to right. SxxWyy: xx percentage reduction in stiffness (S), yy percent reduction in weight (W). Dotted line gives the NREL reference value.

to the tower bending moment, while for the NREL reference the tower bending moment from the rotor weight counteracts that from the thrust force.

For fairing length F40-80, the mean TBM is lowered by 2% compared to F40-90, this is also the case going from F40-90 to F40-100, both effects arising from the change in rotor overhang. The decrease in mean TBM due to softer and lighter blades is approximately 1%. It should be mentioned that although changing the blade properties does change the DEL TBM, mean TBM, and maximum TBM loads, the change incurred by the introduction of the fairing is relatively independent of blade class.

The cone and tilt angles for both the upwind and downwind rotors are kept the same, 5.0° tilt and 2.5° cone. The blades in the upper half of the rotor azimuth are slightly pointing towards the incoming wind direction for the downwind mounted rotor, while the blades on the upwind mounted rotor points slightly away from the incoming wind direction. Due to blade flexibility, this increases the swept area (on the upper half rotor azimuth where the winds are higher) for the downwind rotor, while it decreases it for the upwind rotor (also the NREL reference blades have some flexibility). The power production is, therefore, slightly higher for the downwind rotors by 1% at S10W20 compared to the upwind NREL reference (Fig. 5).

As the blades become even more flexible, e.g., at S20Wyy the power production decreases with decreasing weight. The more flexible and lighter blades deflect and accelerate more than the original blades and capture the wind loads less efficiently.

IV. DISCUSSION

A decrease in blade fatigue loads on downwind mounted rotors was achieved by reducing the tower shadow impact through the use of a fairing tower. This agrees with the studies by Buhl,[13] Janajreh *et al.*[14] and Wilmshurst *et al.*[15] This study further showed that it was sufficient to use a fairing for parts of the tower. This made it possible to reduce the length of the rotor overhang, and thus also to obtain a decrease in mean tower bending moment, while still obtaining a decrease in blade and tower fatigue loads. Including more flexible and lighter blades on the fairing tower, in addition, resulted in blade and tower fatigue loads less than that of the upwind NREL reference.

The present study used the same rotor overhang as for the upwind mounted rotor (when no fairing was present). As the blades on downwind rotors run a smaller risk of hitting into the tower (compared to the upwind configuration), the required clearance could be further reduced compared to the NREL reference, which was not investigated in the present work.

The power production increased for the downwind mounted rotor compared to the NREL reference for blades with flexibility increased by 10% and 15%. The general trend is that using softer and lighter blades gradually decreased the power production for the downwind rotors. For the most flexible blades, the power production was, therefore, somewhat lower than for the NREL reference. This is also in agreement with what Ahlström[22] found, i.e., a considerable

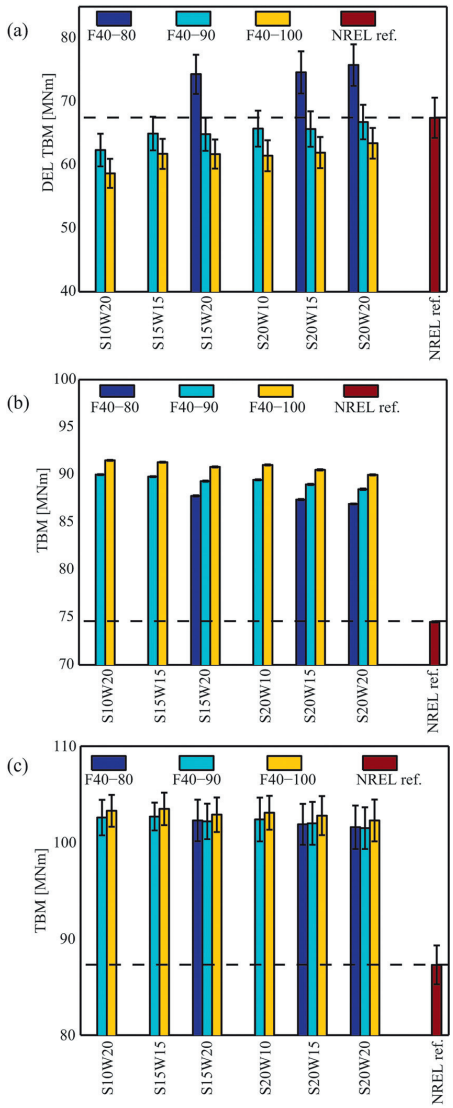

FIG. 4. (a) DEL for the TBM, (b) mean TBM, and (c) maximum TBM for the cases where the DEL blade root flapwise moment is lower than for the NREL reference. The conventional NREL reference is included for comparison. Dotted line gives the NREL reference value.

decrease in power production as the blade tip deflections in flapwise direction exceeded 10% of the blade length.

Buhl[13] questioned the benefits of a fairing around the tower as the increased rotor overhang would increase the mean tower bending moment. This also agrees with our findings, where a significant increase in mean tower bottom bending moment was found for the cases where the blade and tower fatigue loads were lower than for the NREL reference. Lower fatigue loads were found using the larger fairing lengths, corresponding to the larger rotor overhangs. With

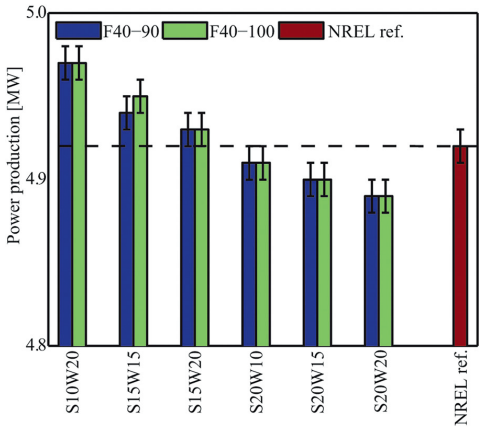

FIG. 5. Mean power production for the cases where the DEL for the TBM is in the same range or lower than for the NREL reference. The conventional NREL reference is included for comparison. Dotted line gives the NREL reference value.

the possibility of further reducing the rotor overhang for downwind rotors, the impact on the mean tower bending moments could likely be reduced. This suggests that an optimal downwind turbine with a fairing would need to be designed with a compromise between increased tower mean loads and decreased fatigue loads. Also, other turbine components could be taken into these considerations, such as in Malcolm and Hansen,[24] where a rather large reduction (18%) in rotor cost/kWh was demonstrated by using softer blades, with strengthening of drive train and tower, increasing their costs by 3% and 1%, respectively.

It should be noted that the fairing was not physically included in the structural model. With the fairing increasing the cross sectional area in the direction of bending, a fairing extending all the way down to the tower bottom will result in the fairing taking some of the mean tower bottom bending moment loads. This would be an interesting idea to study in more detail.

V. CONCLUSION AND FURTHER WORK

Both the blade and tower fatigue loads in a downwind rotor configuration can be reduced compared to the upwind NREL reference, without sacrificing power production. The lowest blade fatigue loads were obtained for a 20% more flexible and lighter blade, with the two largest fairing lengths, amounting to a reduction of 5% relative to the NREL reference (with tower fatigue loads in the same range as for the NREL reference). But the decrease in blade and tower fatigue loads comes at the cost of an increase in mean tower bottom bending moment, approximately 20% at the larger fairing lengths.

A more detailed study of the flow behind the fairing tower (including inflow angles different from 0°) as well as an optimization of the fairing design (for possibly further reduction of the DEL and rotor overhang) would be interesting to pursue.

ACKNOWLEDGMENTS

The work of M.R. was financed by the Research Council of Norway through the project *Offshore Wind Energy in Norway: Setting the Basis*, Contract No. 186952/I30.

[1]T. Ackermann, R. Leutz, and J. Hobohm, "World-wide offshore wind potential and European projects," in *Proceedings Of Power Engineering Society* (Piscataway, 2001), pp. 4–9.
[2]P. E. Morthorst, J. Lemmin, and N.-E. Clausen, *in Proceedings of Offhore Wind Power* (Multi-Science Publications, Brentwood, 2009), pp. 1–13.
[3]G. Moe, "What is the optimum size for a wind turbine?" in *Proceedings of International Conference on Offshore Mechanics Arctic Engineering, OMAE* (San Diego, 2007), pp. 409–416.

[4]J. F. Manwell, J. G. McGowan, and A. L. Rogers, *Wind Energy Explained*, 2nd ed. (Wiley, Chicester, 2010).
[5]P. Jamieson, *Innovation in Wind Turbine Design*, 1st ed. (Wiley, West Sussex, 2011).
[6]T. Burton, N. Jenkins, D. Sharpe, and E. Bossanyi, *Wind Energy Handbook*, 2nd ed. (Wiley, Chicester, 2011).
[7]A. T. Lee and R. G. J. Flay, "Compliant blades for wind turbines," IPENZ Trans. **26**, 7–12 (1999).
[8]M. Reiso and G. Moe, "Blade response on offshore bottom fixed wind turbines with downwind rotors," in *Proceedings of International Conference on Offshore Mechanics Arctic Engineering OMAE* (2010), pp. 499–504.
[9]T. R. Hagen, M. Reiso, and M. Muskulus, "Numerical analysis of turbulent flow past a truss tower for offshore downwind turbines," in *Proceedings of International Offshore Polar Engineering Conference ISOPE* (Maui, 2011), pp. 319–326.
[10]T. R. Hagen, M. Reiso, and M. Muskulus, "Numerical tower shadow modeling for a downwind wind turbine truss tower," in *Proceedings of International Conference on Offshore Mechanics Arctic Engineering OMAE* (Rotterdam, 2011) pp. 859–870.
[11]M. Reiso, M. Muskulus, and G. Moe, "Tower shadow—Experiment comparing wake behind tubular and truss towers," in *Proceedings of International Offshore Polar Engineering Conference ISOPE* (Maui, 2011), pp. 335–341.
[12]M. Reiso, "Root flapwise moment on downwind and upwind rotors with truss and tubular towers," in *Proceedings of 6th EAWE PhD Seminar* (Trondheim, 2010), pp. 267–271.
[13]T. Buhl, "Research in aeroelasticity," Technical Report EFP-2007-II, 2009.
[14]I. Janajreh, R. Qudaih, I. Talab, and G. Chaouki, "Aerodynamic flow simulation of wind turbine: downwind versus upwind configuration," Energy Convers. Manage. **51**(8), 1656–1663 (2010).
[15]S. M. B. Wilmshurst, S. J. R. Powles, and D. M. A. Wilson, "The problem of tower shadow," in *Proceedings of Wind Energy Converssation BWEA* (Oxford, 1985), pp. 95–102.
[16]J. Jonkman, S. Butterfield, W. Musial, and G. Scott, "Definition of a 5-MW reference wind turbine for offshore system development," Technical Report NREL/TP-500-38060, 2009.
[17]L. Bairstow, *Applied Aerodynamics*, 2nd ed. (Longmans, London, 1939).
[18]E. A. Bossanyi, "GH Bladed theory manual," Technical Report 282/BR/009, 2009.
[19]S. R. J. Powles, "The effects of tower shadow on the dynamics of a horizontal-axis wind turbine," Wind Eng. **7**(1), 26–42 (1983).
[20]H. A. Madsen, J. Johansen, N. N. Sørensen, G. C. Larsen, and M. H. Hansen, "Simulation of low frequency noise from a downwind wind turbine rotor," in *Proceedings of the Aerospace Sciences Meeting AIAA* (Reno, 2007), pp. 7549–7560.
[21]M. M. Zdravkovich, *Flow Around Circular Cylinders. Volume 1: Fundamentals* (Oxford University Press, New York, 1997).
[22]A. Ahlström, "Influence of wind turbine flexibility on loads and power production," Wind Energy **9**(3), 237–249 (2006).
[23]M. Reiso and M. Muskulus, "Resolution of tower shadow models for downwind mounted rotors and its effects on the blade fatigue," J. Wind Eng. Ind. Aerodyn. (submitted).
[24]D. J. Malcolm and A. C. Hansen, "WindPACT turbine rotor design study," Technical Report NREL/SR-500-32495, 2002.

Paper 7

A calibration method for downwind wake models accounting for the unsteady behaviour of the wind turbine tower shadow behind monopile and truss towers

By Marit Reiso, Torbjørn Ruud Hagen and Michael Muskulus

Submitted to Journal of Wind Engineering and Industrial Aerodynamics.

A calibration method for downwind wake models accounting for the unsteady behaviour of the wind turbine tower shadow behind monopile and truss towers.

Marit Reiso[a], Torbjørn Ruud Hagen[a†] and Michael Muskulus[a]

[a]Høgskoleringen 7a, Department of Civil and Transport Engineering, Norwegian University of Science and Engineering, NTNU, NO-7491 Trondheim, Norway

Telephone: +47 73 59 46 70

Fax: +47 73 59 70 21

E-mail: marit.reiso@ntnu.no (corresponding author), torbjorn.hagen@owectower.no, michael.muskulus@ntnu.no

Abstract

Traditionally wind turbines are built in the upwind configuration, but the alternative of a downwind rotor has distinct advantages. A main issue with such a configuration is the tower shadow effect on the rotor blades. The presence of the tower generates a complex wind field, consisting of an averaged velocity deficit, unsteady fluctuations from vortex shedding processes and turbulence. Since this tower shadow is commonly simulated using parametric steady wake models, the dynamic behaviour of the wake is not directly accounted for. The present paper suggests a general method calibrating the parametric steady wake models and the turbulence intensity (accounting both for the velocity profile and the unsteady motions) using computational fluid dynamic simulations of the unsteady structural shadow.

Here the method is used in a blade fatigue comparison study. The 15 percent more flexible and lighter blade for the downwind mounted rotors showed a decrease in blade fatigue loads of three, four, and two percent compared to the conventional upwind mounted rotor on a monopile tower for the monopile tower and truss towers at 0 and 22.5 degrees, respectively. This application shows that the truss tower at 0 degree angle seems to result in the lowest blade fatigue loads.

Keywords

Tower shadow, CFD, Powles' model, downwind, truss tower, blade fatigue.

Nomenclature

DEL Damage equivalent load

RFM Blade root flapwise bending moment

[†]Current affiliation: OWEC Tower AS, Storetveitvegen 96, NO-5072, Bergen, Norway

1 Introduction

Reliability is one of the core issues for wind turbines when going offshore, since maintenance is quite expensive and might become difficult at the time of failure due to the necessary weather window. As a consequence, new wind turbine technology is under continuous development for applications in the offshore environment, e.g., new support structure concepts, when pushing for deeper waters.

Wind turbines are complex dynamic structures, which need detailed computational models for their simulation and the necessary iterations between design, analysis and optimization. Most of the simulation technology on the market today is based on approximations that have intrinsic limitations; for new technological concepts such as downwind rotors, truss towers, etc., these simplifications are not fully able to represent a physically accurate model of the wind turbine. Of particular interest here is the complex and unsteady aerodynamic flow around wind turbine towers, which is, as of today, implemented in commercial software codes based on time averaged wake models (Bossanyi, 2009; Moriarty and Hansen, 2005). Most commonly used are varieties of Powles' model (Powles, 1983).

A major advantage of using a downwind mounted rotor, as suggested in the present study, is a potential reduction of the mean blade root flapwise bending moment, due to the possible coning of the blades (Reiso and Moe, 2010). The risk of the blades hitting the tower will be reduced, hence softer (and thereby cheaper and lighter) blades can be used (Ahlström, 2006; Lee and Flay, 1999). Such blades have also proved to decrease the blade fatigue loading (Reiso and Muskulus, 2012b). The main downside of using a downwind mounted rotor is the additional impact-like loading on the blades as they pass through the tower wake. A model scale experiment by Reiso et al. (2011) of the wake behind a full truss tower and a monopile tower seems to favour the truss tower with a more narrow velocity deficit and a lower turbulence intensity.

A truss tower consists of a number of cylindrical members that are arranged in a complex geometric pattern. Even when considering a two-dimensional cross-section, the resulting flow field depends on the spacing between the cylinders and how they are arranged, e.g., side-by-side, tandem or in staggered configuration. Above some critical spacing (that depends on the cylinder arrangement), the flow pattern around the cylinders can be assumed to behave as for a single cylinder. This is an excellent approximation for complex geometries under potential flow (Krause and Muskulus, 2012), but also possible when involving viscous effects. A lot of work has been conducted and reported on such flows around and behind cylindrical structures (e.g., Blevins (1990), Ishigai et al. (1972), Meneghini et al. (2001), Moe et al. (1993), Gao et al. (2010), Zdravkovich (1977), Zdravkovich (1997), Zdravkovich and Namork (1979)), but not many authors have considered the flow behind complex truss structures with diameters and spacing relevant for wind turbine truss towers, and at short-medium distances.

For reliable simulation results based on parameterized steady wake models, the parameters need to be carefully chosen (Coton et al., 2002; Munduate et al., 2004; Wang and Coton, 2001). This can be done by fitting the parameters with data from full scale experiments, as done by Wilmshurst et al. (1985), fitting the parameters of Powles' model for wake width and mean velocity deficit for a monopile and a fairing tower. Hagen et al. (2011a) and Hagen et al. (2011b) suggested a numerical method for fitting the parameters of Powles' model to the mean velocity profile from two dimensional computational fluid dynamic (CFD) simulations, obtaining good agreement for the velocity profiles both for a monopile tower and a truss tower.

Wind turbine loads do not solely result from the steady velocity deficit, but also the dynamics of the unsteady flow around the tower plays an important role, especially for blade loads on downwind mounted rotors. A realistic wind field for such load simulations could be obtained using CFD simulations, but would significantly increase the simulation time, as 10 minute time series are required by the different standards, e.g., IEC 61400-3 (2009), which is computationally infeasible as of today.

The method that is proposed here, instead accounts for the tower shadow (including the unsteady motions), by fitting the parameters of Powles' model and calibrating the turbulence intensity with a number of short CFD simulations. The parameters of Powles' model for the truss tower are fitted using the minimum root-mean-square estimate. Any discrepancy between the mean velocity profile obtained from the CFD simulations and Powles' model is thereafter accounted for in the calibration of the turbulence intensity. The calibrated turbulence intensity value is found as the curve from plotting the blade fatigue loads using the tower shadow model of Powles' (run with a few different trial values for the turbulence intensity) equals the blade fatigue loading obtained using the CFD simulations.

This method replaces the time consuming CFD simulations down with investigations of the flow field behind the towers. The results of this method (parameters for the steady tower shadow and effective values of turbulence intensity) are directly applicable in commercially available software for carrying out full wind turbine simulations. Compared to CFD simulations, this method captures the blade fatigue loading with excellent agreement for the rotor mounted on the monopile tower, while the truss towers at 0 and 22.5 degrees deviates by one and three percent, respectively, which seems an acceptable compromise.

The use of the calibrated Powles' model is demonstrated in a comparison study on blade fatigue for downwind mounted rotors on both truss and monopile towers, using two different blade flexibilities and weights. The fatigue loads are compared with those of the conventional upwind mounted rotor.

2 Methods

The study is divided in two parts – one part suggesting a method for calibrating a parametric tower shadow model and the turbulence intensity with short CFD simulations (section 2.1-2.4). And a second part, using the calibrated model, in a blade fatigue comparison study (section 2.5).

2.1 CFD model

The CFD model is based on earlier work and is described there in detail (Hagen et al, 2011a, b); for completeness, here the most important features are summarized.

The commercial software package Ansys Fluent (Version 12.1.4; Ansys Inc., Canonsburg, USA) was used to simulate the flow fields around two-dimensional cross sections of wind turbine towers. The different members (legs and braces) were approximated by circular cross-sections for simplicity and easy meshing. The following five two-dimensional (horizontal plane) geometrical configurations were considered (Figure 1):

- monopile tower
- truss tower at 0 degrees angle (with respect to the inflow direction); close to X-brace position (later referred as X-braced truss tower at 0 degrees)
- truss tower at 0 degrees angle; close to K-brace position (later referred as K-braced truss tower at 0 degrees)
- truss tower at 22.5 degrees; close to X-brace position (later referred as X-braced truss tower at 22.5 degrees)
- truss tower at 22.5 degrees; close to K-brace position (K-braced truss tower at 22.5 degrees)

The braces were modelled at two different positions (X- and K-brace) in order to assess the influence of cross-sectional geometry (i.e., height) on the results. The inflow was considered at both 0 and 22.5 degrees for the truss towers, to assess the influence of inflow angle. Results for other inflow angles can be found in Hagen et al (2011a).

The distance between the main legs in the truss tower for the two-dimensional CFD simulations was 10.8m (Figure 1). This corresponds to the vertical position in the tower where the part of the blade experiencing the highest power production (about 2/3 along the blade length from the root) will pass. The dimensions of the physical (three-dimensional) and of the CFD model (two-dimensional) for the monopile tower and the truss tower are given in Table 1, the full truss tower geometry is based on work by Long and Moe (2007).

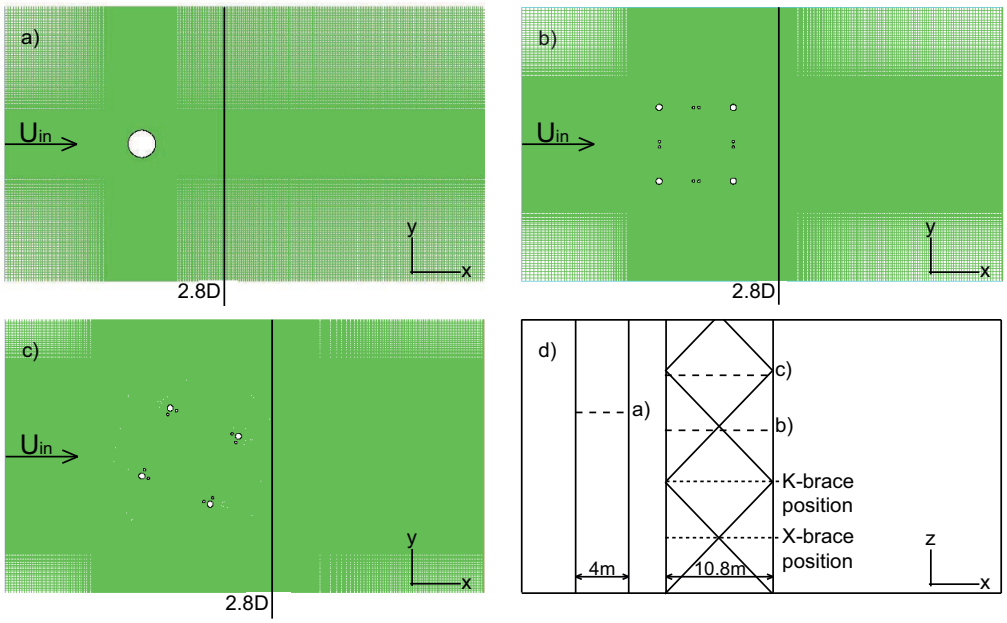

Figure 1. CFD mesh and geometric configuration of the towers; a) monopile, b) X-braced truss tower at 0 degrees, c) K-braced truss tower at 22.5 degrees and d) cross-sections at where a)-c) were calculated. The output data were collected at 2.8D (D = 4.0m, equal to monopile tower diameter) behind the tower centres. Inflow direction, U_{in}, is from the left (similar plots for K-braced and X-braced truss towers at 0 and 22.5 degrees, respectively).

The computational domain spanned 17.5D times 10D in x- and y direction, respectively (x being in the flow direction, and y being transversal to the flow direction, Figure 1). Here D = 4.0m represents the monopile tower diameter. Periodic boundary conditions were used for the upper and lower walls (at y = ±20m), and the right outlet wall was implemented with a velocity reference pressure of 1.0 atmosphere.

The free stream velocity at the inlet (x = -5D) was 12.0m/s, representing a typical operational wind speed for power production under close to maximum operational loads (rotor thrust). A turbulence intensity (defined as the ratio of root-mean-square velocity fluctuations to mean velocity) of 10 percent was used, being typical for the offshore environment, and a turbulence length scale of 1.0m was used, roughly corresponding to the diameter of the larger members in the truss tower (for which the major vortex shedding process and subsequent generation of turbulence is expected). The air density was taken to be $\rho = 1.225 kg/m^3$, with a constant dynamic viscosity of $\mu = 1.789 \cdot 10^{-5}$ kg/(ms), resulting in a kinematic viscosity of $\nu = 1.5 \cdot 10^{-5}$ m^2/s.

The boundary layers around the members were modelled with 30 layers (inner element size 0.0001m, with a growth factor of 1.2) inside an unstructured mesh that was embedded in an

outer structured mesh. The mesh was adaptive with quadrilateral cells and was implemented using Gambit (Version 2.4.6; Ansys Inc., Canonsburg, USA).

Table 1. Physical (three dimensional) and CFD (two dimensional) tower properties for the truss and monopile towers.

Parameter	Truss tower (main leg/brace)	Monopile tower
Three dimensional physical tower properties:		
Diameter [m]	0.90/0.36	3.87-7.00
Number of sections	10	-
Tower height [m]	120	120
Top distance between main legs [m]	4.00/-	-
Bottom distance between main legs [m]	28.0/-	-
Angle against horizontal [^{o}]	84.3/50.0	-
Two dimensional tower properties for CFD simulations:		
Leg spacing [m]	10.80	-
Diameter [m]	0.90/0.36	4.00

The Reynolds-Averaged Navier-Stokes (RANS) equations were complemented with the *k-ω* shear-stress transport (SST) viscosity model (Menter, 1994) and solved numerically. The time step was fixed at dt = 0.005sec, which is both small enough to allow for the resolution of vortex shedding, and to resolve up to 100Hz spectrally. Outputs were sampled 2.8D downstream of the geometric centre of the towers, corresponding to the approximate position where the wind turbine blades will pass through the flow field.

The simulations were validated for the monopile tower by considering the pressure coefficient around its circumference at Reynolds number Re = $3.3 \cdot 10^6$ (Hagen et al, 2011a). Results agreed well with the findings of Warschauer and Leene (1971). The drag coefficient was found to be 0.37, which corresponds to what has been reported by Ong et al. (2009). The non-dimensional size of the boundary layer, y^+ was used to check whether the transition near the cylinder wall was accurately resolved. For super-critical Reynolds numbers one should generally implement $y^+ \leq 5$ (Salim and Cheah, 2009), which is fulfilled in the present work with a y^+_{max} of 3.5.

2.1.1 Post processing

Numerical results were recorded for N = 6000 time steps, corresponding to a flow time of 30 seconds. To ensure fully developed vortex shedding before extracting the output data, 10 000 time steps were simulated prior to writing the output (Nakayama et al., 2010). Time series of local turbulence intensity (including turbulence from the vortex shedding and unsteady motions) and mean velocity profiles were computed.

2.2 Wind turbine simulation

Full wind turbine simulations were run in the commercial software Bladed (version 4.2, GL Garrad Hassan), based on the NREL Offshore 5-MW Baseline Wind Turbine, hereafter referred as the NREL reference (Jonkman et al., 2009). The wind turbine was used in its original configuration, as well as with some applied changes. The turbine was adapted from an upwind to a downwind rotor configuration, and some of the simulations were run with a truss tower instead of the conventional monopile tower. In addition, shaft tilt and cone angles were changed (Table 2).

Table 2. NREL reference properties and applied changes.

Parameter	NREL reference	Changes to NREL reference
Rotor orientation	Upwind	Downwind
Shaft tilt [degrees]	5.0	2.0 [a]
Cone angle [degrees]	2.5	2.0 [a]
Tower	Monopile	Truss and monopile [a]

[a] Only for downwind rotor simulations.

All simulations were run with a mean free stream velocity of 12.0 m/s and with the same wind shear profile, an exponential model with a vertical shear exponent of 0.14. All cases were run using a turbulent wind file pre-calculated from the Kaimal turbulence model (Table 3). In total eight different realizations (random number seeds) were used to obtain more reliable results. A total of 150 and 630 seconds were simulated respectively, for the calibration of the steady wake model (section 2.4) and for the blade fatigue comparison study (section 2.5), with the first 30 seconds removed as transient. For the blade fatigue comparison study, this resulted in time series of 10 minutes length, as required by the IEC 61400-3 standard (IEC, 2009).

The tower shadow was implemented both with the combined Powles' model available in Bladed (section 2.3.1), and alternatively with the unsteady flow field variations from the CFD simulations (section 2.3.2).

Damage equivalent loads (DEL) for the blade root flapwise bending moments (RFM) were calculated. DEL was calculated from Miner's rule by way of a rainflow count of the blade loading time histories. An inverse S-N slope m = 10 and 128 bins for the cycle range were used. The equivalent loads were calculated for a reference frequency of 0.003169Hz, corresponding to $2 \cdot 10^6$ cycles during the total lifetime of 20 years.

Table 3. Kaimal turbulence model parameters.

Width of wind field [m]	150
Lateral number of points (calibration/implementation) [-]	300/50
Height of wind field [m]	200
Vertical number of points [-]	20
Simulation time (calibration/implementation) [sec]	150/630
Lateral spacing (calibration/implementation) [m]	0.5/3.0
Vertical spacing [m]	10.0
Longitudinal spacing [m]	0.48
Mean wind speed [m/s]	12.0
Turbulence length scale:	
Longitudinal [m]	340.2
Transversal [m]	0.1
Vertical [m]	0.1
Turbulence intensity [%]	10

2.3 Tower shadow

The effect of the tower shadow is usually accounted for in full wind turbine simulation software by a constant (but spatially varying) velocity deficit behind the tower, by way of a parameterized model. Here, both the steady model suggested by Powles (1983) and an unsteady CFD simulation of the tower shadow were used.

2.3.1 Steady tower shadow model

In Powles' model the wind velocity U behind a circular member is described in terms of changes to the mean velocity U_0. The model is specified in terms of two non-dimensional parameters: (1) velocity deficit (Δ) at the centre of the wake, and (2) wake width (w). Both parameters are here taken in terms of the member diameter. Recall that y denotes the distance transversal to the free stream velocity and D the tower member diameter, the velocity is given by:

$$U(x,y) = U_0\left(1-\Delta(x)\cos^2\left(\frac{y\pi}{w(x)D}\right)\right), \quad \textbf{(1)}$$

The model is limited to at most one period of the cosine term, and is usually extended laterally with the potential flow solution for arguments of the cosine outside of ±60 degrees (Bossanyi, 2009). The parameters Δ and w depend on the longitudinal distance x from the centre of the tower and usually need to be estimated individually for each transversal.

Powles' model is therefore often supplemented by the following square-root-law in terms of values Δ_r and w_r for some (relative) reference distance x_r (Bossanyi, 2009):

$$\begin{aligned}\Delta(x) &= \Delta_r / \sqrt{x/(x_r D)} \\ w(x) &= w_r \cdot \sqrt{x/(x_r D)}\end{aligned}, \quad \textbf{(2)}$$

This relationship can be theoretically motivated from simple considerations of diffusion processes, and seems to hold well in practice (Powles, 1983). It forms the basis of extending Powles' model from a single cylinder to a multi-member truss tower. As of today, Bladed is the only commercial software that allows for using a tower shadow model for such a multi-member truss type tower. This is achieved by superposition of the solutions for each member:

$$U(x,y) = \sum_{i=1}^{n} U_i(x,y) + (1-n)U_0 = U_0 - \sum_{i=n}^{n} \Delta(x-x_i)\cos^2\left(\frac{(y-y_i)\pi}{w(x-x_i)D}\right), \quad \textbf{(3)}$$

where U_i (i = 1, 2, …, n) represents the velocity field calculated because of the presence of the i-th member, and x_i and y_i represent the coordinates of the centre point of the i –th member. This approach is only a rough approximation of the actual flow field, but we will show that with the right choice of effective parameter values adequate agreement can be reached.

2.3.2 Unsteady tower shadow model

The time series of the tower shadow flow field obtained from the unsteady CFD simulations was implemented without use of the parametric tower shadow model. Since the simulations were only two-dimensional, vertical variations needed to be artificially introduced in order to run three dimensional wind turbine simulations with the CFD tower shadow representation. To account for the vertical variations, the CFD results were shifted by a random offset (in time) for each vertical layer, totally making up 20 layers. This three-dimensional discrete wind file was used in full wind turbine simulations.

As the CFD simulations were limited to 30 seconds (again, due to constraints on computational time), whereof the first 5 seconds were removed as transient, the results of the CFD simulations were recycled six times. In principle the cyclic nature of the tower shadow wind field could result in biased results for, e.g., blade fatigue loading, but since the tower

shadow is superposed with turbulent fluctuations and additionally averages out vertically along the blades, this seems unlikely.

To summarize, the simulated unsteady tower shadow implemented here assumes vertically independent two-dimensional flows, with no three-dimensional cross-flows, on which additional three-dimensional turbulent variations (with vertical cross-flow) were superposed. The resulting three-dimensional wind fields were written to Bladed wind files, for later use in the software.

2.4 Calibration of Powles' steady wake model

For reliable wind turbine simulations when using steady parameterized wake models, it is crucial that the parameters are well fitted. For Powles' model this applies to two parameters; the velocity deficit (Δ) and the wake width (w). The reference length, x_r (Equation 2) was taken to be 2.8 monopile diameters (D = 4.0m), and the reference velocity deficit (Δ_r) and wake width (w_r) parameters were found by fitting the average transversal velocity profiles resulting from the CFD simulations, minimizing the root mean square (RMS) difference. This estimation was performed for each tower profile individually and also globally for the truss tower by minimizing the maximum RMS over all four configurations simultaneously (truss tower at 0 and 22.5 degrees at both X- and K-brace position).

What is new here is that in addition to fitting the steady wake parameters, the turbulence (originating from both the vortex shedding and the sub-grid turbulence parameterization in the CFD simulations) is accounted for by calibrating the turbulence intensities (TI) used with the (globally) fitted Powles' model. Full wind turbine simulations were carried out using the tower shadow both from the globally fitted Powles' model (using four different trial values for the TI) and the CFD simulations. The results for the blade fatigue were plotted. The optimum TI to be used with Powles' model was obtained where the curve for the CFD tower shadow intercepted with the trend-line through the four different TI's used with Powles' model. This method also accounts for any discrepancy in the mean velocity profile from the fitted Powles' model and the CFD simulations.

For the calibration of TI, Powles' model was used for the same cross sectional geometries as for the CFD simulations, i.e. a monopile tower with constant diameter, D = 4.0m, and truss towers with constant main leg spacing of 10.8m. Two different setups, X- and K-brace, were run with each of the two truss tower arrangements, 0 and 22.5 degrees respectively.

The tower shadow models were implemented in the wind field file through a MatLab script (MathWorks version R2012a). The mean tower shadow wake was superposed with random realizations of the turbulence from the Kaimal spectra, as is standard in wind turbine load simulations, refer e.g., Bossanyi (2009). A similar script was used for the CFD tower shadow, but instead of the mean tower shadow wake, time series of the wake including vortex

shedding were used. In addition, the turbulence from the sub-grid parameterization was obtained by scaling realizations of turbulence from the Kaimal spectrum with values for the local turbulence intensity (time series) recorded during the simulations. The final wind field files were again normalized to unit standard deviation before being imported to the Bladed software for full wind turbine simulations. With the tower shadow present in the wind field file, the tower shadow module in Bladed was disabled.

The simulations were carried out using a grid resolution of 300 x 20 points across the lateral and vertical domain of 150m x 200m, at a longitudinal resolution of 25Hz, which has been found sufficient for such structures (Reiso and Muskulus, 2012a). The Kaimal spectra had a maximum resolution of 50 points across the 150m lateral domain, and linear interpolation (without increasing spectral resolution) was used to fit the Kaimal spectra with the tower shadow resolution of 300 points.

2.5 Blade fatigue comparison study

The second part of the study is a blade fatigue comparison study. Full wind turbine simulations were performed using both the original NREL reference blade and an adjusted NREL blade. The adjusted NREL blade is a 15 percent more flexible and 15 percent lighter blade compared to the NREL reference blade. The value of 15 percent was chosen as it has shown good performance in power production as well as a decrease in blade fatigue loading behind both a monopile and a fairing tower (Reiso and Muskulus, 2012b). This is a simplified adjustment, where the blade geometry is kept equal to that of the NREL reference. As both the stiffness and weight were decreased by the same amount, the blade eigenfrequency stayed intact (Ahlström, 2006). The NREL reference blade was used for both the upwind and downwind rotor configurations, while the adjusted NREL blade was implemented for the downwind configurations only.

The tower shadow and tower dam (upwind rotor) effects were implemented using the inbuilt functions in GH Bladed, with the physical tower geometries given in Table 1. For the downwind configurations, the velocity deficits, wake widths and turbulence intensities obtained from the calibration of Powles' model (section 2.4) were used. The conventional upwind mounted rotor on a monopile tower was included for reference and the tower dam effect was derived assuming potential flow (correction factor set to 1), which is the current standard in wind turbine simulations (Bossanyi, 2009). With the Bladed software a limitation of 50 lateral points across the domain exist, and this maximum was used (lateral domain size of 150m), with a vertical and longitudinal resolution equal to that used in section 2.4, i.e., 20 points (across a vertical domain of 200m) and 25Hz (Table 3).

3 Results

3.1 Calibrated steady wake model

It should first be mentioned that the velocities at the boundaries of the CFD domain (at approximately y/D = ±5, Figure 2) overestimated the free stream velocity of 12m/s with a mean offset of 2.5 percent for the monopile tower, an overestimation that was present also for the truss tower configurations (with a 3.0 percent overestimation), Figure 2. This overestimation originates from the limited size of the computational domain, and is a numerical artefact due to the periodic boundary conditions, but does not affect the validity of this approach. If used in an industrial application, a larger domain will lead to slightly more accurate parameter estimates.

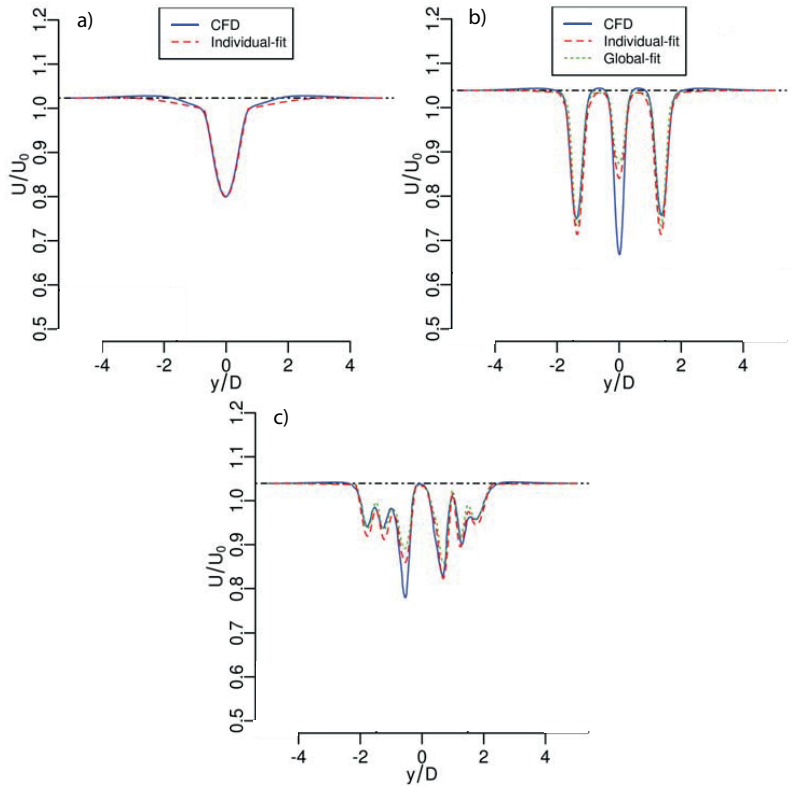

Figure 2. Normalized (with respect to free stream velocity) mean wind velocity profiles at reference position 2.8D (D = 4.0m) behind the towers (dips corresponding to the approximate position of the tower legs and braces); a) monopile, b) X-braced truss tower at 0 degrees, c) X-braced truss tower at 22.5 degrees (K-braced truss towers not shown). For the truss towers, both individual (broken lines) and global fits (dotted lines) of the combined Powles' model are shown (parameter values given in Table 4).

The mean velocity profile represented by Powles' model for the monopile tower (Figure 2a), accurately reproduces the CFD profile, with reference velocity deficit and wake width parameters of $\Delta_r = 0.218$ and $w_r = 1.804$, respectively (Table 4). The only discrepancy was a slight underestimation at transversal position ±2D.

Table 4. Individual and global fitted Powles' model parameters for the monopile tower and the X-braced and K-braced truss towers at 0 and 22.5 degree angle towards the incoming wind direction.

Tower geometry	Individually fitted values [a]		Globally fitted values [a]	
	Velocity deficit (Δ)	Wake width (w)	Velocity deficit (Δ)	Wake width (w)
Monopile	0.218	1.804	-	-
X-braced truss tower at 0 degrees	0.197	2.295	0.185	1.914
K-braced truss tower at 0 degrees	0.241	1.995	0.185	1.914
X-braced truss tower at 22.5 degrees	0.217	2.027	0.185	1.914
K-braced truss tower at 22.5 degrees	0.249	1.813	0.185	1.914

[a] Reference position 2.8D (D = 4.0 m).

For the truss tower arrangements some discrepancies appeared. The central velocity deficit behind the X-braced truss tower at 0 degrees underestimated the CFD results by roughly 25 percent for the individually fitted parameters (Figure 2b). For the globally fitted parameters the underestimation of the dip was even larger, around 31 percent. Powles' model for the K-braced truss tower at 0 degrees represented the results of the CFD simulations better than for the X-brace, with discrepancies at the two dips (at transversal position ±1.5D) of 2 and 18 percent for the individually and globally fitted values, respectively (Figure 2c).

For the truss tower at 22.5 degrees, Powles' model for the K-brace showed the largest discrepancy from the CFD simulations, with a maximum underprediction of the mean velocity profile (at transversal position -1.5D) of 14 and 21 percent for the individually and globally fitted parameters, respectively (Figure 2e). The maximum underprediction for the X-brace at transversal position -0.5D was 10 and 14 percent, respectively (Figure 2d).

The reference wake width parameters for all truss tower configurations were larger than that of the monopile tower ($w = 1.804$, Figure 2a), with a broad scatter from slightly higher for the K-braced truss tower at 22.5 degrees ($w = 1.813$, Figure 2e), to 27 percent higher for the X-braced truss tower at 0 degrees ($w = 2.295$, Figure 2b). The globally fitted value was six percent higher than for the monopile tower, $w = 1.914$. For the reference velocity deficit, only the two K-brace configurations showed a larger velocity deficit than the monopile tower (Δ =

0.218), approximately 12-13 percent higher ($\Delta = 0.241$ and $\Delta = 0.249$, respectively). Here the globally fitted value was 15 percent lower ($\Delta = 0.185$) than the reference velocity deficit parameter for the monopile tower.

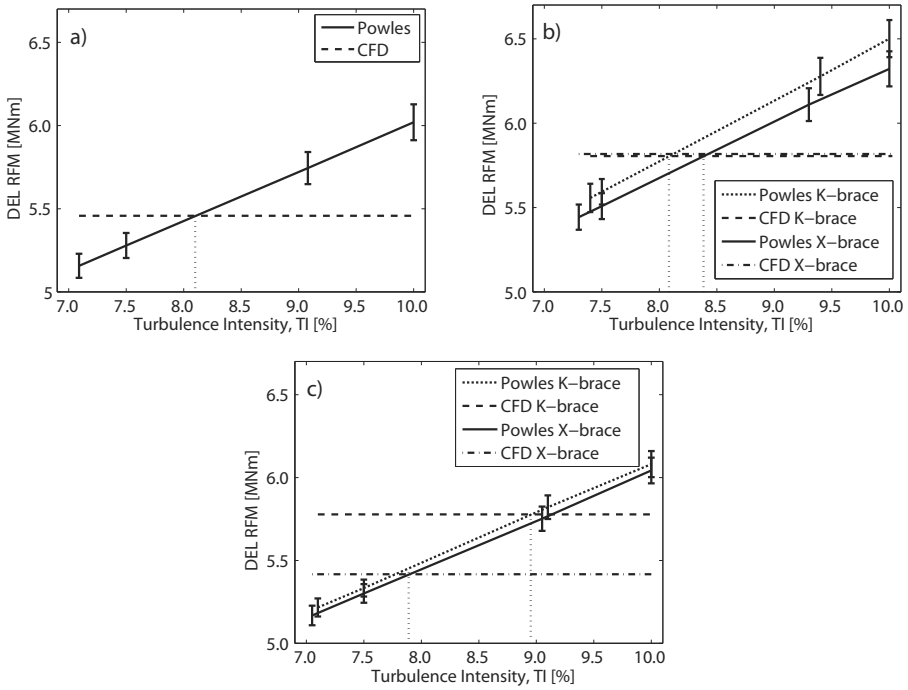

Figure 3. Damage equivalent loads (DEL) for the blade root flapwise bending moment (RFM) at different turbulence intensities (TI); a) monopile, b) truss tower at 0 degrees and c) truss tower at 22.5 degrees. Curves are shown for the CFD tower shadow at constant TI and the Powles' tower shadow model with four different values of the TI.

For full wind turbine simulations with a realistic truss tower, consisting of both X- and K-brace sections, the turbulence intensity was taken as the average of the values for the two cross sections. For the truss tower at 0 and 22.5 degrees, this resulted in a TI of 8.23 and 8.43 percent, respectively (Figure 3b and Figure 3c). The respective root mean square errors for the X-brace and K-brace of the two tower angles were 0.10 and 0.37 percent. Simulations run with the calibrated turbulence intensities showed a deviation of the DEL of ±1.0 and ±3.0 percent for the truss tower at 0 and 22.5 degrees, respectively (Table 5).

With the use of the steady wake parameters (Δ and w) from Figure 2, the turbulence intensities were calibrated. The lowest turbulence intensity was found for the monopile tower, 8.11 percent, Figure 3a.

An interesting finding is the linear shape of the trend-line ($R^2 = 1$) between the DEL RFM for the different TI's.

Table 5. Damage equivalent loads (DEL) for the blade root flapwise bending moment (RFM) obtained from the CFD simulations and the Powles' model; the latter is using the calibrated turbulence intensities.

	CFD [MNm]	Powles model with calibrated TI [MNm]
Monopile	5.46	5.45
K-braced truss tower at 0 degrees	5.81	5.85
X-braced truss tower at 0 degrees	5.80	5.76
K-braced truss tower at 22.5 degrees	5.78	5.60
X-braced truss tower at 22.5 degrees	5.42	5.58

3.2 Blade fatigue comparison study

The damage equivalent loads (DEL) for the blade root flapwise moment (RFM) in the turbulent wind cases (with additional turbulent variations in the incoming wind field) were significantly higher (by approximately 20 percent) than for the steady flow with only the mean tower shadow profiles (Figure 4). The latter features fewer fluctuations in the flow behind the towers, and hence resulted in reduced DEL RFM. For comparison, the conventional upwind mounted rotor on a monopile tower was included (using the potential flow model), and showed a similar difference, but with a 40 percent increase in DEL RFM from the steady to the turbulent wind case.

The steady wind simulations do not allow for realistic blade fatigue estimates, but were performed in order to isolate the relative effect from the tower shadow and the turbulent wind. The turbulent wind disturbs and averages out the velocity deficit profile of the tower shadow, which can be seen from the smaller relative difference in DEL RFM between the upwind and downwind rotor configurations in the turbulent wind cases (deviating by a maximum of 7 percent, Figure 4), compared to the steady wind cases (deviating by 11-27 percent, Figure 4).

In addition, with the smaller difference in DEL RFM between the upwind and downwind rotor configurations in the turbulent wind cases, the adjusted NREL blades gave a decrease in DEL RFM compared to the upwind mounted rotor by 3, 4 and 2 percent for the monopile tower and truss towers at 0 and 22.5 degrees, respectively. This is a different finding than for the steady wind cases, where an increase was found for the downwind mounted rotors, 11, 13 and 14 percent for the monopile and truss towers at 0 and 22.5 degrees, respectively.

The lowest DEL RFM for the downwind rotors in the turbulent wind cases was found for the flexible blade on the truss tower at 0 degrees, while the steady wind cases showed the lowest DEL RFM for the flexible blade on the monopile tower.

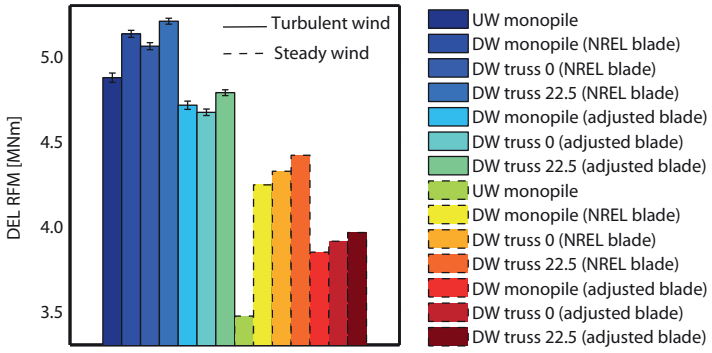

Figure 4. Damage equivalent loads (DEL) for blade root flapwise bending moment (RFM) for upwind (UW) and downwind (DW) mounted rotors on a monopile tower and a truss tower, latter both aligned at 0 and 22.5 degrees with respect to the inflow direction. Downwind rotors are run with two different blade flexibilities and weights. Steady and turbulent wind refers to the mean tower deficit and the Kaimal spectrum with additional turbulence intensity, respectively.

4 Discussion

4.1 Calibrated steady wake model

Intuitively one could think that the monopile tower (having the largest apparent solidity) would be the tower with the largest velocity deficit. But the largest velocity deficit was found behind the two dimensional K-braced truss tower at 0 degrees (well reproduced by the individually fitted Powles' model). The large velocity deficit can be explained from the interaction between the closely spaced main leg and brace (centre to centre distance of one meter) in the K-brace configuration. This agrees with literature, such as Zdravkovich (1977), Gao et al (2010) and Blevins (1990), where both interaction effects and increased velocity deficits (compared to two single cylinders that do not interact) were reported for closely spaced cylinders. With the present tower aligned at 0 degrees, two and two K-brace configurations were arranged in tandem, and the flow field behind the first K-brace would have insufficiently recovered (Powles, 1983) before reaching the second K-brace, further increasing the total velocity deficit behind the K-braced truss tower at 0 degrees.

Powles' model significantly underestimated the central dip in the X-braced truss tower at 0 degrees (25 and 31 percent for the individually and globally fitted parameters). As the model uses simple superposition of the flow fields for the individual truss tower members (Equation

3), the interaction effects between the brace members were not accounted for, which would have given a larger velocity deficit, as shown by, e.g., Gao et al (2010).

The X- and K-braces at 22.5 degrees represent the configuration more frequently encountered in practice, where the inflow is not aligned with the structure, and these results should therefore be considered more relevant. Also the discrepancies between Powles' model and the CFD results were smaller at 22.5 degrees compared to the 0 degree truss tower. The staggered arrangement of the truss tower members at 22.5 degrees exhibited an increased velocity recovery, as fewer tandem arrangements were present compared to the truss tower at 0 degrees, this also agrees with, e.g., Ishigai et al (1972).

Using one set of wake parameters, i.e., the globally fitted parameters for Powles' model (Figure 2), raises the question of the validity of the model, as its predictions deviate more from the CFD profiles. Using the calibrated turbulence intensity resulted in deviations of one and three percent in response for the truss tower at 0 and 22.5 degrees, respectively, which seems an acceptable result. If a more accurate result is required, the parameters may be fitted individually for each truss tower angle with respect to the incoming wind direction. Although a trivial modification of the procedure, this will only be practically applicable if commercial software is updated accordingly.

It should be noted that unsteady CFD simulations with fully turbulent inflow would result in additional turbulent mixing behind the tower structures. And that this, to a certain extent, is expected to reduce the structured vortex shedding compared to the present study, where the turbulence from the turbulent wind and a realization of the sub-grid turbulence is simply superposed onto the CFD time series of the tower shadow.

The linear trend-line between the different TI's benefit the method, as the simulations using Powles' model can be limited to 2-3 trial values of the different TI's, thereby decreasing the number of simulations.

The method improves the reliability of wind turbine simulations through a more accurate representation of the tower shadow, and is directly applicable in the software Bladed. Hence the time consuming CFD simulations are reduced to simulating a few cross sections of the relevant tower geometries to obtain the unsteady velocity profile which can be used in the fitting and calibration of Powles' model and an effective (fatigue-equivalent) turbulence intensity, respectively. The full 3-dimensional shapes of the towers are accounted for in the Bladed software, with the mean velocity deficit being compiled from Equations (1-3) at each height.

4.2 Blade fatigue comparison study

A study by Reiso and Muskulus (2012a) showed that the main contribution to blade fatigue loads on downwind mounted rotors came from the mean velocity deficit and turbulence, and

minor contributions from the additional turbulence and unsteady motions originating from the vortex shedding and the presence of the structure. This was also seen in this study, with a 40 and 20 percent increase in blade fatigue loads for the up- and downwind mounted rotors, respectively, when including turbulence. However, the turbulence from the vortex shedding and the presence of the structure need to be accounted for, for accurate tower shadow representation and reliable simulation results. With their minor contribution, these fluctuations can be approximated through adjusting the turbulence intensity, and thereby excluding the need for full CFD simulations.

The largest blade fatigue loads for the downwind mounted rotors were reported for the blade behind the truss tower at 22.5 degrees angle with the incoming wind direction (for both steady and turbulent wind cases), despite the fact that the velocity deficit was approximately 62 percent larger and the wake width only 17 percent lower for the truss tower at 0 degrees (Figure 2). A possible explanation to this could again be the influence the turbulence has on disturbing the velocity profile of the tower shadow, where the turbulence intensity has the capability to average out the deeper deficits of the more narrow velocity profiles of the truss tower at 0 degrees to a larger extent than for the wider truss tower at 22.5 degrees. This would also explain why the lowest blade fatigue loads were found behind the monopile tower in the steady wind cases, while they were found for the truss tower at 0 degrees in the turbulent wind cases.

5 Conclusion and further work

A method for fitting Powles' model and calibrating the value of the effective turbulence intensity with CFD simulations was demonstrated. This improves the reliability of wind turbine simulations using Powles' model, and the method is directly applicable in commercial software (Bladed). The time consuming CFD simulations are reduced to short studies for the relevant tower geometries. The mean velocity profiles from the CFD simulations were used to fit the velocity deficit and wake width parameters of Powles' model, while the unsteady and turbulent behaviour of the CFD simulations were accounted for through an increase in the turbulence intensity (with respect to an outcome variable of interest, which here was damage equivalent structural loading). Some discrepancies between the mean velocity profiles obtained from the CFD simulations and Powles' model occur under the linear superposition of the different flow fields, and this can be accounted for, to a large extent, through an increase in the turbulence intensity. With the use of globally fitted parameters, a blade fatigue load discrepancy of only one and three percent was found for the truss tower at 0 and 22.5 degrees, respectively.

The method is general and could also be used for other steady wake models, e.g., Blevins (1990), Schlichting and Gersten (2000) and the JET wake model by Madsen et al. (2007), as well as for other structures where it is important to account for the unsteady and turbulent behaviour of the downwind wind field caused by the structure itself.

The method was used for three dimensional tapered towers, showing a decrease in blade fatigue loads using 15 percent more flexible and 15 percent lighter blades of three, four and two percent for the monopile tower and the truss tower at 0 and 22.5 degrees, respectively, compared to the upwind mounted rotor.

6 Acknowledgement

The work of Marit Reiso was financed by the Research Council of Norway (NFR) through the project *Offshore Wind Energy in Norway: Setting the Basis*, contract no. 186952/I30.

7 References

Ahlström, A., 2006. Influence of wind turbine flexibility on loads and power production. J. Wind Energy 9, 237-249.

Blevins, R.D., 1990. Flow-induced vibration, Van Nostrand Reinhold, New York.

Bossanyi, E.A., 2009. GH Bladed theory manual. Technical report 282/BR/009. Garrad Hassan and Partners Limited, Bristol.

Coton, F.N., Wang, T., Galbraith, R.A.M., 2002. An examination of key aerodynamic modelling issues raised by the NREL blind comparison. Wind Energy 5, 199-212.

Gao, Y., Yu, D., Tan, S., Wang, X., Hao, Z., 2010. Experimental study on the near wake behind two side-by-side cylinders of unequal diameters. Fluid Dyn. Res. 42, 1-13.

Hagen, T.R., Reiso, M., Muskulus, M., 2011a. Numerical analysis of turbulent flow past a truss tower for offshore downwind turbines, Proc. Int. Offshore Polar Eng. Conf., ISOPE, Maui, pp. 319-326.

Hagen, T.R., Reiso, M., Muskulus, M., 2011b. Numerical tower shadow modeling for a downwind wind turbine truss tower, Proc. Int. Conf. Offshore Mech. Arct. Eng., OMAE, Rotterdam, pp. 859-870.

IEC, 2009. Wind Turbines - Part 3: Design Requirements for Offshore Wind Turbines. Technical report IEC 61400-3. International Electrotechnical Commission, IEC, Geneva.

Ishigai, S., Nishikawa, E., Nishimura, K., Cho, K., 1972. Experimental study on structure of gas flow in tube banks with tube axes normal to flow. I. Karman vortex flow from two tubes at various spacings. Bull. Jpn. Soc. Mech. Eng., JSME 15, 949-956.

Jonkman, J., Butterfield, S., Musial, W., Scott, G., 2009. Definition of a 5-MW Reference Wind Turbine for Offshore System Development. Technical report NREL/TP-500-38060, Golden.

Krause, L., Muskulus, M., 2012. Modeling of tower influence for a full-height truss tower wind turbine with the source panel method, Proc. Int. Offshore Polar Eng. Conf. ISOPE, Rhodes, pp. 417-422.

Lee, A.T., Flay, R.G.J., 1999. Compliant blades for wind turbines. IPENZ Trans. 26, 7-12.

Long, H., Moe, G., 2007. Truss Type Towers in Offshore Wind Turbines, Proc. European Offshore Wind Conf. Exhib., EWEA, Berlin.

Madsen, H.A., Johansen, J., Sørensen, N.N., Larsen, G.C., Hansen, M.H., 2007. Simulation of low frequency noise from a downwind wind turbine rotor, Collect. Tech. Pap. Aeros. Sci. Meet. AIAA, Reno, pp. 7549-7560.

Meneghini, J.R., Saltara, F., Siqueira, C.L.R., Ferrari, J.A., 2001. Simulation of flow interference between two circular cylinders in tandem and side-by-side arrangements. J. Fluids Struct. 15, 327-350.
Menter, F.R., 1994. Two-equation eddy-viscosity turbulence models for engineering applications. AIAA 32, 1598-1605.
Moe, G., Domben, T., Steen, P.E., 1993. Vibrations of a circular cylinder in the wake of a larger cylinder, Proc. 2nd European Conf. Struc. Dyn.: EURODYN. Publ by A.A. Balkema, Trondheim, pp. 1083-1083.
Moriarty, P.J., Hansen, A.C., 2005. AeroDyn theory manual. Technical report NREL/EL-500-36881, Golden.
Munduate, X., Coton, F.N., Galbraith, R.A.M., 2004. An investigation of the aerodynamic response of a wind turbine blade to tower shadow. J. Solar Energy Eng. 126, 1034-1040.
Nakayama, A., Okamoto, D., Takeda, H., 2010. Large-eddy simulation of flows past complex truss structures. J. Wind Eng. Ind. Aerodyn. 98, 133-144.
Ong, M.C., Utnes, T., Holmedal, L.E., Myrhaug, D., Pettersen, B., 2009. Numerical simulation of flow around a smooth circular cylinder at very high Reynolds numbers. Marine Struc. 22, 142-153.
Powles, S.R.J., 1983. The effects of tower shadow on the dynamics of a horizontal-axis wind turbine. J. Wind Eng. 7, 26-42.
Reiso, M., Moe, G., 2010. Blade response on offshore bottom fixed wind turbines with down-wind rotors, in: Proc. Int. Conf. Offshore Mech. Arct. Eng. OMAE, Shanghai, pp. 499-504.
Reiso, M., Muskulus, M., 2012a. Resolution of Tower Shadow Models for Downwind Mounted Rotors and its Effects on the Blade Fatigue. Unpublished results.
Reiso, M., Muskulus, M., 2012b. The simultaneous effect of a fairing tower and increased blade flexibility on a downwind mounted rotor. Unpublished results.
Reiso, M., Muskulus, M., Moe, G., 2011. Tower shadow - Experiment comparing wake behind tubular and truss towers, Proc. Int. Offshore Polar Eng. Conf. ISOPE, Maui, pp. 335-341.
Salim, S.M., Cheah, S.C., 2009. Wall y+ strategy for dealing with wall-bounded turbulent flows, Int. MultiConf. Eng. Comp. Scientists 2009. IMECS 2009. Newswood Limited, Hong Kong, pp. 2165-2170.
Schlichting, H., Gersten, K., 2000. Boundary-Layer Theory, Springer.
Wang, T., Coton, F.N., 2001. A high resolution tower shadow model for downwind wind turbines. J. Wind Eng. Ind. Aerodyn. 89, 873-892.
Warschauer, K.A., Leene, J.A., 1971. Experiments on mean and fluctuating pressures of circular cylinders at cross flow at very high Reynolds numbers, Proc. 3rd Int. Conf. Wind Eff. Build. Struc., pp. 305-315.
Wilmshurst, S.M.B., Powles, S.J.R., Wilson, D.M.A., 1985. The problem of tower shadow, Proc. Wind Energy Convers. BWEA, Oxford, pp. 95-102.
Zdravkovich, M.M., 1977. Review of flow interference between two circular cylinders in various arrangements. Trans. ASME., I, J. Fluids Eng. 99, 618-633.
Zdravkovich, M.M., 1997. Flow around circular cylinders. Volume 1: Fundamentals, Oxford University Press, New York.
Zdravkovich, M.M., Namork, J.E., 1979. Structure of interstitial flow between closely spaced tubes in staggered array, Flow Induc. Vib., Symp. Natl. Congr. Press. Vessel Pip. Tech., San Francisco, pp. 41-46.

Appendix B - Derivation of the turbulence intensity from RANS simulations

This derivation of the turbulence intensity from the RANS simulations was originally given in Hagen [117], and is reconstructed here. First; the turbulence intensity is given as:

$$TI_{tot} = \frac{\sqrt{\sigma^2}}{V_0}, \tag{1}$$

where V_0 is the free stream wind velocity and σ^2 the variance. In unsteady RANS model simulations, the total variance consist of two parts:

- One part that comes from the unsteady motions (i.e. the ensemble mean velocity, $\langle V(t) \rangle$), and
- One part that comes from the sub-grid parametrization, quantified by the turbulent kinetic energy, which is the ensemble variance of the velocity at each time point t ($\sigma^2_{TKE(t)}$).

For clarity, the following notations are used:
i ensemble index,
N total number of realizations in the ensemble,
$\langle\rangle$ ensemble mean,
j time index,
T total number of time steps,
$\overline{V}$ time averaged velocity.

Unsteady motions

To obtain the variance from the unsteady motions ($\sigma^2_{unsteady}$), the time average of the velocity is first derived:

$$\overline{V} = \frac{1}{T}\sum_{j=1}^{T} V(t_j) = \frac{1}{T}\sum_{j=1}^{T} \langle V(t_j)\rangle \,, \tag{2}$$

since the fluctuations are zero-mean. Then the variance from the unsteady motions becomes:

$$\sigma^2_{unsteady} = \frac{1}{T}\sum_{j=1}^{T} \left(\langle V(t_j)\rangle - \overline{V}\right)^2 \tag{3}$$

Sub-grid parametrization

The turbulent kinetic energy (TKE) is given through the RANS simulations. It is based on the following physical relation and connected to the instantaneous variance of the modelled turbulent fluctuations by the relationship:

$$TKE = \frac{1}{2}\left(\left\langle \left(V_x(t) - \langle V_x(t)\rangle\right)^2\right\rangle + \left\langle \left(V_y(t) - \langle V_y(t)\rangle\right)^2\right\rangle\right) \approx \left\langle \left(V(t) - \langle V(t)\rangle\right)^2\right\rangle, \tag{4}$$

where x and y denotes the velocity components in the alongwind and transversal directions, respectively. This results in:

$$\sigma^2_{TKE(t)} = lim_{N\to\infty}\frac{1}{N}\sum_{i=1}^{N} \left(V_i(t) - \langle V(t)\rangle\right)^2 , \tag{5}$$

where V_i(t) is the i-th realization of the time series (unknown quantity in RANS simulations) in the ensemble, and $\langle V(t)\rangle$ is the ensemble mean of the velocity at time t.

Further the variance for the time averaged turbulent kinetic energy ($\sigma^2_{\overline{TKE}}$) is defined:

$$\sigma^2_{\overline{TKE}} = \frac{1}{T}\sum_{j=1}^{T} \sigma^2_{TKE(t)} \tag{6}$$

This gives the total variance (σ^2) from the RANS simulations:

$$\sigma^2 = lim_{N\to\infty}\frac{1}{N}\sum_{i=1}^{N}\cdot\frac{1}{T}\sum_{j=1}^{T}\left(V(t_j)-\overline{V}\right)^2$$

$$= lim_{N\to\infty}\frac{1}{N}\sum_{i=1}^{N}\cdot\frac{1}{T}\sum_{j=1}^{T}\left(\left(\langle V(t_j)\rangle-\overline{V}\right)+\left(V(t_j)-\langle V(t_j)\rangle\right)\right)^2 \tag{7}$$

Expanding the square we are left with these terms:

$$lim_{N\to\infty}\frac{1}{N}\sum_{i=1}^{N}\cdot\frac{1}{T}\sum_{j=1}^{T}\left(\langle V(t_j)\rangle-\overline{V}\right)^2=\sigma^2_{unsteady} \tag{8}$$

$$lim_{N\to\infty}\frac{1}{N}\sum_{i=1}^{N}\cdot\frac{1}{T}\sum_{j=1}^{T}\left(V(t_j)-\langle V(t_j)\rangle\right)^2$$

$$=\frac{1}{T}\sum_{j=1}^{T}lim_{N\to\infty}\frac{1}{N}\sum_{i=1}^{N}\left(V(t_j)-\langle V(t_j)\rangle\right)^2$$

$$=\frac{1}{T}\sum_{j=1}^{T}\sigma^2_{TKE}(t_j)=\sigma^2_{\overline{TKE}} \tag{9}$$

$$2\cdot lim_{N\to\infty}\frac{1}{N}\sum_{i=1}^{N}\cdot\frac{1}{T}\sum_{j=1}^{T}\left(\langle V(t_j)\rangle V(t_j)-\langle V(t_j)\rangle^2-\overline{V}V(t_j)+\overline{V}\langle V(t_j)\rangle\right)=0 \tag{10}$$

Therefore the total variance is:

$$\sigma^2 =^2_{unsteady} +\sigma^2_{\overline{TKE}}, \tag{11}$$

and the total turbulence intensity, TI_{tot}, from the RANS simulations becomes:

$$TI_{tot}=\frac{\sqrt{\sigma^2}}{V_0}=\frac{\sqrt{\sigma^2_{unsteady}+\sigma^2_{\overline{TKE}}}}{V_0} \tag{12}$$

Bibliography

[1] SRC. SRC - Available: http://www.eng.src-vertical.com/information/ infobasic/, downloaded 06/01/2013.

[2] J.F. Manwell, J.G. McGowan, and A.L. Rogers. *Wind Energy Explained - Theory, Design and Application*. Wiley, Chichester, 2008.

[3] P. Vølund and J. Hansen. Middelgrunden 40 MW offshore wind farm near Copenhagen, Denmark, installed year 2000. *Dep. Wind Energy, SEAS Denmark*, 2000.

[4] D. Wilson and P. Roopa. Dreaming with BRICs: The path to 2050. *Goldman Sachs*, 99:1–24, 2003.

[5] Energiewende - German plans to cut carbon emissions with renewable energy are ambitious, but they are also risky. Available: http://www.economist.com/node/21559667, downloaded 06/01/2013.

[6] S. Ropenus. BWE - German Wind Energy Association. Available: http://www.wind-energie.de/en/policy/offshore, downloaded 03/01/2013.

[7] M. Bilgili, A. Yasar, and E. Simsek. Offshore wind power development in Europe and its comparison with onshore counterpart. *Renew. Sustain. Energy Reviews*, 15:905–915, 2011.

[8] A. Karnstedt. Karte der verteilung von windkraftanlagen (windparks) in Deutschland. Available: http://en.wikipedia.org/wiki/file:windkraftanlagen in deutschland.png, downloaded 03/01/2013.

[9] C.L. Archer and M.Z. Jacobson. Evaluation of global wind power. *J. Geophys. Res.*, 110:1–20, 2005.

[10] G. Gaudiosi. Offshore wind energy in the world context. In *Proc. of World Renewable Energy Congress (WREC1996), Denver, CO*, pages 899–904, 1996.

[11] G. Moe. What is the optimum size for a wind turbine? In *Proc. of the 26th International Conference on Offshore Mechanics and Arctic Engineering (OMAE2007), San Diego, CA*, pages 1–8, 2007.

[12] P. Jamieson. *Innovation in wind turbine design*. Wiley, Chichester, 2011.

[13] J. Paska, M. Salek, and T. Surma. Current status and perspectives of renewable energy sources in Poland. *Renew. and Sust. Energy Reviews*, 13:142–154, 2009.

[14] P.E. Morthorst, J. Lemming, and N.E. Clausen. *Offshore Wind Power*. Multi-Science Publishing, Brentwood, 2009.

[15] T. Ackermann, R. Leutz, and J. Hobohm. World-wide offshore wind potential and European projects. In *Proc. of Power Engineering Society Summer Meeting (IEEE2001), Vancouver, BC*, pages 4–9, 2001.

[16] D.R.S. Verelst and T.J. Larsen. Yaw stability of a free-yawing 3-bladed downwind wind turbine. In *Proc. 6th PhD Seminar on Wind Energy in Europe, European Academy of Wind Energy (EAWE), Trondheim*, pages 29–32, 2010.

[17] A. Lee and R. Flay. Compliant blades for wind turbines. *IPENZ Trans.*, 26:7–12, 1999.

[18] J.C. Glasgow, D.R. Miller, and R.D. Corrigan. *Comparison of upwind and downwind rotor operations for the DOE/NASA 100-kW Mod-0 wind turbine.* Tech. Rep. NASA-TM-81744, National Aeronautics and Space Administration, Cleveland, OH, 1981.

[19] G.R. Frederick and J.M. Savino. *Summary of tower design for large horizontal axis wind turbines.* Tech. Rep. NASA-TM-87166, National Aeronautics and Space Administration, Cleveland, OH, 1986.

[20] R.W. Righter. *Wind energy in America: A history.* Oklahoma University Press, Norman, 1996.

[21] J.L. Collins and R.K. Shaltens. *Experience and assessment of the DOE-NASA Mod-1 2000-kilowatt wind turbine generator at Boone, North Carolina.* Tech. Rep. NASA-TM-82721, National Aeronautics and Space Administration, Cleveland, OH, 1982.

[22] P.C. Putnam. *Power from the wind.* Van Nostrand Reinhold, New York, 1948.

[23] T. Fischer. *Executive summary - WP4: Offshore foundations and support structures.* Upwind project, Contract No. 019945(SES6), 2011.

[24] C. Bartsch. Fact-sheet Alpha Ventus. *Bundesministerium für Umwelt, Naturschutz und Reaktorsicherheit*, 2012.

[25] RWE. Nordsee ost - RWE's first German offshore wind farm. *RWE Innogy*, 2013.

[26] N.L. Pedersen and A.K. Nielsen. Optimization of practical trusses with constraints on eigenfrequencies, displacements, stresses, and buckling. *Struct. Multidisc. Optim.*, 25:436–445, 2003.

[27] B. Skaare, T.D. Hanson, R. Yttervik, and F.G. Nielsen. Dynamic response and control of the Hywind demo floating wind turbine. In *Proc. of the European Wind Energy Conference and Exhibition (EWEC2011), Brussel*, pages 53–57, 2011.

[28] A. Bossler. *Floating offshore wind foundations: Industry consortia and projects in the United States, Europe and Japan*. www.maine-intl-consulting.com, Main(e) International Consulting LLC, Bremen (ME), 2012.

[29] S.M.B. Wilmshurst, S.J.R. Powles, and D.M.A. Wilson. The problem of tower shadow. In *Proc. of the 7th British Wind Energy Association Conference (BWEA1985), London*, pages 95–102, 1985.

[30] I. Janajreh, R. Qudaih, I. Talab, and C. Ghenai. Aerodynamic flow simulation of wind turbine: Downwind versus upwind configuration. *Energy Convers. and Manag.*, 51:1656 – 1663, 2010.

[31] T. Buhl. *Research in aeroelasticity*. Tech. Rep. EFP-2007-II, DTU, Risø National Renewable Energy Laboratory, Roskilde, 2009.

[32] H. Long and G. Moe. Preliminary design of bottom-fixed lattice offshore wind turbine towers in the fatigue limit state by the frequency domain method. *J. Offshore Mech. Arct. Eng.*, 134:1–10, 2012.

[33] P. Jamieson and A. Jaffrey. Advanced wind turbine design. *J. Solar Energy Eng.*, 119:315–320, 1997.

[34] P. Jamieson, C. Hornzee-Jones, E.M. Moroz, and R.W. Blakemore. *General electric company (assignee) variable diameter wind turbine rotor blades.* Patent no. US 6, 972,498 B2, 2005.

[35] GL Germanischer Lloyd. *Guideline for the certification of offshore wind turbines*. Tech. Rep. GL Wind 2004, Hamburg, 2004.

[36] Det Norske Veritas. *Design of offshore wind turbine structures*. Tech. Rep. DNV-OS-J101, Høvik, 2013.

[37] International Electrotechnical Commission. *Wind turbines - Part 3: Design requirements for offshore wind turbines*. Tech. Rep. IEC:2009 61400-3, Geneva, 2009.

[38] A.J. Brand, J. Peinke, and J. Mann. Turbulence and wind turbines. In *Proc. 13th European Turbulence Conference, Warsaw*, pages 1–9, 2011.

[39] R.D. Blevins. *Flow-Induced Vibrations*. Van Nostrand Reinhold, New York, 1990.

[40] M.M. Zdravkovich. *Flow around circular cylinders, Vol. 1*. Oxford University Press, Oxford, 1997.

[41] T. Sarpkaya. *Wave forces on offshore structures*. Cambridge University Press, Cambridge, 2010.

[42] S. Ishigai, E. Nishikawa, K. Nishimura, and K. Cho. Experimental study on structure of gas flow in tube banks with tube axes normal to flow. Part 1, Karman vortex flow from two tubes at various spacings. *Bull. JSME*, 15:949–956, 1972.

[43] M.M. Zdravkovich. Review of flow interference between two circular cylinders in various arrangements. *J. Fluids Eng.*, 99:618–633, 1977.

[44] J.R. Meneghini, F. Saltara, C.L.R. Siqueira, and J.A. Ferrari. Simulation of flow interference between two circular cylinders in tandem and side-by-side arrangements. *J. Fluids Struct.*, 15:327–350, 2001.

[45] Y. Gao, D. Yu, S. Tan, X. Wang, and Z. Hao. Experimental study on the near wake behind two side-by-side cylinders of unequal diameters. *Fluid Dyn. Res.*, 42:1–13, 2010.

[46] T. Sørensen, M.L. Thøgersen, P. Nielsen, A. Grötzner, and S. Chun. *Adapting and calibration of existing wake models to meet the conditions inside offshore wind farms.* Danish Energy Authority J.nr. 79029-0031, EMD International A/S, Aalborg, 2008.

[47] J.F. Ainslie. Calculating the flowfield in the wake of wind turbines. *J. Wind Eng. Ind. Aerodyn.*, 27:213–224, 1988.

[48] P.-Å. Krogstad and P.E. Eriksen. 'Blind test' calculations of the performance and wake development for a model wind turbine. *Renewable Energy*, 50:325–333, 2013.

[49] S. R. J. Powles. The effects of tower shadow on the dynamics of a horizontal-axis wind turbine. *Wind Eng.*, 7:26–42, 1983.

[50] E.A. Bossanyi. *GH Bladed Theory Manual.* Tech. Rep. 282/BR/009, Garrad Hassan, Bristol, 2009.

[51] P.J. Moriarty and A.C. Hansen. *AeroDyn theory manual.* Tech. Rep. NREL/EL-500-36881, National Renewable Energy Laboratory, Golden, CO, 2005.

[52] C. Bak, H.A. Madsen, and J. Johansen. Influence from blade-tower interaction on fatigue loads and dynamics. In *Proc. of the European Wind Energy Conference and Exhibition (EWEC2001), Copenhagen*, pages 394–397, 2001.

[53] H. Schlichting and K. Gersten. *Boundary-layer theory.* Springer, Berlin, 2000.

[54] H.A. Madsen, J. Johansen, N.N. Sørensen, G.C. Larsen, and M.H. Hansen. Simulation of low frequency noise from a downwind wind turbine rotor. In *45th AIAA Aerospace Sciences Meeting and Exhibit, Reno, NV, Paper No. AIAA-2007-623*, pages 1–12, 2007.

[55] T. von Karman. Progress in the statistical theory of turbulence. In *Proc. National Academy of Sciences (PNAS1948)*, pages 530–539, 1948.

[56] J.C. Kaimal, J.C. Wyngaard, Y. Izumi, and O.R. Coté. Spectral characteristics of surface layer turbulence. *Q.J.R. Meteorol. Soc.*, 98:563–589, 1972.

[57] T. Burton, D. Sharpe, N. Jenkins, and E. Bossanyi. *Wind Energy Handbook*. Wiley, Chichester, 2008.

[58] E.L. Petersen, N.G. Mortensen, L. Landberg, J. Højstrup, and H.P. Frank. Wind power meteorology. Part I: Climate and turbulence. *Wind Energy*, 1:25–45, 1998.

[59] R.I. Harris. Some further thought on the spectrum of gustiness in strong winds. *J. Wind. Eng. Ind. Aerodyn.*, 33:461–477, 1990.

[60] ESDU. *Characteristics of atmospheric turbulence near the ground. Part II: Single point data for strong winds (neutral atmosphere)*. Tech. Rep. ESDU 85020, Engineering Science Data Unit, UK, 1985.

[61] R.W. Thresher, W.E. Holley, C.E. Smith, N. Jafarey, and S.-R. Lin. *Modeling the response of wind turbines to atmospheric turbulence*. Tech. Rep. RL0/2227-81/2, Oregon State University, OR, 1981.

[62] J. Mann. The spatial structure of neutral atmospheric surface-layer turbulence. *J. Fluid Mech.*, 273:141–168, 1994.

[63] K. Saranyasoontorn, L. Manuel, and P.S. Veers. A comparison of standard coherence models for inflow turbulence with estimates from field measurements. *J. Solar Energy Eng.*, 126:1069–1082, 2004.

[64] E. Simiu and R.H. Scanlan. *Wind effects on structures*. Wiley, New York, 1986.

[65] J. Høystrup. A simple model for the adjustment of velocity spectra in unstable conditions downstream of an abrupt change in roughness and heat flux. *Bound.-Layer Meteorol.*, 21:341–356, 1981.

[66] International Electrotechnical Commission. *Wind turbines - Part 1: Design requirements*. Tech. Rep. IEC:2005 61400-1, Geneva, 2005.

[67] International Electrotechnical Commission. *Wind turbine generator systems - Part 1: Safety requirements*. Tech. Rep. IEC:1998 61400-1, Geneva, 1998.

[68] H.R. Olesen, S.E. Larsen, and J. Højstrup. Modelling velocity spectra in the lower part of the planetary boundary layer. *Bound.-Layer Meteorol.*, 29:285–312, 1984.

[69] F. Irgens. *Continuum mechanics*. Springer, Berlin, 2008.

[70] D.C. Wilcox. *Turbulence modeling for CFD*. La Cañada, CA: DCW Industries, 2006.

[71] S.B. Pope. *Turbulent flows*. Cambridge University Press, Cambridge, 2010.

[72] U. Piomelli and E. Balaras. Wall-layer models for large-eddy simulations. *Annu. Rev. Fluid Mech.*, 34:349–374, 2002.

[73] S.B. Pope. A lagrangian two-time probability density function equation for inhomogeneous turbulent flows. *Phys. Fluids*, 26:3448–3450, 1983.

[74] L. Prandtl. Über ein neues formelsystem für die ausgebildete turbulenz. *Nach. Akad. Wiss. Göttingen Math-Phys.*, pages 6–19, 1945.

[75] L. Prandtl. Über die ausgebildete Turbulenz. *ZAMM*, 5:136–139, 1925.

[76] T. Cebeci. *Analysis of turbulent flows*. Elsevier, Amsterdam, 2004.

[77] P.R. Spalart and S.R. Allmaras. One-equation turbulence model for aerodynamic flows. *Rech. Aerosp.*, 1:5–21, 1994.

[78] P. Bradshaw, D.H. Ferriss, and N.P. Atwell. Calculation of boundary layer development using the turbulent energy equation. *J. Fluid Mech.*, 28:593–616, 1967.

[79] B.S. Baldwin and T.J. Barth. *A one-equation turbulence transport model for high Reynolds number wall-bounded flows*. NASA Tech. Memorandum 102847, National Aeronautics and Space Administration, Moffett Field, CA, 1990.

[80] J.C. Rotta. Statistische theorie nichthomogener Turbulenz. *Z. Phys.*, 129:547–572, 1951.

[81] A.N. Kolmogorov. The equations of turbulent motion in an incompressible fluid. *Izvestia Acad. Sci. USSR Phys.*, 6:56–58, 1942.

[82] P.G. Saffman. A model for inhomogenous turbulent flow. *Proc. R. Soc. London Ser. A*, 317:417–433, 1970.

[83] C.G. Speziale, R. Abid, and E.C. Anderson. Critical evaluation of two-equation models for near-wall turbulence. *AIAA*, 30:324–331, 1992.

[84] W.P. Jones and B.E. Launder. The prediction of laminarization with a two-equation model of turbulence. *Int. J. Heat Mass Transf.*, 15:301–314, 1972.

[85] B.E. Launder and B.I. Sharma. Application of the energy-dissipation model of turbulence to the calculation of flow near a spinning disc. *Lett. Heat Mass Transf.*, 1:131–138, 1974.

[86] F. Menter. Two-equation eddy-viscosity turbulence models for engineering applications. *AIAA*, 32:1598–1605, 1994.

[87] B.E. Launder, G.J. Reece, and W. Rodi. Progress in the development of a Reynolds-stress turbulent closure. *J. Fluid Mech.*, 68:537–566, 1975.

[88] C.G. Speziale. On nonlinear k-l and k-ϵ models of turbulence. *J. Fluid Mech.*, 178:459–475, 1987.

[89] A. Yoshizawa. Statistical analysis of the deviation of the Reynolds stress from its eddy viscosity representation. *Phys. Fluids*, 27:1377–1387, 1984.

[90] S.M. Salim and S.C. Cheah. Wall y+ strategy for dealing with wall-bounded turbulent flows. In *Proc. International Multi-Conference of Engineers and Computer Sciences (IMECS2009), Hong Kong*, pages 1–6, 2009.

[91] S. Yarlanki, B. Rajendran, and H. Hamann. Estimation of turbulence closure coefficients for data centers using machine learning algorithms. In *Proc. of the 13th IEEE Intersociety Conference on Thermal and Thermomechanical Phenomena in Electronic Systems (IEEE2012), San Diego, CA*, pages 38–42, 2012.

[92] J. Jonkman and M.L. Buhl. *FAST User's Guide*. Tech. Rep. NREL/EL-500-38230, National Renewable Energy Laboratory, Golden, CO, 2005.

[93] T.J. Larsen and A.M. Hansen. *How 2 HAWC2, the user's manual*. Tech. Rep. Risø-R-1597(ver. 3-1), Risø National Laboratory, Roskilde, 2007.

[94] A. Myhr, K.J. Maus, and T.A. Nygaard. Experimental and computational comparisons of the OC3-Hywind and tension-leg-buoy (TLB) floating wind turbine conceptual designs. In *Proc. of the 21st International Offshore and Polar Engineering Conference (ISOPE2011), Maui, HI*, pages 353–360, 2011.

[95] *Fedem user's guide, release 7.0*. Fedem Technology, Trondheim, 2012.

[96] WindSim. manual. Available: http://www.tudelft.nl/en/research/knowledge-centres/duwind/windsim/, downloaded 20/02/2013.

[97] P.E. Thomassen, P.I. Bruheim, S. Loup, and L. Frøyd. A novel tool for fem analysis of offshore wind turbines with innovative visualization techniques. In *Proc. of the 22nd International Offshore and Polar Engineering Conference (ISOPE2012), Rhodes*, pages 374–379, 2012.

[98] J.R. Morison, M.P. O'Brien, J.W. Johnson, and S.A. Schaaf. The force exerted by surface waves on piles. *Petroleum trans.*, 189:149–154, 1950.

[99] J. Jonkman and W. Musial. *Offshore code comparison collaboration (OC3) for IEA task 23 offshore wind technology and deployment*. Tech. Rep. NREL/TP-5000-48191, National Renewable Energy Laboratory, Golden, CO, 2010.

[100] W. Popko, F. Vorpahl, A. Zuga, M. Kohlmeier, J. Jonkman, and A. Robertson et al. *Offshore code comparison collaboration continuation (OC4), Phase I - Results of coupled simulations of an offshore wind turbine with jacket support structure*. NREL/CP-5000-54124, National Renewable Energy Laboratory, Golden, CO, 2012.

[101] D. Simms, S. Schreck, M. Hand, and L.J. Fingersh. *NREL Unsteady aerodynamics experiment in the NASA-Ames wind tunnel: A comparison of predictions to measurements*. Tech. Rep. NREL/TP-500-29494, National Renewable Energy Laboratory, Golden, CO, 2001.

[102] F.N. Coton, T. Wang, and R.A.McD. Galbraith. An examination of key aerodynamic modelling issues raised by the NREL blind comparison. *Wind Energy*, 5:199–212, 2002.

[103] X. Munduate, F.N. Coton, and R.A.McD. Galbraith. An investigation of the aerodynamic response of a wind turbine blade to tower shadow. *J. Solar Energy Eng.*, 12:1034–1040, 2004.

[104] T. Wang and F.N. Coton. A high resolution tower shadow model for downwind wind turbines. *J. Wind Eng. Ind. Aerodyn.*, 89:873–892, 2001.

[105] M.H. Snyder and W.H.Jr. Wentz. *Dynamics of wakes downstream of wind turbine towers*. Tech. Rep. NASA-CP-2185, National Aeronautics and Space Administration, Cleveland, OH, 1981.

[106] T. Wang, F. Coton, and R. Galbraith. An examination of two tower-shadow modelling strategies for downwind wind turbines. In *36th AIAA Aerospace Sciences Meeting, Reno, NV, Paper No. AIAA-98-0022*, pages 20–30, 1998.

[107] R.W. Thresher, A.D. Wright, and E.L. Hershberg. A computer analysis of wind turbine blade dynamic loads. *J. Solar Energy Eng.*, 108:17–25, 1986.

[108] P.-Å. Krogstad and J.A. Lund. Study of the performance of a model turbine. *Wind Energy*, 15:443–457, 2012.

[109] M.O.L. Hansen, J.N. Sørensen, S. Voutsinas, N. Sørensen, and H.Aa. Madsen. State of the art in wind turbine aerodynamics and aeroelasticity. *Prog. Aerosp. Sci.*, 42:285–330, 2006.

[110] L.J. Vermeer, J.N. Sørensen, and A. Crespo. Wind turbine wake aerodynamics. *Prog. Aerosp. Sci.*, 39:467–510, 2003.

[111] F. Zahle, N.N. Sørensen, and J. Johansen. Wind turbine rotor-tower interaction using an incompressible overset grid method. *Wind energy*, 12:594–619, 2009.

[112] J. Jonkman, S. Butterfield, W. Musial, and G. Scott. *Definition of a 5-MW Reference Wind Turbine for Offshore System Development*. Tech. Rep. NREL/TP-500-38060, National Renewable Energy Laboratory, Golden, CO, 2009.

[113] H.H. Bruun. *Hot-wire anemometry: Principles and signal analysis*. Oxford University Press, Oxford, 1995.

[114] M.C. Ong, T. Utnes, L.E. Holmedal, D. Myrhaug, and B. Pettersen. Numerical simulation of flow around a smooth circular cylinder at very high Reynolds numbers. *Marine Struc.*, 22:142–153, 2009.

[115] L. Bairstow. *Applied aerodynamics*. Longmans Green and Co., London, 1939.

[116] J.A. Nelder and R. Mead. A simplex method for function minimization. *Comput. J.*, 7:308–313, 1965.

[117] T.R. Hagen. *Numerical simulations of flow past a truss tower with an evaluation of tower shadow models for wind turbines*. NTNU, Norwegian University of Science and Technology, Trondheim, 2011.